# TRANSFER OF TRIPLET EXCITONS IN SINGLET FISSION-SILICON SOLAR CELLS

Experiment and Theory Towards Breaking the Detailed-Balance Efficiency Limit

BENJAMIN DAIBER

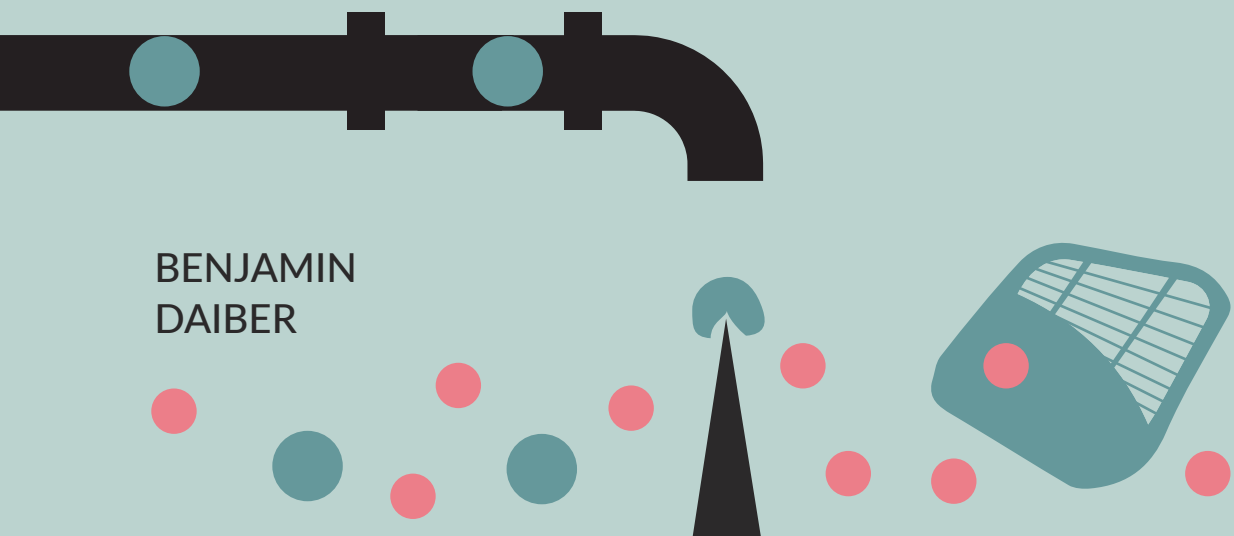

BENJAMIN DAIBER

# TRANSFER OF TRIPLET EXCITONS IN SINGLET FISSION-SILICON SOLAR CELLS



Ph.D. Thesis, University of Groningen, December 2020

Benjamin Daiber

Ph.D. Examining committee:
Prof. M.W.B. Wilson
Dr. J. Clark
Prof. M.A. Loi
Prof. M.S. Pchenitchnikov
Prof. F.C. Grozema

The work described in this thesis was performed between November 2016 and December 2020 at AMOLF, Science Park 104, 1098 XG Amsterdam, The Netherlands and financed by the Netherlands Organization for Scientific Research (NWO).

Printed by GVO drukkers & vormgevers B.V.
Cover Design by Loes Kema

This document was typeset using the `classicthesis` style for LaTeX developed by André Miede. The style was inspired by Robert Bringhurst's seminal book on typography *"The Elements of Typographic Style"*.

A digital version of this thesis can be downloaded at amolf.nl

university of groningen

# Transfer of Triplet Excitons in Singlet Fission-Silicon Solar Cells

Experiment and Theory Towards Breaking the Detailed-Balance Efficiency Limit

**PhD thesis**

to obtain the degree of PhD at the
University of Groningen
on the authority of the
Rector Magnificus Prof. C. Wijmenga
and in accordance with
the decision by the College of Deans.

This thesis will be defended in public on

9 April 2021 at 12.45 hours

by

**Benjamin Daiber**

born on 21 February 1992
in Stuttgart, Germany

**Supervisor**
Prof. B. Ehrler

**Co-Supervisor**
Dr. E. Alarcón-Lladó

**Assessment committee**
Prof. M.A. Loi
Prof. M.S. Pchenitchnikov
Prof. F.C. Grozema

# PROPOSITIONS

accompanying the dissertation

## Transfer of Triplet Excitons in Singlet Fission-Silicon Solar Cells
### Experiment and Theory Towards Breaking the Detailed-Balance Efficiency Limit

by

Benjamin Daiber

1. Quenching of delayed PL can be used to detect transfer of triplet excitons into another semiconductor.
2. The wrong assumption about the noise distribution can systematically change your fitting results.
3. Singlet fission can improve the silicon solar cell with many different transfer mechanisms.
4. FRET can be efficient even into an indirect bandgap semiconductor like silicon, if the donor-acceptor distance is small.
5. Transfer of triplet excitons from an organic semiconductor into silicon can be enabled by controlling the polymorphism of tetracene.
6. Doing the right thing is becoming harder, the longer you wait, but you have to wait long enough to know what is right.
7. Once you think your problem has a trivial solution you have found a good solution.
8. Science would work better with an alphabetical author list.
9. The simplest way of explaining a graph or concept is the most understandable and will have the largest impact.
10. What the reviewers accept as sufficient is arbitrary in first approximation.

Dedicated to everyone who has treated me with kindness and love,

helped me on my journey, big and small.

# CONTENTS

# 1 INTRODUCTION

This chapter will introduce the basics of solar cell physics, organic semiconductors and singlet fission, which will help in the understanding of the following chapters. We will also quickly introduce the need for solar cell efficiency gains and provide the context of solar cells in the green energy transition.

## 1.1 SOLAR CELLS AND THE GREEN ENERGY TRANSITION

Manmade global warming is a key challenge in the next 20 years. We have to reduce the emission of greenhouse gasses drastically if we want to avoid the devastating effects of global warming. The Intergovernmental Panel on Climate Change says in its fifth assessment report that we have to reduce the amount of greenhouse gasses starting immediately if we want to limit global warming below 2 °C [102]. Electrical power generation is currently a large emitter of greenhouse gasses, so a climate neutral alternative to fossil power plants is urgently needed. Solar cells are one such technology for green energy generation, promising because of their scalability and low cost [72]. In many places in the world it is now cheaper to install new solar cells than to *run* existing coal power plants [67]. Compared to nuclear power the lower capital cost, construction time, and the lack of nuclear waste is an advantage. Wind energy is another green energy source that is complementary to the installation of solar cells since the wind and sun are often active in different parts of the day, increasing the availability of electricity in the grid. However, wind power is not easily scalable, the cheaper on-shore wind parks often lead to citizen complaints and a slow roll out, and off-shore wind turbines are three

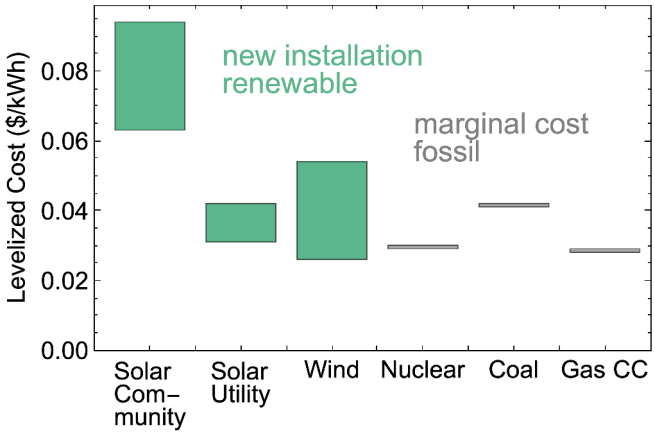


**Figure 1.1:** Select LCOE's taken from Lazard LCOE 14.0 [67]. Solar on the utility scale and wind power is now competitive with the marginal cost of running and maintaining fossil fuel power plants.

times more expensive to construct, operate and maintain [132]. Cost is the driving force in the energy market, any technology that is scalable and has a lower cost than the existing power plants will dominate over time. A good metric to compare the cost of energy generation between different technologies is the levelized cost of energy (LCOE), which takes the sum of all cost over the power plant lifetime into account. The investment bank Lazard has released a study of LCOE for 2020, a selection of costs are reproduced in Figure 1.1. The gray bars in Figure 1.1 are the marginal costs for keeping paid-off power plants running, which is, amazingly, in the same price region as installing a new wind or solar cell power plant.

If current technology is already so competitive, where is the need for new solar cell materials and designs? First, we have to accelerate growth, current installation speeds are not fast enough to meet expected future demand even with constant 30 % year-over-year growth until 2030 [46]. We will need a large overcapacity to electrify our economy. The transportation sector is currently transformed by the advent of the electric vehicle, but other fields like heating and cooling are also expected to increase electric energy consumption dramatically. Especially heating

during winter in the global north will need vast amounts of electricity, which will require us to install much more solar cell capacity. Unfortunately the increased demand falls in a time with lower average irradiance levels. An overcapacity plus some storage will also allow us to alleviate the problem of intermittent irradiation during the day and night cycle and between winter and summer. Hydrogen is also discussed as a fuel for heating, aviation, trucks and shipping. Currently hydrogen is generated by splitting natural gas into $CO_2$ and hydrogen, so-called grey hydrogen. We will need large amounts of cheap electricity to replace this process with electrolysis.

The costs of silicon solar cells have fallen dramatically already, but since silicon solar cell generation is energy intensive, there is a lower cost limit, although it is unclear where exactly it is [72]. The energy payback time for silicon solar cells is currently around 1 year [92]. The main way of reducing the cost of electricity generated by solar cells is the increase of solar cell efficiency. Installation, land and upkeep are fixed costs and are always expensive, so even a free solar cell would only cut costs by around 50% [92]. These fixed costs do not increase for higher efficiency solar cells, which makes efficiency gains the main goal for much of the solar cell manufacturers nowadays.

However, silicon solar cells are already very efficient. The theoretical maximum for silicon solar cell efficiency that can ever be achieved is 29.4 %, the so-called Auger limited detailed-balance limit [130]. The currently reported record silicon solar cell has an efficiency of 26.7 % (90 %(!) of the theoretical maximum), achieved with concerted efforts over the last 40 years [40]. It is clear that additional gains will be even harder to achieve, and additional efficiency gains with novel solar cell concepts are needed. One of these novel concepts is the singlet fission-silicon solar cell. In this concept high-energy light is absorbed in a separate layer that can then split the energy and inject it into a conventional solar cell like silicon. This concept has the potential for cheap manufacturing, since the underlying solar cell would remain largely untouched. In the following we will discuss how a conventional solar cell works, the principles behind organic semiconductors and singlet fission, and the challenges that arise

when combining organic and inorganic semiconductors to increase solar cell efficiencies.

## 1.2 INORGANIC SEMICONDUCTORS AND SOLAR CELLS

**SEMICONDUCTORS** Semiconductors are the building blocks for all solar cells, that allows us to extract the energy of light as usable electrical energy. When a photon hits a semiconductor it can generate an electron-hole pair, which can then be extracted with extraction layers and metallic contacts to drive an electrical load. Each semiconductor has a bandgap, which is the energy difference between the electron in the conduction band and the hole in the valence band. If the incoming photon has an energy smaller than the bandgap it will not be absorbed and can therefore not be used to generate power. In case of a photon energy with an energy larger than the bandgap energy the photon will be absorbed, but the excess energy will be lost as heat. Both of these loss mechanisms are fundamental when using a single bandgap, because the bandgap energy is very well defined but the solar spectrum is very broad, there are always photons that will not be used efficiently. This concept is visualized with the real solar spectrum and the silicon bandgap in Figure 1.2.

**EFFICIENCY LIMIT** A practical question is which semiconductor we should select to have the most efficient solar cell. This question has been answered by a detailed-balance calculation using a standardized input spectrum of the sun [115]. The optimal bandgap is between 1.1 eV and 1.5 eV, which is fortunate since there are many known materials that have this bandgap. Silicon is one of them, with a bandgap of 1.1 eV it has a high theoretical maximum efficiency above 31 %.

**SILICON** Most of the installed solar cells in the world are silicon solar cells [92], all aspects have been optimized for performance. This includes surface passivation, which prevents electrons and holes from recombining at the surface. The surface also usually has a micrometer-scale pyramidal

texture which decreases reflection losses and leads to higher currents. The surface with pyramids will look matte, as compared to bare silicon wafers that reflect visible light and look metallic to the eye. On top of the pyramidal structure a thin passivation layer is applied. This binds the dangling hydrogen atoms at the interface of silicon which are recombination centers. Often this passivation layer also acts as an additional antireflection coating, as in the case of silicon-nitride layers, which is the origin of the blue hue of many silicon solar cells. There are also effective ways of separating electron and hole by doping silicon with impurities.

One route for a new generation of solar cells is to keep all the aforementioned knowledge and technology for efficient silicon solar cells and use new materials as an add-on to increase efficiency.

Silicon is an indirect semiconductor, which means that a photon alone is not enough to form an electron hole pair across the bandgap, a phonon is also needed for the transition. Phonons are quasiparticles of the modes of vibrations in a crystal and their momentum is needed to absorb a photon in an indirect bandgap semiconductor. For solar cells this additional requirement is detrimental, it leads to lower light absorption coefficients which requires the silicon layer to be thick. To absorb 90 % of the light incident on earth (AM1.5) the silicon layer needs to be at 50 µm thick, in the absence of any additional light trapping scheme [139].

**EXCITONS IN SILICON** Upon absorption of a photon, an electron-hole pair is created that is very close in space. Electron and hole are Coulombically bound in a state called the exciton. In inorganic semiconductors like silicon this state is of little importance since the binding energy is small and electron and hole are readily separated. The binding energy is inversely proportional to the dielectric constant. The high dielectric constant of silicon is 11.7 leading to a binding energy of 14.7 meV [58], smaller than $k_B T = 25\,\text{meV}$, the thermal energy of a particle at room temperature. In other materials the exciton binding energy is much larger than $k_B T$, as we will see in the next section about organic semiconductors. This leads to very different behaviors of the semiconductor, including the main topic of the thesis, singlet fission.

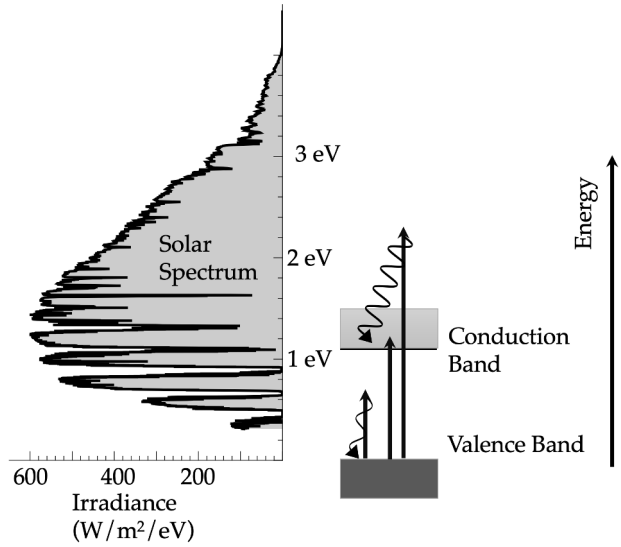


**Figure 1.2:** Solar spectrum and valence and conduction band of silicon. Photons with an energy smaller than the bandgap will not be absorbed, photons with a larger energy than the bandgap will be absorbed, but the additional energy will be lost through thermalization.

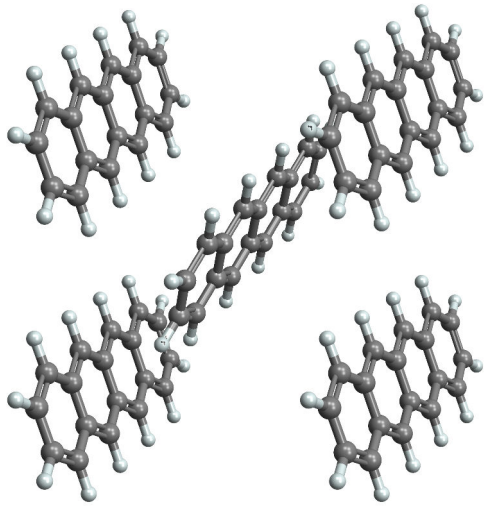

**Figure 1.3:** Molecular crystal of tetracene, an organic semiconductor consisting of four benzene rings that exhibits efficient singlet fission and is the focus of this thesis.

## 1.3 ORGANIC SEMICONDUCTORS

Organic semiconductors consist of covalently bound carbon and hydrogen atoms, that form amorphous molecular films, polymers and molecular crystals. They usually have a larger bandgap of $(2-3)$ eV [60], which means they absorb light in the visible and appear colorful to the human eye. In the following we will shortly introduce the optoelectronic behavior of molecular crystals, starting with a single molecule.

**WAVEFUNCTIONS IN ORGANIC MATERIALS** Each molecule has a so-called molecular wavefunction, which describes the volume that an electron occupies. These volumes are also called orbitals, each with different energies corresponding to their distance from the positively charged nucleus. There are different kinds of orbitals depending on their angular momentum quantum number. In carbon there are p-orbitals and s-orbitals, filled with electrons in the lowest possible energy state. Two close carbon atoms will lead to a hybridization of the orbitals called sp-

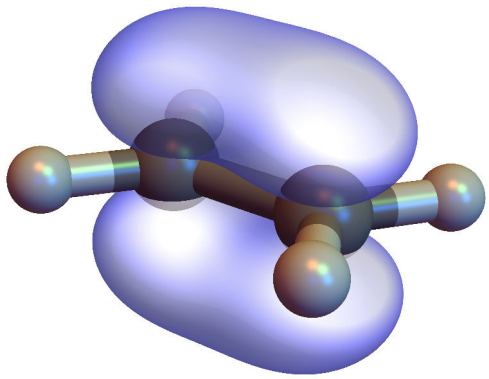

**Figure 1.4:** Wavefunctions (blue) of the π-bond in ethene. Hydrogen atoms are grey, carbon atoms are black. Modified, based on work of Günther Gsaller "Some examples of molecular orbitals" CC BY 3.0

Orbital, two electrons in such orbitals can form a bond, the strong σ-bond. If two electrons in p-orbitals overlap they form a more delocalized and weaker π-bond, the base for all organic semiconductors. Figure 1.4 shows the π-bond orbitals for ethene, a simple organic molecule.

**HOMO AND LUMO** We shall now discuss the energy levels of the electrons in these new bonds. The wavefunctions of the two electrons in a bond can interfere either constructively, leading to a state with so called bonding-character which leads to a new state with lower energy, or destructively, with so-called anti-bonding character and a higher energy level. This energy split is depicted in Figure 1.5, the anti-bonding orbitals are denoted with a star. This energy difference is very important, since we can excite an electron across it. Just like in inorganic semiconductors where the excitation happens across the bandgap, in organic semiconductors we excite an electron from the highest occupied molecular orbital (HOMO) to the lowest unoccupied molecular orbital (LUMO) by absorbing a photon of the appropriate energy. The difference in energy is determined by the exchange integral of the two electron orbitals. The exchange integral can be expressed as the interaction of the positive nucleus

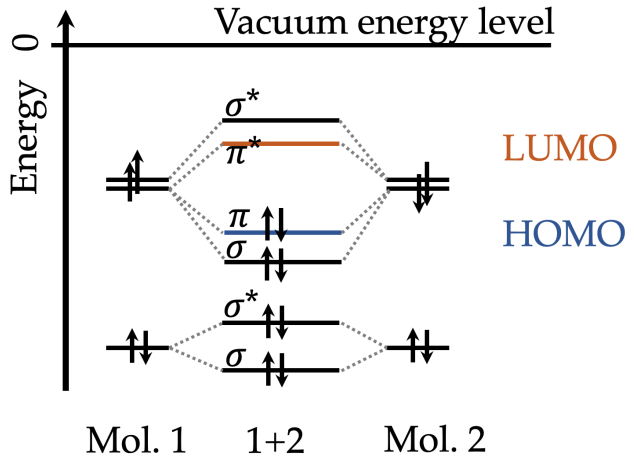


**Figure 1.5:** Electronic structure of ethene. Bonds form from single molecule orbitals. HOMO and LUMO are orbitals with an energy difference in the UV, larger organic molecules have lower HOMO-LUMO gaps with absorption in the visible spectrum of light. All electrons are in the ground state.

and the overlap of the two electrons centered around two different atoms. Luckily, for many organic semiconductors the energy difference between HOMO and LUMO is a couple $eV$, the same as photons in visible light, making them attractive for solar cell applications.

**EXCITONS** An exciton is a multi-electron state of a molecule, taking all electrons into account. In our previous case where we excited an electron from the HOMO to the LUMO we also have to take into account all the interactions between electrons and the smaller probabilities that an electron occupies higher lying orbitals. The main contribution to the state will still be from one electron in the HOMO and one in the LUMO, so it is common to omit all other states and depict that as an excited state exciton, called $S_1$ or singlet exciton. However, it is important stress that the singlet exciton is a multi electron state and has a different, smaller, energy than the HOMO-LUMO energy difference. The difference between

ground and excited singlet state, called the optical bandgap, is indeed the actual energy that a photon needs to have to excite the molecule, which can be slightly different from the HOMO-LUMO gap, also called the electrical bandgap, that we described before.

The *singlet* exciton state refers to the exciton spin state, described by the spin wavefunctions of all electrons. If we have two electrons with two spin states, called up and down and a total spin of 1, we can arrange the electrons in four states, three triplet states $\left(|\uparrow\uparrow\rangle, \frac{1}{\sqrt{2}}(|\uparrow\downarrow\rangle + |\downarrow\uparrow\rangle), |\downarrow\downarrow\rangle\right)$ and one singlet state $\left(\frac{1}{\sqrt{2}}(|\uparrow\downarrow\rangle - |\downarrow\uparrow\rangle)\right)$. The difference in energy between the triplet and singlet states is the exchange energy, twice the exchange integral between the two electrons. If the wavefunction overlap is large between the spin-up and down electrons in the HOMO and LUMO for example, the exchange energy will be large and the triplet exciton will be at a much lower energy than the singlet exciton.

The triplet exciton cannot be accessed optically, we cannot directly photoexcite from the ground state singlet exciton to the triplet exciton, absent a spin flip or spin mixing from heavy atoms that lead to intersystem crossing between the singlet and triplet exciton states. This, however, also means that triplet excitons cannot be directly converted to light when they relax back to their ground state, the triplet exciton is therefore called a *dark state*. A welcome side-effect of a dark state is that the fast optical relaxation pathway is not available, which leads to a long lifetime of triplet exciton states in the μs range, allowing for more time to extract or convert energy of a triplet state.

## 1.4 SINGLET FISSION

Singlet fission is the process of converting an excited singlet exciton state into two triplet excitons with about half the energy each. Since two triplet excitons together have spin 0, just as the singlet exciton, this is a spin-allowed process, and can be both fast and efficient. Since singlet fission is an effective way of splitting the higher energy of singlet excitons in organic semiconductors, it can be used to increase the efficiency of a

single junction solar cell. In this scheme, we absorb high-energy photons in the organic semiconductor, singlet fission generates two triplet excitons that we then have to inject into a lower-bandgap semiconductor where the electrical energy can be extracted. Effectively we then created a solar cell with two bandgaps with a higher detailed-balance efficiency limit of 42 % [22], but with potentially only one material needing to be optimized for charge extraction.

The simplest way of depicting the singlet fission process is shown in Equation 1.1 and Figure 1.6. An excited singlet exciton in an organic material can be converted readily, on a subpicosecond time scale [119], into a correlated triplet pair (TT) that is overall still a spin-singlet state. If the coupling energy of the (TT) state is not too large then over time the TT state can lose spin-coherence and diffuse into two independent triplet exciton states, usually on two different molecules. This process is also spin allowed, since the two spins of the free triplets also add up to zero, but may, over time, lose spin coherence.

$$S_0 + S_1 \rightleftharpoons (TT) \rightleftharpoons T_1 + T_1 \tag{1.1}$$

The two free triplet excitons can then diffuse in the organic semiconductor and have to be transferred into another semiconductor or disassociated into free electrons and holes.

We can also monitor the density of singlet excitons over time and will find that the quenching of the singlet state, and with it the photoluminescence is related to the singlet fission efficiency. Certain singlet fission materials like tetracene also allow for the backwards process, where two triplets recombine to form a singlet exciton which can then decay radiatively, called triplet-triplet annihilation (TTA). We can detect TTA as delayed photoluminescence. This delayed photoluminescence can be used to monitor the triplet population, and any quenching or transfer mechanisms will be visible as a reduced delayed photoluminescence intensity.

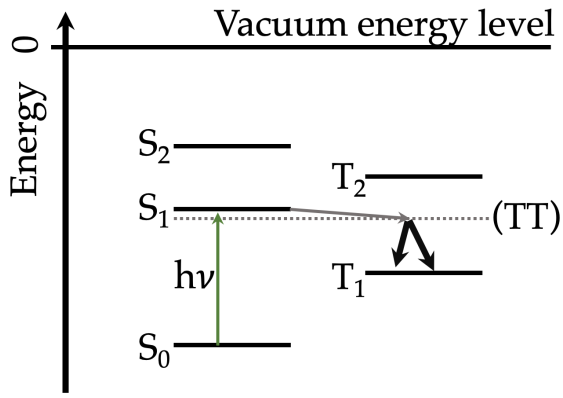


**Figure 1.6:** States involved in the singlet fission process, as described in Equation 1.1

**SINGLET FISSION SOLAR CELLS** The main unresolved problem in the realization of the singlet fission solar cell is about how the energy of the triplet excitons can be used to generate electricity.

Since the triplet exciton is a dark state, singlet fission cannot be used as a spectral downshifting layer that converts blue to red light. However, triplet excitons can be transferred into inorganic quantum dots like PbS which can emit light of the energy of the triplet excitons [21]. The quantum dots used for this purpose consist of heavy atoms that provide a large spin-orbit coupling, leading to spin mixing so the spin quantum number is no longer a good quantum number. Quantum dot emission and absorption can be tuned by changing their size, which is on the order of few nanometers, by exploiting the quantum confinement effect. Tuning the energy to accept the triplet excitons of many different singlet fission materials makes quantum dots very versatile.

Another example for the successful application of a singlet fission solar cell is the disassociation of triplet excitons in pentacene at a PbS quantum dot interface [28].

Attempts at disassociating the triplet exciton at disassociating the triplet exciton with an electron accepting layer of $C_{60}$ fullerenes have also been reported and may also be viable, if the efficiencies are increased [76].

The most elegant solution would be the direct transfer of triplet excitons into a bulk semiconductor like silicon, which has recently been shown to occur when deploying a thin $HfO_xN_y$ interlayer between tetracene and silicon [29].

**UPCONVERSION SYSTEMS** The reverse process of singlet fission, triplet-triplet annihilation, should also be mentioned as it is a closely related process that can offer insights and tools useful for singlet fission solar cells. The upconversion layer absorbs low-energy photons, generates triplets via intersystem crossing and their energy is then transferred into an annihilator where two triplet excitons are combined to emit a high energy photon towards a solar cell [36], or in biological tissue to activate medicine with blue light [106].

Recently, direct transfer of a triplet exciton has been reported between a lead-halide perovskite and rubrene [86] which is relevant for singlet fission solar cells as it is the inverse process and shows that transfer of a band-like semiconductor excitation into a triplet state of an organic semiconductor is possible.

## 1.5 RESEARCH QUESTIONS AND OUTLINE

The main goal of this work was to realize a singlet fission solar cell by facilitating and investigating the transfer of triplet excitons at a semiconductor interface.

How can we transfer triplet excitons over longer distances if they are dark states? Is it possible to exploit FRET transfer from quantum dots to silicon for that purpose and achieve high transfer efficiencies?

We investigate the FRET efficiency from quantum dots into silicon in Chapter 2.

Since there are many different triplet transfer processes available, what are the challenges of realizing each of them, and if efficient triplet transfer is achieved, what is the effect of the transfer mechanism on the singlet fission-silicon solar cell efficiency? Can we, and should we search for different singlet fission materials with different singlet exciton energies?
We calculate the solar cell efficiencies for three transfer schemes in Chapter 3

If transfer of triplet excitons is the goal, can we use optical measurements to detect it, rather than building a complete solar cell? What are the limits of detection for triplet exciton transfer and how can we eliminate other influences of sample to sample variation and other quenching pathways to isolate the signal of triplet transfer?
We describe a new method of combining optical and height measurements of tetracene islands on silicon samples to detect triplet quenching in Chapter 4.

What kind of interlayer between tetracene and silicon can enable the transfer of triplet excitons, and what influence does the orientation of the triplet molecules have on transfer efficiency? How can we be sure to detect triplet transfer, and can we quantify the transfer efficiency?
We show a solar cell with triplet transfer in Chapter 5 and quantify the triplet transfer efficiency using a singlet fission model to describe delayed photoluminescence decay data.

# 2 ENHANCING SILICON SOLAR CELLS WITH SINGLET FISSION: THE CASE FOR FÖRSTER RESONANT ENERGY TRANSFER USING A QUANTUM DOT INTERMEDIATE

This chapter is based on the following publication [126]:

Stefan Wil Tabernig*, Benjamin Daiber*, Tianyi Wang and Bruno Ehrler "Enhancing silicon solar cells with singlet fission: the case for Förster resonant energy transfer using a quantum dot intermediate" In: *Journal of Photonics for Energy* 8.02 (2018)

One way for solar cell efficiencies to overcome the Shockley–Queisser limit is downconversion of high-energy photons using singlet fission (SF) in polyacenes like tetracene (Tc). SF enables generation of multiple excitons per high-energy photon, which can be harvested in combination with Si. In this work, we investigate the use of lead sulfide quantum dots (PbS QDs) with a band gap close to Si as an interlayer that allows Förster resonant energy transfer (FRET) from Tc to Si, a process that would be spin-forbidden without the intermediate QD step. We investigate how the conventional FRET model, most commonly applied to the description of molecular interactions, can be modified to describe the geometry of QDs between Tc and Si and how the distance between QD and Si, and the QD bandgap affects the FRET efficiency. By extending the acceptor

dipole in the FRET model to a 2-D plane, and to the bulk, we see a relaxation of the distance dependence of transfer. Our results indicate that FRET efficiencies from PbS QDs to Si well above 50 % are possible at very short but possibly realistic distances of around 1 nm, even for QDs with relatively low photoluminescence quantum yield.

## 2.1 INTRODUCTION

The domination of the solar cell market by silicon led to the search of add-ons that could increase efficiency while also maintaining low cost. One possible way to increase efficiency is by downconverting high-energy light using an organic material that exhibits singlet fission (SF).

In a single-junction solar cell, photons with energy above the bandgap can excite an electron into the conduction band. Excess energy is lost, as the charge carriers quickly thermalize to the band edge. Downconversion schemes minimize the energy lost by thermalization, by converting high-energy photons to lower-energy charge carriers. Downconversion via SF can improve on the single-junction Shockley–Queisser [22, 115] efficiency limit, raising it from 33.7 % to 44.4 % [47].

SF in organic semiconductors describes the conversion of a singlet exciton into two triplet excitons, conserving spin. In tetracene (Tc), SF is faster (90 ps) [141] than other decay channels, which leads to a yield of almost two triplet excitons per absorbed photon. The resulting triplet excitons cannot relax radiatively to the singlet ground state, as this process is spin-forbidden, leading to a long triplet lifetime. In Tc, the energy of the triplet excitons (1.25 eV) [131] is close to the bandgap of silicon (1.12 eV), allowing in principle for the triplet excitons to be injected into silicon (Si). In one possible realization, the triplet exciton energy is first transferred into a lead sulphide (PbS) quantum dot (QD) [129] interlayer and subsequently transferred into Si [104, 146] (see Figure 2.1). Once the triplet exciton is in the QD, the presence of lead with strong spin-orbit coupling leads to intersystem crossing of singlet and triplet states. The spin triplet and singlet excitons are energy degenerate ($\sim 3$ meV) [57], which leads

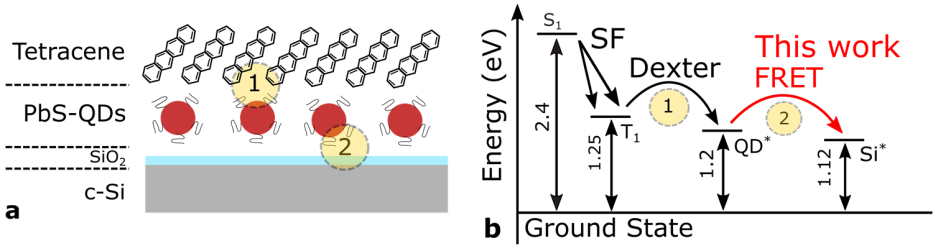


**Figure 2.1:** (a) Illustration of the SF-FRET geometry. A Tc-layer lies on top of the PbS-QD (+ ligands) monolayer, which is on top of c-Si. The two yellow circles indicate the two energy transfer steps, namely Tc→QD (1) and QD→Si (2). (b) The Jablonski diagram, with the FRET process between QDs and Si highlighted in red. $S_1$ and $T_1$ correspond to the first excited singlet and triplet state in Tc, respectively. The excited states of the QD and Si are indicated by QD* and Si*

to efficient spin mixing. Hence, the exciton can decay radiatively, in principle allowing for energy transfer into Si via photon emission or Förster resonant energy transfer (FRET). Transfer into lead sulfide [129] and lead selenide [125] QDs was recently demonstrated with high efficiency ($> 90\,\%$) [129]. While energy transfer from core/shell CdSe/ZnS QDs into c-Si [146] as well as inter-QD FRET for cases, where energy was transferred among the same QD species [15, 16, 75] and between two different QD species [15, 138], has been demonstrated, energy transfer from PbS QDs into Si with a QD bandgap close to the one of c-Si remains to be shown.

One of the processes competing with FRET is the emission of photons by the QDs and the reabsorption in Si. For that process to be efficient, careful light management to funnel photons into silicon is required. In addition, the low external quantum efficiency of the Si cell near the

indirect band edge might somewhat limit the achievable efficiency. Direct energy transfer in the form of FRET would be an elegant solution to allow for higher efficiency, as FRET can outcompete radiative energy transfer at distances smaller than the system-specific Förster distance $R_0$, which is around 8 nm in the case of FRET between PbS QDs [16, 70]. Once the exciton resides in Si it will contribute to charge generation, as the extraction efficiency of state-of-the-art Si solar cells is close to unity. Thus, the SF-FRET geometry could lead to additional current in Si solar cells, if short distances between the donor and acceptor can be achieved.

Apart from radiative energy transfer or FRET, other transfer mechanisms are also possible in the Tc-QD-Si geometry. The triplets from Tc could be transferred directly into silicon, bypassing the QDs. This would happen via the Dexter energy transfer mechanism [24, 104], which proceeds *via* correlated two-electron transfer. In this case, the excited electron of the triplet exciton would be transferred into the excited state in Si, while a ground-state electron from Si transfers into the Tc HOMO. Dexter energy transfer could also act as a transfer channel from the PbS QDs into Si. However, the Dexter transfer efficiency falls exponentially with distance from donor to acceptor due to the required wave function overlap. Thus, Dexter energy transfer is only relevant for short distances $< 1$ nm. The QD ligands already contribute to a $\sim 1$ nm separation between donor and acceptor. Hence, the overall contribution of Dexter energy transfer will presumably be negligible compared to FRET, which has a weaker distance dependency.

Sequential charge transfer from Tc or the PbS QDs to Si is another possible pathway for exciton dissociation, meaning that the electron would be transferred into Si and a hole would transfer from Si into Tc (or vice versa). This mechanism would require sandwiching the active layer between electrodes and is hence undesirable compared to the FRET or Dexter mechanisms.

Here, we establish the theoretical requirements for FRET between PbS QDs and Si, considering the QD bandgap, the distance between Si and QDs, and the geometry of the interface. We find that FRET can be 80 % efficient when the QDs are within 2.5 nm to the surface of Si, even for QDs with a bandgap close to the Si bandgap. This is a much shorter distance

compared to inter-QD FRET or organic molecules, mostly because the molar absorption coefficient of Si is very low near the band edge. We further find that the distance dependence is somewhat relaxed when considering the Si surface as a plane or bulk acceptor. Finally, we lay out the path to prepare the Si surface to allow for efficient FRET from Tc into Si. Once efficient transfer of energy between QDs and Si can be achieved experimentally, SF could provide a direct path toward more efficient Si solar cells with minimal need for changes of the Si cell geometry.

## 2.2 FÖRSTER RESONANT ENERGY TRANSFER

The FRET efficiency of excitons from QDs into Si, $\eta_{FRET}$, is defined in Equation 2.1. The main goal of this work is to determine how $\eta_{FRET}$ depends on donor–acceptor distance, on the bandgap of the QDs, and on the geometry of the system. The FRET efficiency $\eta_{FRET}$ compares the FRET rate $k_{FRET}$ to all the competing rates, defined as the exciton decay rate of the QD donor in absence of the silicon acceptor $k_{D,0}$ [77]:

$$\eta_{FRET} = \frac{k_{FRET}}{k_{D,0} + k_{FRET}} \tag{2.1}$$

where $k_{D,0} = 1/\tau_{D,0}$ and $\tau_{D,0}$ represents the donor exciton lifetime in absence of an acceptor.

FRET is a distance-dependent energy transfer mechanism between two molecules, which are approximated to be point dipoles. Förster derived an expression for the FRET rate [32], which depends on the emission spectrum of the donor, absorption spectrum of the acceptor, donor lifetime, and donor-acceptor distance. The classical as well as quantum mechanical approach both lead to Equation 2.2 [32, 77]:

$$k_{FRET}(R_{DA}) = \frac{1}{\tau_{D,0}} \left( \frac{R_0}{R_{DA}} \right)^6 \tag{2.2}$$

where $R_{DA}$ represents the distance between donor and acceptor and $R_0$ is the Förster distance. $R_0$ determines how strongly the FRET rate depends on the distance and is given by Equation 2.3 [77]:

$$R_0^6 = \frac{9000}{128\pi^5 N_A} \times \frac{Q_D \kappa^2 J}{n^4} \tag{2.3}$$

In Equation 2.3, the prefactor summarizes several numerical constants and Avogadro's number $N_A$. $Q_D$ is the donor photoluminescence quantum yield (PLQY), $\kappa^2$ is a parameter that depends on the relative orientation between donor and acceptor dipole, and $n$ represents the refractive index of the medium separating donor and acceptor. The parameter $J$ is commonly referred to as spectral overlap integral as it represents the spectral matching of the donor emission and acceptor absorption spectra and is calculated as follows in Equation 2.4 [77]:

$$J = \int_0^\infty \overline{f_D}\,(\lambda)\, \alpha_{M,A}\,(\lambda)\, \lambda^4 \, d\lambda \tag{2.4}$$

The overlap integral contains the normalized emission spectrum of the donor $\overline{f_D}\,(\lambda)$and the molar absorption coefficient of the acceptor $\alpha_{M,A}\,(\lambda)$, integrated over the wavelength $\lambda$ [gray area in Figure 2.2]. We can use the far-field absorption coefficient of silicon for the near-field (Förster) coupling, because FRET has been measured to also be phonon assisted [146].

Figure 2.2 depicts $\alpha_{M,Si}$ and $\overline{f_D}$ as a function of energy. The FWHM assumed for the QD PL is 200 meV, in agreement with literature [71, 81, 110]. The refractive index of the separating medium depends on how one accounts for the contributions of the dielectric functions of the QD itself, the surrounding ligand, and the spacer material. Following Yeltik et al. [146], we consider the average of refractive indices in a straight line from QD to the silicon surface. We approximate the refractive index as constant for different spacer thicknesses. As such, $n_{SiO_2} = 1.45$ is used,

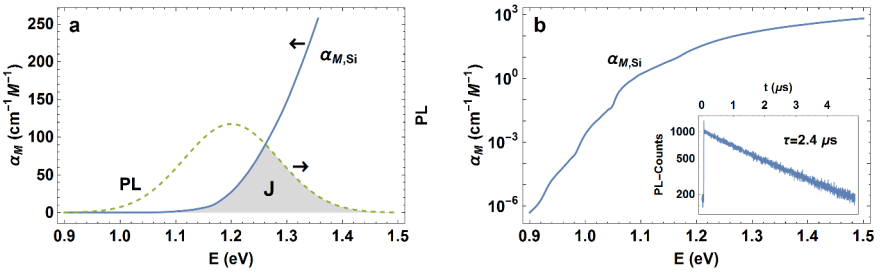


**Figure 2.2:** (a) $\alpha_{M,Si}$ and PL of 1.2 eV PbS QDs as a function of photon energy. The gray shaded area indicates the spectral overlap between the QD donor and the Si acceptor (J). $\alpha_{M,Si}$was taken from Green and Keevers[42] and the PL spectrum was modeled as a Gaussian centered at 1.2 eV with a FWHM of 200 meV, which corresponds to a broadening of $\sigma = 84$ meV. The PL has arb. units. (b) Molar absorption coefficient of silicon $\alpha_{M,Si}$ as a function of photon energy. The inset shows the measured transient PL lifetime for 1.2 eV PbS QDs in solution.

which is the index of the $SiO_2$ spacer layer in between the QDs and the Si bulk. In fact, the QDs and the ligands will also influence the overall refractive index, as the light will be influenced by an effective medium given that the wavelength of emission is much larger than the distances involved in our system. The refractive index of the QDs is well above 1.45, and the refractive index of the organic ligands is between 1.45 for oleic acid (OA)[18] and 1.5 (3-mercatopropyonic acid)[78] for most organic ligands. Inorganic ligands like $ZnI_2$ are very short so we can neglect their influence on the electromagnetic field. However, since the ligands do not fill the entire volume [81], we deem the approximation of $n = 1.45$ valid for distances larger than 1 nm. The orientation parameter $\kappa^2$ depends on the relative transition dipole orientation of donor and acceptor [77]. Since the QDs have rotational symmetry, the dipole orientation in the QDs will be isotropic, which yields $\kappa^2_{iso} = 23.17$. The quantum yield of PbS-QDs depends on various factors, including size [82], excitation wavelength [39], QD concentration [39], ligands [114], and whether they are in solution or in solid state. The choice of QD size is important because

the corresponding bandgap has to be lower than the Tc triplet exciton energy and higher than the Si bandgap, to ensure that both transfer processes are downhill in energy. We choose QDs with emission centered at 1.2 eV, which corresponds to an average size of 3.4 nm [82]. The PLQY for these QDs ranges from 20 % to 55 % [39] in solution and up to 15 % in films [1]. We determined the radiative lifetime of our 1.2 eV PbS QDs (see Appendix for details on QD synthesis and PL lifetime measurement) in octane as $\tau_{PbS} = 2.4\,\mu s$ (inset Figure 2.2(b)), which is in good agreement with literature [16, 71, 82]. For a more accurate description of the FRET rate, the measured lifetime of the QDs in solution should be replaced by the QD lifetime measured after deposition on quartz, to obtain the reference value for "infinite" donor–acceptor separation $\tau_{D,0}$.

We exclude the effects of parasitic absorption in the QD layer because we assume a submonolayer QD coverage. To be specific, the ideal QD coverage to maximize transfer and minimize QD-absorption would be a submonolayer coverage, where the inter-QD spacing is far bigger than the inter-QD Förster radius of 8 nm [16, 70]. Making this assumption allows us to neglect any significant contributions of inter-QD FRET. Inter-QD FRET should be regarded as an undesirable decay channel because screening more QDs increases the chance to find a surface trap state, and there will be a tendency to transfer toward lower energy QDs. The upper limit for the QD spacing is determined by the Tc triplet diffusion length. In the final geometry, the QD coverage has to be dense enough to allow all Tc triplets to diffuse toward a QD, meaning that the ideal QD separation corresponds to the triplet diffusion length of around 400 nm [2, 133]. Such a QD coverage absorbs less than 0.01 % of the solar spectrum, and thus, we can neglect absorption of the incident light by QDs (see Appendix for details on this estimate).

In the following, we calculate $R_0$, which is the distance for that the transfer efficiency reaches 50 % in the dipole–dipole model. While this is not exactly the case for the plane and bulk geometries we will introduce later, $R_0$ is still a useful quantity to estimate separation distances. As can be seen in the upper plot of Figure 2.3, the values for $R_0$ vary from 0.9 nm to up to 1.5 nm, depending on the QY and bandgap of the QDs. The steep loss of transfer efficiency below the bandgap of silicon (around 1.12 eV)

can be attributed to the exponential decrease in the absorption coefficient. The largest QD bandgap for which energy transfer from triplet excitons in Tc was observed is 1.23 eV [129], and we indicate the QD bandgap range by the gray area in Figure 2.3. The bottom panel of the same figure shows the FRET efficiency, which obeys a relatively steep slope around 1.2 eV, compared to higher bandgaps, suggesting the importance of a careful choice of the QD bandgap. The bottom plot of Figure 2.3 shows FRET efficiencies for 1 nm and 2 nm separation distances, with varying QY. Changes in distance by only 1 nm around $R_0$ lead to an efficiency increase of up to 75 %. The efficiencies at 1 nm separation saturate for bandgaps slightly higher than required in the given geometry at values close to 100 %. It is worth noting that high FRET efficiencies ($> 65\,\%$) can be achieved at realistic distances (1 nm) even for a low QY (20 %).

## 2.3 INFLUENCE OF GEOMETRY

Up until now, we have calculated the FRET efficiencies according to a dipole–dipole model that does not take into account the extended nature of the silicon acceptor geometry. We introduce two potentially more accurate descriptions of the FRET rate in our system, in the following referred to as "dipole—infinite plane model" and "dipole—bulk model," similar to earlier approaches [75, 142]. Our final geometry will probably be best represented by the bulk model, and in the following, we show how it differs from the more conventionally used dipole–dipole description laid out above.

The silicon acceptor occupies one half-space instead of being a point-dipole, leading to a modification of Equation 2.2 [65, 120]. For the dipole-infinite plane model, the zero-dimensional dipole acceptor is substituted with a 2-D acceptor extended over the x-y plane, assuming that the acceptor dipole of FRET mainly resides on the surface of Si (see Equation 2.5):

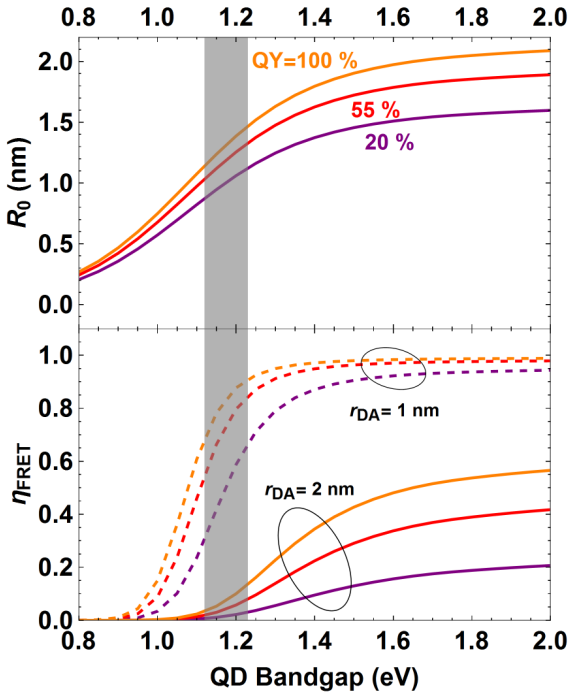


**Figure 2.3:** The upper graph shows the QD bandgap dependence of the Förster distance $R_0$ for different quantum yields. In the bottom figure, the FRET efficiency as function of QD bandgap is depicted. Dashed lines represent a donor–acceptor distance of 1 nm, solid lines correspond to 2 nmseparation. The colors correspond to the same QYs as in the upper figure. The gray shaded region in both plots indicates the bandgap range from 1.12 to 1.23 eV, which is the range relevant for the transfer from Tc into Si.

$$
\begin{aligned}
k_{FRET} &= \sigma_{Si} \int_0^{\infty} \int_0^{2\pi} \frac{r}{\left(R_{DA}\left(r_{DA}, r\right)\right)^6} dr d\phi \\
&= \sigma_{Si} \frac{R_0^6}{\tau_{D,0}} \int_0^{\infty} \int_0^{2\pi} \frac{r}{\left(\sqrt{r_{DA}^2 + r^2}\right)^6} dr d\phi \\
&= \sigma_{Si} \frac{R_0^6}{\tau_{D,0}} \times \frac{\pi}{2 r_{DA}^4}
\end{aligned}
\tag{2.5}
$$

where $R_{DA}\left(r_{DA}, r\right)$ is the distance from the donor dipole to an infinitesimal acceptor dipole, and $\sigma_{Si}$ is the density of silicon atoms on a <111> silicon surface ($\sigma_{Si} = 7.8\,nm^{-2}$). After integration over the Si surface (r is the radial component in polar/cylindrical coordinates), the rate only depends on the distance component perpendicular to the surface, thus on $r_{DA}$. The parameterizations used are illustrated in Figure 2.5(b).

While this model is closer to the physical reality, it only considers the Si surface. In order to include the Si bulk, we can integrate Equation 2.5 over the half space occupied by Si, which leads to Equation 2.6:

$$
\begin{aligned}
k_{FRET} &= \rho_{Si} \frac{\pi R_0^6}{2\tau_{D,0}} \int_0^{-\infty} \frac{1}{\left(z'\left(z, r_{DA}\right)\right)^4} dz \\
&= \rho_{Si} \frac{\pi R_0^6}{2\tau_{D,0}} \int_0^{-\infty} \frac{1}{\left(z\left(\frac{n_{Si}}{n}\right) + r_{DA}\right)^4} dz \\
&= \rho_{Si} \frac{\pi R_0^6}{\tau_{D,0}} \left(\frac{n}{n_{Si}}\right) \frac{1}{r_{DA}^3}
\end{aligned}
\tag{2.6}
$$

For the integration, $z'\left(z, r_{DA}\right)$ is split into the integration variable for the half space z and the distance from the donor to the surface of the bulk acceptor $r_{DA}$, and $\rho_{Si}$ is the density of silicon atoms ($\rho_{Si} = 50\,nm^{-3}$). The additional prefactor $n/n_{Si}$ arises because we have to consider the

refractive index of the part of bulk silicon between the infinitesimal acceptor and the QD donor as part of the separating medium. We use a refractive index of 3.55 for silicon $n_{Si}$, corresponding to the relevant energy region (1.2 eV) [42]. A derivation can be found in the Appendix. We note that the prefactor is independent of distance between donor and acceptor. Mathematically, this is due to the choice of integration limits and leads to an effective Förster distance $R_{0,eff} = \left(\frac{n_{SiO_2}}{n_{Si}}\right)^{\frac{1}{6}} R_0$.

Figure 2.4 shows the FRET efficiencies for both models introduced above. From comparison with the bottom panel of Figure 2.3, it becomes obvious that for 2 nm separation, the FRET efficiencies are improved considerably up to around 85 % for the dipole—infinite plane model in the relevant region compared to 15 % for the dipole—dipole model, whereas the values for 1 nm do not change significantly. This occurs due to the different distance dependencies in different models and acceptor dipole densities ($\rho_{Si}$and $\sigma_{Si}$) in different models, as shown in Figure 2.5. Figure 2.5 shows that the point model has the steepest distance dependency, which is relaxed in the planar geometry, and the efficiency drop with distance in the bulk model is the most shallow. The efficiency is unity for small separations $r_{da}$ for all models and drops to almost zero at 2 nm for the point model, 8 nm for the plane model, and is nonzero even for separations exceeding 10 nm for the bulk model.

Usually the characteristic length for FRET, the distance at which the transfer efficiency is 50 %, is in the order of 10 nm (QD-QD FRET of 8 nm [16, 70]) which is considerably longer than in the case of QD-silicon energy transfer which we discuss in this paper. However, the FRET distance becomes larger going from point (1.8 nm) to plane (2.8 nm) to bulk (3.5 nm) model. The slope is mainly determined by the distance dependence of the FRET rate (Equation 2.1) which changes from $r^{-6}$ (point model) to $r^{-4}$ (plane model) to $r^{-3}$ (bulk model). The absolute efficiencies going from point to plane to bulk model are larger because the FRET rate is dominant compared to base rate $k_{D,0}$ (Equation 2.1). The underlying reason for the larger efficiencies is that there are more acceptors available in bulk ($\rho_{si}$) compared to plane ($\sigma_{Si}$) and point (one acceptor) models.

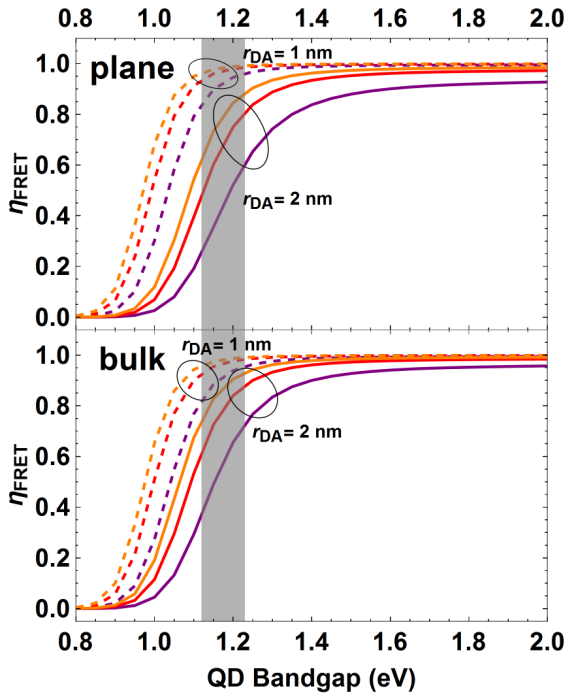


**Figure 2.4:** FRET efficiencies for the "dipole-infinite plane model" (top) and the "dipole-bulk model" (bottom). Dashed and continuous lines represent 1 nm and 2 nm separation, respectively. The gray shaded region indicates the bandgap range of interest. The colors correspond to the same QY values as in Figure 2.3.

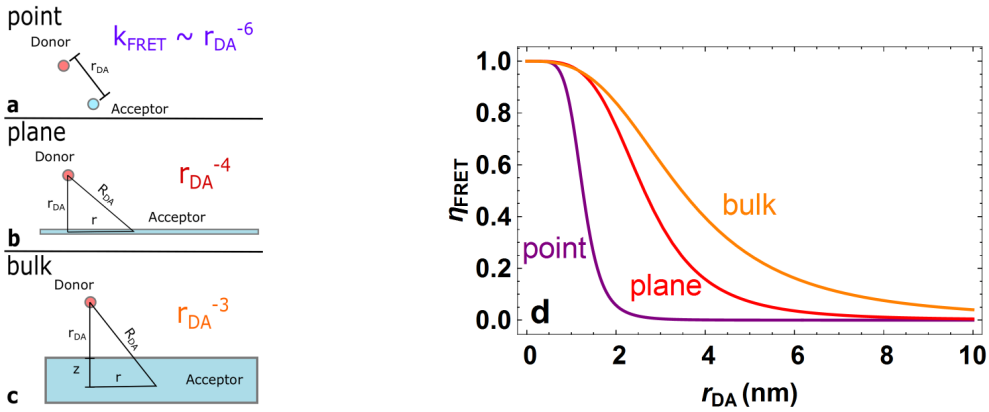


**Figure 2.5:** The three pictures on the left show the three different models ((a) dipole–dipole, (b) dipole–infinite plane, (c) dipole–bulk) and the corresponding donor acceptor distance dependencies obtained by starting from Equation 2.2 and integrating over a distance, surface, or space. The colors indicate which lines in (d) the dependencies correspond to. (d) The graph shows the FRET efficiency for those three models at distances in the order of $R_0$. The QD bandgap is 1.2 eV and the QD QY is 55 %, corresponding to $R_0 = 1.26$ nm.

With increasing distance, first dipole-plane and then dipole-bulk interactions become relatively stronger as they take into account more area/volume. Which model most accurately describes the distance dependence in our QD-silicon geometry? While the bulk-model represents the geometry more accurately, one could argue that due to the strong distance dependence of FRET, the majority of the interaction occurs already at the surface, so the plane-model might be valid after all. However, the spatial extend of the Bloch waves in silicon will ultimately govern the transition geometry.

We note that the mathematical treatment shown here does not take into account that part of the electromagnetic field is reflected by silicon, which leads to a reduced donor lifetime for small distances according to CPS theory [14]. Furthermore, the exciton in the QD could be more accurately described as an extended dipole. The point-dipole approximation is no longer valid if the distance between donor and acceptor is on the order of the exciton (QD) size. If the separation between electron and hole (1.8 nm for PbS QDs [39]) is taken into account, the near field will no longer be accurately described by the $r^{-3}$ dependence used in the FRET derivation. The final step would be the addition of a quantitative description of Dexter transfer [24], which is a possibly competing charge-mediated energy transfer. Dexter transfer has an exponential distance dependence, which leads to transfer distances of around 1 nm but it does not depend on the absolute molar absorption coefficient of silicon (only on the spectral shape), which could make Dexter rates comparable with FRET rates in this case.

A factor that greatly affects $k_{FRET}$ is the overlap between QD emission and Si absorption spectra. The QD absorption energy must be lower than the Tc triplet exciton energy and the emitted energy of the QD must be above the Si bandgap. The broadening of the QD emission spectrum leads to additional losses when the emission spectrum broadens beyond the given limits. Sharper QD emission spectra could be achieved with a QD ensemble with sharper size distribution [51]. Apart from that, the Stokes shift might influence the choice of QD size strongly. We now assumed emission at 1.2 eV, which means that the absorption of the QDs would occur at a higher energy. However, the absorption is limited by the fact

that Tc triplet states impose an upper boundary for the QD bandgap of around 1.25 eV.

## 2.4 CONCLUSION

In conclusion, we showed that FRET from PbS QDs to silicon is possible with sufficiently high FRET efficiencies, even for QDs that have a bandgap close to silicon and low PLQY. While efficient FRET is only possible over small separation distances in the order of a few nanometers, those distances are physically feasible, given careful engineering of the interface.

It is of great importance that the emission and absorption peak of the QDs are between the Tc triplet exciton energy and the bandgap of Si, with a narrow emission spectrum. Hence, to obtain high FRET efficiency for using SF to improve silicon solar cells, a narrow size distribution of adequate QDs leading to a narrow PL peak and to fine tuning of the bandgap and emission yield of the QDs is necessary. Additionally, the silicon surface needs to be passivated electrically and against oxidation with a very thin (sub-nm) layer. Such layers can be achieved with thin metal oxides [111] or self-assembled monolayers of organic molecules [9]. In case of the organic molecules, they could also act as covalent linkers and passivating ligands for the QDs.

## 2.5 APPENDIX

### QD Synthesis and Passivation

The colloidal PbS QDs were synthesized via the hot injection method [49]. In order to obtain the 1.2 eV QDs we measured, we used a previous recipe [8]. Most chemicals were purchased from Sigma-Aldrich. For those that were not, the distributor will be indicated. The octadecene is degassed heating to 80 °C. A 20 ml syringe is filled with 0.213 ml

of bis(trimethylsilyl)sulphide (synthesis grade) together with 10 mL of octadecene (technical grade 90%) in a glove box ($< 0.5\,\mathrm{ppm}\,H_2O$; $< 0.5\,\mathrm{ppm}\,O_2$) environment. 0.45 g of PbO (99.999 %, Alpha Aesar), 1.34 g of OA (technical grade 90%), and 14.2 g of octadecene are mixed together in a three-necked Schlenk flask. At a temperature of 95 °C and under vacuum, this forms a clear solution. Then, the temperature is increased to around 170 °C in a nitrogen environment. Now, the Schlenk flask containing the lead precursor is transferred to a heating mantle, which is at room temperature. As soon as the temperature has reached the injection temperature of 150 °C (for 1.2 eV QDs), the sulphur precursor is injected into the flask with the solution being vigorously stirred. When the solution has cooled down to 35 °C, 20 mL of acetone are added.

For surface passivation with $I_2$, we follow Lan et al. [66]. After the completed synthesis, the QDs are precipitated with acetone in a glovebox. After centrifuging for 4 to 10 min at 4000 to 5000 rpm, the residual liquid is disposed of, which is followed by vacuum-drying of the precipitate overnight. The QDs are then redispersed in toluene ($\geqslant$ 99.9 %) to obtain a concentration of 150 $\mathrm{mg/ml}$. Now, a 25 mM iodine (99.999 %) in toluene solution is added to the QD solution at a 1:5 ratio and stirred for 24 h. Afterwards, the QDs are precipitated with methanol and centrifuged at 1500 to 5000 rpm for 2 to 5 min. The residual fluid is disposed of, and after a night of vacuum-drying, the QDs are dispersed in octane to obtain a 37.5 $\mathrm{mg/ml}$ solution.

This solution is then diluted with octane to obtain a 4.4 $\mathrm{mg/ml}$ solution, which was used in the lifetime measurements.

### PL Lifetime Measurement

The photoluminescence decay of the 1.2 eV bandgap PbS QD was measured in a home-built time-correlated single-photon counting (TCSPC) system consisting of a 640 nm pulsed laser (PicoQuant LDH-D-C-640) with a repetition rate of 0.2 MHz as an excitation source controlled by a PicoQuant PDL 828 "Sepia II". The signal was collected by a single-photon avalanche diode (SPAD) detector (Micro Photon Devices, MPD-5CTD)

connected to a PicoQuant HydraHarp 400 multichannel picosecond event timer. The laser has a power of 14.6 $\mu W$ at the used repetition rate. The laser light was filtered out of the collection path by a Chroma ZET 642-nf notch filter and a Chroma ET 655lp long-pass filter. The TCSPC decays were collected for 5 min.

### Introduction of Bulk Silicon as Additional Separating Medium in the Dipole—Bulk Model

The distance between the QD donor and the infinitesimal dipole acceptor located at an arbitrary spot somewhere in the silicon bulk can be described as $r_{DA} + z = z\prime$. Here, $z\prime$ is the total separation distance and $r_{DA}$ and $z$ are the parts in the $SiO_2$ medium and in silicon, respectively. For simplicity, we now calculate the case for $z\prime$ perpendicular to the silicon surface (Figure 2.6), but the following derivation holds for any angle between the donor–acceptor connection line and the silicon surface.

The total refractive index $n_{tot}$ can be calculated from the effective medium approximation, where $n_{tot}$ is the weighted sum of the two individual indices, for $SiO_2$, $n_{SiO_2}$ and silicon $n_{Si}$:

$$n_{tot}\,(r_{DA} + z) = n_{SiO_2} \times r_{DA} + n_{Si} \times z$$

Solving for $n_{tot}$ leads to

$$n_{tot} = \frac{n_{SiO_2} \times r_{DA} + n_{Si} \times z}{r_{DA} + z} = n_{SiO_2} \left( \frac{r_{DA} + \frac{n_{Si}}{n_{SiO_2}} z}{r_{DA} + z} \right)$$

$$R_0'^6 = \frac{9000 \ln(10)}{128 \pi^5 N_{AV}} \times \frac{Q_D \kappa^2 J}{n_{tot}^4}$$

The obtained expression has to be substituted into a new Förster distance, $R\prime_0$, following Equation 2.3:

$$
\begin{aligned}
R_0'^6 &= \frac{9000\ln(10)}{128\pi^5 N_{AV}} \times \frac{Q_D \kappa^2 J}{n_{tot}^4} \\
&= \frac{9000\ln(10)}{128\pi^5 N_{AV}} \times \frac{Q_D \kappa^2 J}{n_{SiO_2}^4} \left( \frac{r_{DA} + \frac{n_{Si}}{n_{SiO_2}} z}{r_{DA} + z} \right)^{-4} \\
&= R_0^6 \left( \frac{r_{DA} + z}{r_{DA} + \frac{n_{Si}}{n_{SiO_2}} z} \right)^4
\end{aligned}
$$

where $R_0$ is the ordinary Förster distance for $SiO_2$ as separating medium. This can now be substituted into the equation for the FRET rate, which we obtained after integration over the surface:

$$
\begin{aligned}
k_{FRET} &= \frac{\pi}{2} \int_0^\infty \frac{R_0'^6}{(r_{DA} + z)^4} dz \\
&= \frac{\pi}{2} R_0^6 \int_0^\infty \frac{1}{(r_{DA} + z)^4} \left( \frac{r_{DA} + z}{r_{DA} + \frac{n_{Si}}{n_{SiO_2}} z} \right)^4 dz \\
&= \frac{\pi}{2} R_0^6 \int_0^\infty \frac{1}{\left( r_{DA} + \frac{n_{Si}}{n_{SiO_2}} z \right)^4} dz \\
&= \frac{\pi}{2} R_0^6 \frac{n_{SiO_2}}{n_{Si}} \int_0^\infty \frac{1}{u^4} du \\
&= -\frac{\pi}{6} R_0^6 \frac{n_{SiO_2}}{n_{Si}} \left( 0 - \frac{1}{r_{DA}^3} \right) \\
&= \frac{\pi}{6} R_0^6 \left( \frac{n_{SiO_2}}{n_{Si}} \right) \frac{1}{r_{DA}^3}
\end{aligned}
$$

The equations above show the derivation of the $n/n_{Si}$ prefactor in Equation 2.6 of the main text. For the integration, substitution of variables was used with $u = r_{DA} + \frac{n_{Si}}{n} z$.

### Estimate of the Fraction of Light That is Absorbed by the PbS QD Layer

As a conservative estimate, we assume that the QDs are separated by 50 nm on a square lattice, which is well below the triplet diffusion length [2, 133]. This means that one QD occupies an area of 50 nm × 50 nm. The QDs are approximated as spheres with a radius of 1.75 nm, which corresponds to a bandgap of 1.2 eV. The volume of the QDs was calculated and divided by the area occupied by one QD, which gives an effective QD layer thickness across the whole geometry of $d_{QD,eff} = 9 \times 10^{-3}$ nm. With this effective layer thickness, we estimated the relative absorption of incident light by the QDs by using the Beer–Lambert law, as shown in Equation 2.7:

$$I_{QD}(\lambda) = I_0(\lambda) \times \exp\left(-\alpha_{QD}(\lambda)\, d_{QD,eff}\right) \tag{2.7}$$

Here, $I_{QD}(\lambda)$ stands for the intensity of light behind the QD layer. $I_0(\lambda)$ is the incident light intensity for which we used the AM1.5 solar spectrum [52]. $\alpha_{QD}(\lambda)$ denotes the wavelength-dependent absorption coefficient of PbS QDs [48]. The relative intensity loss due to the QDs can then be calculated, as shown in Equation 2.8, with the integrals going over the whole wavelength range:

$$\Delta I_{rel} = \frac{\int \left(I_0(\lambda) - I_{QD}(\lambda)\right) d\lambda}{\int I_0(\lambda)\, d\lambda} \tag{2.8}$$

This leads to a relative intensity loss of $\Delta I_{rel} = 0.006\%$, which confirms our assumption that QD absorption is negligible in our geometry.

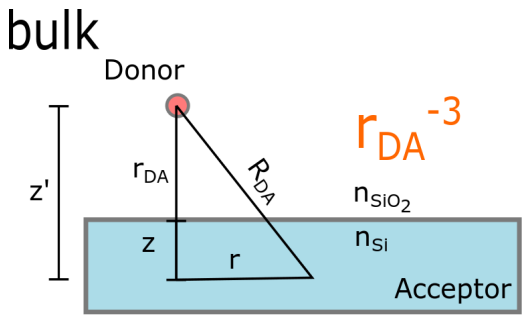


**Figure 2.6:** Illustration of the geometry for the bulk integration of kFRET.

# 3 REALISTIC EFFICIENCY LIMITS FOR SINGLET FISSION SILICON SOLAR CELLS

This chapter is based on the following publication:

Benjamin Daiber, Koen van der Hoven, Moritz H. Futscher, and Bruno Ehrler, "Realistic Efficiency Limits for Singlet Fission Silicon Solar Cells", *in Preparation* (2020)

Singlet fission is a carrier multiplication mechanism that could make silicon solar cells much more efficient. We calculated the efficiency potential of three technologically relevant singlet fission-silicon solar cell implementations. We assume realistic but optimistic parameters for a singlet fission material and we investigate the effect of singlet energy and entropic gain as well as relevant loss mechanisms. If the transfer of triplet excitons occurs via charge transfer, where the triplet exciton is dissociated at the interface, the maximum efficiency is 34.6 % at a singlet energy of 1.85 eV. The viable range of singlet fission materials is large, many materials with singlet energies from 1.3 eV to 3 eV can improve on the silicon solar cell efficiency. For the Dexter-type triplet energy transfer the maximum efficiency is 32.9 % with an optimal singlet energy of 2.15 eV, enhancing the silicon efficiency is only possible with singlet fission materials that have triplet energies larger than the silicon band gap. For Förster Resonant Energy Transfer (FRET), the triplet excitons are first transferred into an emitter, e.g. a quantum dot, which can then undergo FRET into silicon. For this transfer route the maximum efficiency is 28.7 %

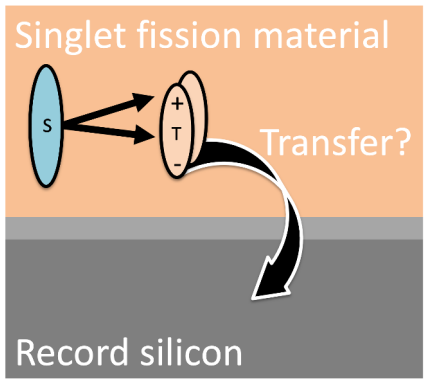


**Figure 3.1:** Schematics of the simulated singlet fission and transfer process.

at 2.33 eV which is lower than the previous two because of additional parasitic absorption and transfer losses into the quantum dots. We show that the efficiency gain from singlet fission is larger the more efficient the silicon base cell is, which stands in contrast to tandem perovskite-silicon solar cells.

## 3.1 INTRODUCTION

Solar cells are the most important cornerstone of transitioning the world's energy production from a fossil-based system to a $CO_2$ neutral future. The main solar cell technology in use today is based on silicon. Silicon solar cells have shown large improvements in efficiencies and cost, the technology is mature and highly optimized. However, the record efficiency of silicon solar cells has improved only slightly from ~ 24 % to 26.7 % in the past 20 years [87] because it gets harder and harder to improve the already highly optimized cell structure and material quality. Including Auger recombination in the thermodynamic detailed-balance limit of solar cell efficiency leads to a theoretical maximum efficiency of silicon solar cells of 29.4 % [130]. The efficiency of the record silicon solar

cell is 26.7 % [41], which is a remarkable 91 % of the theoretical maximum. New approaches are needed to improve the efficiency further. In this paper we calculate the realistic efficiency potential of singlet fission-silicon solar cells with three different geometries and transfer mechanisms, each with distinct advantages and challenges. These results can inform the practical application and search for new singlet fission materials.

Silicon has a fairly low bandgap energy (1.12 eV), above which photons are absorbed. A large fraction of the photons of the solar spectrum have a higher energy and will lose their excess energy to thermalization losses. These high-energy photons can be converted into electricity more efficiently if they are split into multiple photons or excitations with and energy above the silicon bandgap. If such downconversion can be applied to silicon, we can build on the vast knowledge of silicon solar cells without the need for large changes in silicon solar cell architecture.

Singlet fission is an example of a downconversion process that can potentially increase the efficiency of silicon solar cells by using the solar spectrum more efficiently. High-energy photons are absorbed in the singlet fission material and form a spin-0 singlet exciton. In certain organic materials like poly-acenes and perylene diimides (PDIs) this singlet exciton will split into two spin-triplet excitons of roughly half the energy of the singlet exciton [118]. For an efficient implementation, this singlet fission layer would be placed on top of a silicon solar cell, absorb all the high-energy light, convert each photon into two triplet excitons, and transfer their energy or charge into the silicon solar cell. The absorption-coefficients of organic materials are high at the energies of the molecular transitions [61]. Singlet fission can also be a very efficient process with efficiencies close to 200% in pentacene [140], meaning each singlet generates two triplet excitons. The main bottleneck for the singlet fission-sensitized silicon solar cells is the transfer of excitons from the absorber layer into silicon.

Here we simulate how efficient a singlet fission-silicon solar cell could be given realistic materials and device parameters. We find that the broadband absorption of typical singlet fission materials needs to be improved, for example by sensitization schemes. The most efficient implementation based on a record-efficiency silicon solar cell would be the charge transfer

from triplet excitons into silicon with the highest efficiency of 34.6 %. This efficiency maximum is reached at a surprisingly low singlet exciton energy of 1.85 eV with a realistic entropic gain of 100 meV. The simplest triplet transfer implementation, Dexter transfer, could also achieve high efficiency (32.9 %) but puts a stronger constraint on the singlet energy. FRET shows the lowest efficiency potential of 28.7 % because of additional loss channels. Finally, we compare the behavior to perovskite-silicon tandem solar cells and find that singlet fission shows the largest efficiency improvements for efficient silicon base cells, while tandem solar cells show a larger efficiency improvement for less efficient silicon base cells.

## 3.2 METHODS

We model the singlet fission-silicon solar cell by calculating the absorption and exciton generation in the singlet fission layer, the resulting triplet excitons are then transferred into a silicon solar cell model assuming three different transfer mechanisms. The injection of these additional charge carriers in the silicon solar cell changes the short circuit current, open circuit voltage and fill factor in a nontrivial manner, depending on the transfer mechanism. We therefore start with the description of a silicon solar cell current-voltage curve and then add the singlet fission current to the generated current in the silicon solar cell.

The silicon solar cell current-voltage curve is calculated with a diode master equation following previous work [33]. The radiative recombination current calculated with the absorbed photons that have to be equal to the emitted photons of a black body at room temperature, following the detailed-balance argument. The non-radiative recombination is modeled following De Vos et al. [23] and adjusted for the charge transfer case as described below. Shockley-Read-Hall (SRH) and Auger recombination are described with a diode equation with an ideality factor of 1 for SRH and $\frac{3}{2}$ for Auger recombination [130]. The SHR recombination prefactor is a fitting parameter for each solar cell. The Auger recombination is modeled using an Auger coefficient that is dependent on the temperature

and the intrinsic charge carrier density [130]. Unless otherwise stated we use the record 26.7 % interdigitated back contact silicon solar cell from Kaneka [41] as a base silicon cell.

The absorption in the singlet fission layer is modeled using the Lambert-Beer law. Upon absorption of a photon a singlet exciton is formed which can undergo the singlet fission process. Singlet fission takes place with a certain efficiency up to 200 % which is reached in pentacene [140]. We set this efficiency in our model to 190 %, to account for inefficiencies in different singlet fission materials. TIPS-Tetracene for example has a singlet fission efficiency of 180 % [121]. Each absorbed photon in our model leads to 1.9 triplet excitons at half the singlet exciton energy.

However, the energy of the triplet excitons is not necessarily half of the singlet exciton energy. In some materials like pentacene it is less than half the energy, while in others like tetracene two triplet excitons can actually carry more energy than the singlet exciton energy. This surprising observation seems to violate thermodynamics, since the two triplet excitons originate from one singlet exciton. The relevant measure here is the free energy that includes the enthalpy (which we commonly refer to as energy) but also an entropy term. This entropy term allows for the free energy to increase during a reaction (one singlet to two triplet excitons) if the gain in the number of states and therefore the entropy gain is significant. The gain in free energy from the entropy term can be up to 220 meV in PDIs (endoergic *and* efficient singlet fission [25]) and 200 meV in tetracene [62]. We therefore include an entropic gain of 100 meV during singlet fission in the realistic case and an entropic gain of 300 meV as an optimistic case. The entropic gain stems from the fact that the singlet state has a lower entropy than the two triplet excitons. The number of states that the delocalized singlet state can occupy is lower compared to the two localized triplets, who can reside on many different combinations of molecules, thus the number of states and entropy is larger. In tetracene this entropic gain is the driving force for singlet fission [62], and other materials could be engineered or selected for a high entropic gain by optimizing the singlet and triplet delocalization and crystal structure.

We consider three different schemes of harvesting the energy of the triplet excitons for the silicon solar cell. The transfer of charges from

triplet excitons into silicon, where the exciton is dissociated at the interface, the transfer of energy where the whole triplet energy is transferred into silicon, or the transfer of the triplet exciton energy into an intermediate emitter which then transfers the energy into silicon by FRET.

**CHARGE TRANSFER** Modeling charge transfer requires adjusting the recombination current if the triplet exciton energy is smaller than the silicon bandgap. This approach assumes that we can change the absolute energy position of the highest occupied molecular orbital (HOMO) and lowest unoccupied molecular orbital (LUMO) such that the LUMO aligns with the valence band of silicon. If $E_{Triplet} < E_{Silicon}$ the recombination current is higher and the recombination gap is smaller by the difference of the bandgap and triplet energy, as seen in equation 3.1, adjusted from the general recombination equation [23, 89].

$$J_{Rad0} = q\frac{2\pi}{c^2h^3}\int_{E_{Si}}^{\infty}\frac{E_n^2}{\exp\left(E_n-\left(E_{Si}-E_{Triplet}\right)\right)-1}dE_n \tag{3.1}$$

**DEXTER TRANSFER** The Dexter transfer model assumes that the energy transfer is possible if the triplet energy with entropy gains is larger than the silicon bandgap, assuming a perfect absolute energy alignment of the singlet fission material HOMO and LUMO and silicon valence and conduction band energy respectively. If the triplet energy is smaller than the silicon bandgap, then the transfer could still be thermally activated. Since the triplet excitons have a certain temperature and do not interact, we use the Maxwell-Boltzmann distribution in energy for an ideal gas for the probability density of triplet excitons:

$$f_E\left(E,T\right) = 2\sqrt{\frac{E}{\pi}}\left(\frac{1}{kT}\right)^{\frac{3}{2}}\exp\left(-\frac{E}{2kT}\right)$$

We then integrate over all energies above $\Delta E$, the difference of silicon bandgap and triplet energy. This gives us the probability of excitons that have enough energy to overcome $\Delta E$ due to the energy distribution at

room temperature. We normalize by the integral over all energies to get a probability. For all $\Delta E < 0$ the triplet energy is larger than silicon bandgap and the probability is 1, which also follows from the limit $\Delta E \to 0$.

$$P_{Dexter} = \frac{\int_{\Delta E}^{\infty} f_E\,(E, 300K)\,dE}{\int_{0}^{\infty} f_E\,(E, 300K)\,dE}$$

**FRET TRANSFER** FRET transfer is modeled by using a previously published model for FRET transfer efficiency from a quantum dot to a bulk silicon acceptor. The distance between donor (quantum dot) and acceptor (bulk silicon) is set to 1 nm. The quantum dot has an emission energy of the singlet fission triplet energy including entropy gains and a FWHM of 0.2 eV. This assumes that there is no Stokes shift. This is optimistic but since there is only a very dilute layer of quantum dots necessary and we assume that the quantum dots will be monodisperse, this which allows for a very small Stokes shift [136].

## 3.3 RESULTS

### 3.3.1 Absorption in the singlet fission material

The absorption of any downshifting material should be large so that the maximum number of incoming photons can be absorbed and undergo the downshifting mechanism to multiply carriers and increase the photocurrent. Singlet fission takes place in organic molecules with a relatively large singlet-triplet exciton energy splitting, thus with a large exchange energy. Often these molecules are conjugated molecules. The absorption of these organic molecules is considered to be strong because the absorption coefficient is relatively high compared to other semiconductors [61]. However, this is only the case at the absorption peaks at the specific energies of the pi-orbital transitions, leading to a narrow absorption spectrum if compared to the band-to-band absorption of most inorganic semiconductors. Since the solar spectrum is broadband and reaches from energies of ca. 0.3 eV (4000 nm) to 4 eV (310 nm), the fraction of absorbed

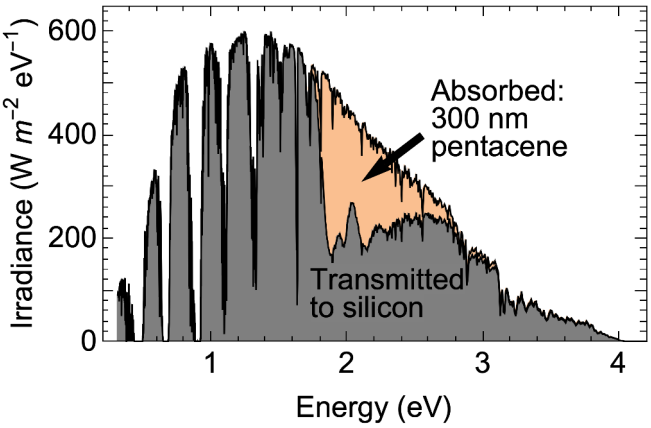


**Figure 3.2:** AM1.5 Spectrum split into the light absorbed in a 300 nm thick pentacene layer and light that is transmitted through the pentacene layer to the bottom silicon solar cell. Even a thick 300 nm pentacene layer only absorbs 32 % of the light with an energy above the singlet energy.

light of most singlet fission materials is very low. To illustrate this point we show the absorbed solar irradiance in a thin pentacene layer of 300 nm (Figure 3.2). Thicknesses below 300 nm are typical for films used in singlet fission solar cells [28, 76]. This thickness is also the order of the triplet exciton diffusion length in polycrystalline pentacene of $(40-80)$ nm and single crystal pentacene $(350-800)$ nm [98]. Figure 3.2 shows that only 32 % of the power above the singlet energy is absorbed. 67 % of the light above the singlet exciton energy is transmitted and is lost to the singlet fission process. Instead, the light is absorbed in the silicon solar cell below the singlet fission absorber, where it adds current but does not benefit from carrier multiplication. Even for a film thickness of 1000 nm, around three times the single-crystal triplet diffusion length, we still lose 34 % of the solar power above the pentacene singlet exciton energy.

The small fraction of absorbed photons from the solar spectrum in typical singlet fission materials like pentacene and tetracene directly translates into a smaller photocurrent gain. To illustrate this point, we

have calculated the theoretical maximum solar cell efficiency for a system that is ideal, where the only loss mechanism is incomplete absorption. We perform a detailed balance type calculation, with the tetracene and pentacene absorption spectra but otherwise 200 % efficient singlet fission, no non-radiative recombination except Auger recombination in silicon, and no parasitic absorption. In case of pentacene there is a voltage penalty since the triplet energy is smaller than the silicon bandgap. The recombination of charge carriers in the dark ($J_0$) does not happen across the silicon bandgap but instead across a smaller gap equivalent to the triplet energy, since this is the smallest energy difference where recombination can occur. The larger recombination due to the smaller energy gap in turn leads to a reduced voltage. Figure 3.3 shows the efficiency of a tetracene-silicon and pentacene-silicon solar cell as a function of tetracene or pentacene thickness, including the limits for an ideal absorber with the respective absorption onsets (horizontal lines in Figure 3.3). The dashed horizontal line shows the silicon-Auger limit, the solid lines represent the efficiency limits of tetracene and pentacene if they were ideal absorbers, which is also the limit for large thicknesses. We use energy at which tetracene and pentacene start to absorb as the absorption onset of the ideal absorber, which explains the discrepancies with the singlet exciton energies. In this ideal case even a very thin tetracene layer increases the current, but the efficiency gain keeps rising for layer thicknesses well above the polycrystalline triplet diffusion length of ~ 600 nm [2]. A pentacene layer however would have to be at least 950 nm thick to improve on the silicon Auger limit, which is many times the diffusion length of triplets in polycrystalline pentacene [98].

Below we assess the influence of different loss factors on the efficiency potential of singlet fission-silicon solar cells. Because of the poor broadband absorption, we treat the absorption of our theoretical materials as ideal in the following, absorbing all light above the singlet energy. This broadband absorption could be achieved by using a sensitizing layer, as in a recent study where perovskite quantum dots were used as a broadband absorber, then the excitons are transferred into a singlet fission material where they can undergo singlet fission [73]. This additional layer makes use of the efficient band-to-band absorption, with the penalty of a certain

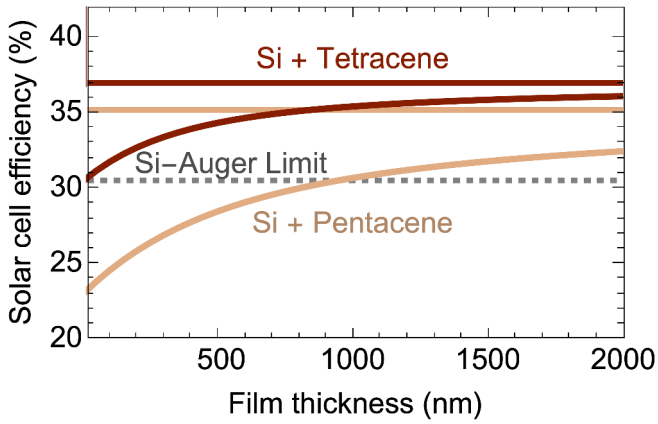


**Figure 3.3:** Detailed balance limit with the Auger recombination of silicon taken into account (dashed gray line) for an AM1.5 spectrum. The efficiency limit of a singlet fission-silicon cell based on this silicon base cell with tetracene and pentacene layers of different thicknesses, tetracene in red and pentacene in orange with an ideal absorber case of the respective materials as horizontal lines. The singlet energy/absorption onset is 1.7 eV for pentacene and 2.3 eV for tetracene. Triplet energies are 0.86 eV for pentacene and 1.25 eV for tetracene. The singlet fission efficiency is set to 2 and no additional loss channels are assumed.

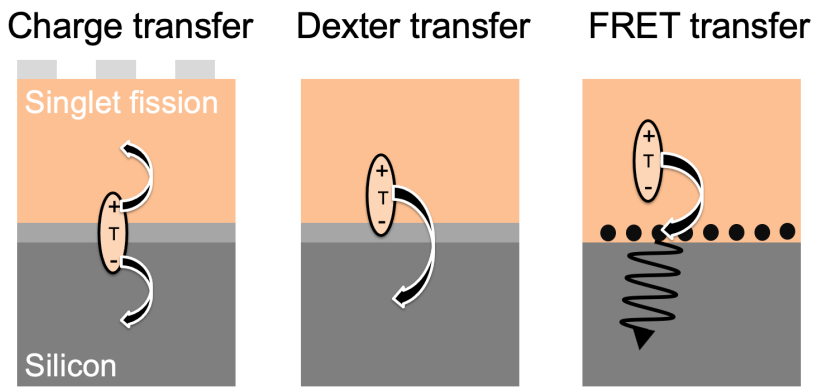


**Figure 3.4:** Schematics of the three transfer schemes discussed in this paper. *Charge transfer* includes the disassociation of the triplet exciton at the interface and subsequent transfer of both electron and hole independently. *Dexter transfer* entails the transfer of the energy of the triplet exciton into silicon by concurrently transferring electron and hole. *FRET* transfer consists of the transfer of the triplet exciton energy into a quantum dot with subsequent transfer of the energy from quantum dot into silicon via FRET.

transfer loss from the sensitizer to the singlet fission material. Since this first sensitizing study already reports a singlet exciton transfer efficiency of 80 % and additional gains are likely possible, we do not explicitly take this transfer step loss into account in the following calculations.

### 3.3.2 Different Transfer Mechanisms

In the following we calculated the efficiency for three distinct transfer schemes, charge transfer, Dexter transfer and FRET. We use the record silicon solar cell with an efficiency of 26.7 % [41] as a base cell into which additional current from singlet fission is injected. We explore the influence of different loss mechanisms and the difference between the transfer schemes, depicted in Figure 3.4.

#### 3.3.2.1 Charge transfer

Triplet excitons can be transferred into a silicon solar cell by charge transfer. In this transfer mechanism, the triplet exciton is dissociated into electron and hole at the interface between singlet fission material and silicon. $C_{60}$ and other fullerenes are often used as an electron acceptor for singlet fission materials and can efficiently dissociate the triplet excitons [17, 91]. Here we assume that the electron is transferred into silicon and the hole has to travel through the singlet fission material to an additional set of contacts on top of the singlet fission layer. The holes from the photocurrent generated in silicon need to transfer through the singlet fission material as well. The additional contacts and the long diffusion through the singlet fission layer will lead to additional losses. A variation of this transfer scheme is to use silicon top contacts to accept the singlet fission holes by adding an additional electron blocking layer around the contacts, in between the singlet fission layer and the metal of the contacts. If the hole mobility of a singlet fission material is high this buried contact could eliminate the need for additional top contacts which would reduce parasitic absorption losses. In our model we assume a doubled series resistance and a 3 % parasitic absorption loss from the additional top contacts. Further we assume 95 % efficient triplet generation and a 95 % efficient triplet disassociation leading to an overall triplet yield of 1.805 per absorbed photon. We discuss the requirements for the hole mobilities in the singlet fission material below.

An important element of modeling the charge transfer is the voltage penalty that applies if the triplet energy is smaller than the silicon bandgap. The radiative recombination will then occur between the smallest energy gap of the cell, which in this case is between the HOMO of the singlet fission material and the silicon conduction band. We assume ideal alignment of the LUMO of the singlet fission material and the silicon conduction band. By the smaller effective bandgap the dark recombination current increases which leads to a voltage penalty for triplet energies smaller than the silicon bandgap. In Figure 3.5 we plot the solar cell efficiency of the charge transfer-singlet fission-silicon solar cell as a function of the singlet energy of the singlet fission material. The singlet energy is

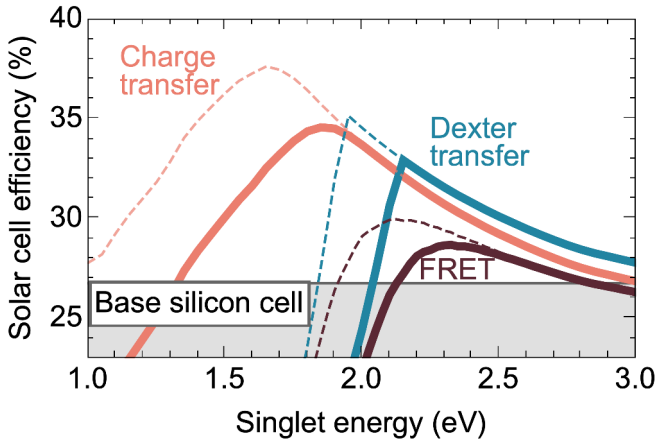


**Figure 3.5:** Solar cell efficiency of charge transfer, Dexter energy transfer, and FRET as a function of the singlet energy of a theoretical singlet fission material. The horizontal grey line is the record silicon solar cell that forms the bottom cell for the simulated singlet fission solar cells with the different transfer schemes. Thick lines assume a 100 meV entropy gain, dashed lines assume an optimistic 300 meV entropy gain. We show the charge transfer (orange), Dexter transfer (blue) and FRET (red) efficiencies. The most efficient transfer mechanism is the Charge transfer, which also shows the widest possible range of potential singlet fission materials.

also the absorption onset of our ideal absorber. The triplet energy is half of the singlet energy, plus an entropic gain term. The entropic gain can dramatically increase the efficiency of a singlet fission-solar cell as shown by the dashed lines in Figure 3.5.

**OPTIMAL ENERGY** Naively, the maximum singlet fission-silicon solar cell efficiency could be expected at a singlet exciton energy of 2.2 eV, twice the silicon bandgap of 1.1 eV. However, this is not the case as seen in Figure 3.5. The optimum singlet energy depends both on the transfer scheme and the entropic gain that is assumed. The charge transfer model shows the maximum solar cell efficiency of 34.6 % at a singlet exciton energy of 1.85 eV at 100 meV entropy gain, considerably lower than twice

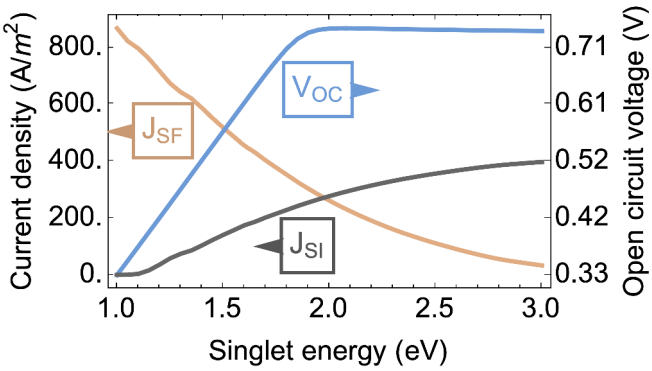


**Figure 3.6:** Different parts of the charge transfer solar cell efficiency for different singlet energies. We can see that the voltage penalty decreases the $V_{OC}$ below a singlet energy of 1.8 eV. $J_{SF}$ increases with lower singlet energy, since more absorbed photons can be converted in the singlet fission process. The current generated in silicon decreases.

the silicon bandgap. To explain this behavior, we show the three most important quantities for the singlet fission-silicon solar cell efficiency: the short circuit current from the singlet fission layer ($J_{SF}$), the silicon cell ($J_{Si}$), and the silicon solar cell open-circuit voltage ($V_{OC}$), in Figure 3.6 with the same x-axis of singlet energy as in Figure 5. $J_{SF}$ continuously increases with lower singlet energy thanks to an increased number of absorbed photons that can create two triplet excitons. At the same time $J_{Si}$ decreases, but not as quickly since every photon absorbed by the silicon cell generates at most one electron-hole pair. The voltage penalty, as seen in the decreasing $V_{oc}$ with decreasing singlet energy appears slightly below twice the silicon bandgap because of the entropic gain. Initially, the increase in photocurrent compensates the drop in voltage so that the efficiency optimum is in a regime where the solar cell suffers voltage penalty. The penalty only starts to reduce the efficiency at below 1.85 eV. The fill factor also decreases, similarly to $V_{oc}$, albeit not as strongly. We omit the fill factor from Figure 3.6 for clarity.

#### 3.3.2.2 *Influence of Entropy*

The entropic gain discussed earlier also leads to an increased efficiency and lower optimal singlet energy. Figure 3.5 shows the absolute efficiency gain plotted for 100 meV entropic gain and 300 meV entropic gain. We only consider the entropic gain during the singlet fission process in the singlet fission material. Since there is also a certain density of states in silicon it is conceivable that an increased number of available states inside silicon could also lead to an additional entropy gain. Since the a change in entropy during the process will lead to a gain in Gibbs free energy, G *via* $\Delta G = -T\Delta S$ with the temperature T and the change in entropy $\Delta S$. The increased Gibbs free energy could therefore increase ($\Delta G < 0$) or decrease ($\Delta G > 0$) the transfer efficiency. The change in entropy can be calculated with the formula $\Delta S = k_B \left(\ln \Omega_S - \ln \Omega_T\right)$ by counting the states in silicon $\Omega_S$, and the available states of the free triplet exciton $\Omega_T$.

We will now perform a rough calculation for the entropy gain for the transfer between tetracene and silicon. The number of states of a triplet excitons in tetracene has been calculated by Kolomeiskiy et al. [62] by calculating the number of molecules within the Dexter radius of $(10 - 20)$ Å. The number of molecules accessible for a triplet exciton is 19 for a Dexter radius of 10 Å, 37 for a radius of 15 Å and 61 for a dexter radius of 20 Å.

We can estimate the number of states in silicon by integrating square-root dependence of the density of states (units: $\frac{1}{cm^3 eV}$) from the conduction band edge to 150 meV above the band edge. We use 130 meV since this is the difference in energy between the tetracene triplet exciton and silicon. Different effective masses for electrons and holes in silicon are taken into account, and the integral is split into two with integration boundaries for electron and hole from the bandedge to 75 meV above. This calculation leads to a density of states of $0.12\,nm^{-3}$. In silicon the exciton size is much larger than the Dexter radius since the dielectric constant is large ($\sim 11$) which leads to a large Wannier exciton of around 9 nm radius. This leads to a large number of states available within the sphere occupied by the Wannier exciton in silicon, namely 448. This change in the number of available states would lead to an additional en-

tropy gain of 76 meV if the triplet state in tetracene has a Dexter radius of 10 Å, 59 meV for a Dexter radius of 15 Å, and 46 meVfor a Dexter radius of 20 Å.

The additional entropy term could be beneficial to the transfer efficiency and potentially the solar cell efficiency. We calculated the entropy gain by using exciton radii which is presumably only realistic for a direct Dexter exciton transfer. Other transfer mechanisms might behave differently and our naive assumptions might not hold.

In Figure 3.5 we can see that a higher entropy term would extend the possible singlet fission materials to lower singlet energies, as low as 1.65 eV at 300 meV entropy gain, where the efficiency is calculated to be 37.6 %. We therefore conclude that it would be hugely beneficial if we could control and increase the entropy gain to increase the singlet fission-silicon solar cell efficiency. Also, most synthetic efforts towards new singlet fission molecules aim for singlet energies above 2 eV. However, our results show that low-bandgap singlet fission materials are potentially even more interesting, since the peak of increased solar cell efficiency is very broad thanks to the charge transfer and the entropy gain.

#### *3.3.2.3 Space Charge limited current*

Since the charge transfer scheme involves transport of holes from the singlet fission material and silicon through tetracene, the low mobility of organic singlet fission materials like tetracene will make charge extraction inefficient. This will be especially problematic since organic semiconductors have poor broadband absorption as described earlier, which necessitates thick singlet fission absorber layers. To estimate the necessary hole mobilities and the resulting maximum thicknesses for any singlet fission-layer, we model the system using the Mott-Gurney law of space charge limited current. This model assumes that the contacts are not introducing any additional barriers, that the holes are not transported via traps or that the cell operates above the trap filling voltage. The space-charge limited current then becomes

$$J(V) = \frac{9}{8}\epsilon\mu\frac{V^2}{L^3}$$

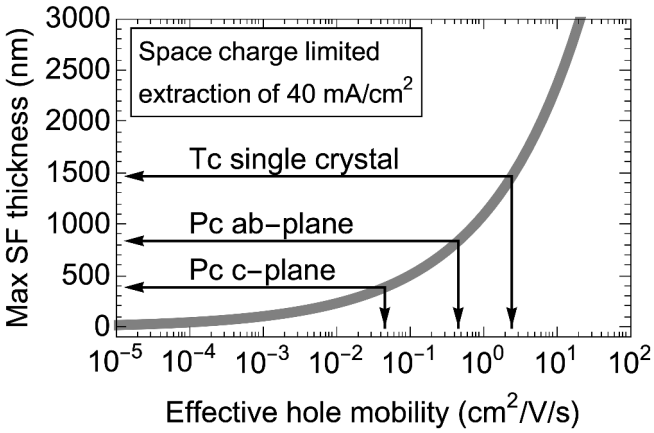


**Figure 3.7:** Maximum singlet fission layer thickness as a function of effective hole mobility. We assume a voltage drop of 0.36 eV and an extracted current of 40 $^{mA}/_{cm^2}$.

with $\epsilon$ the singlet fission-material permittivity, $\mu$ the hole mobility, and L the layer thickness. We assume that we have to extract a typical current from the silicon cell of 40 $^{mA}/_{cm^2}$ through the singlet fission layer and that half of the silicon voltage drops over the singlet fission layer, set to $V = 0.36\,V$. With these assumptions we can solve for the thickness as a function of mobility as shown in Figure 3.7. We show three characteristic singlet fission materials, a best-case scenario of single crystal tetracene with a mobility of 2.4 $^{cm^2}/_{Vs}$ [107] would allow for a maximum layer thickness of ~ 1500 nm, which would lead to an ideal efficiency of 36 % (Figure 3.3). The mobility in polyacenes is typically anisotropic [45], requiring aligned growth of the singlet fission material for optimal performance. For pentacene the mobilities in two different crystal axes have a value of 0.45 $^{cm^2}/_{Vs}$ in the ab-plane and a 10 times lower mobility in the c-plane direction [45]. In real devices, the transport would most likely occur in the low-mobility c-plane since that is the preferred growth direction on silicon [122, 123], which would limit the singlet fission layer thickness to 400 nm.

Since there is a long history of research towards high-mobility organic materials for organic transistors [90] that has yet to overcome mobilities above $20\,\mathrm{cm^2/Vs}$ this is most likely a hard problem to solve with molecular engineering. However, if we use a sensitizer to efficiently absorb the light, we could design a much thinner singlet fission layer combined with a thick absorber layer that also has a high mobility (e.g. a metal halide perovskite), which in turn puts lower requirements on the necessary hole mobility in the organic layer. Another strategy is the use of a bulk heterojunction, used in organic solar cells to overcome low mobilities by mixing the donor and acceptor phases resulting in much shorter transport distances for example with a bulk heterojunction between the singlet fission material and a hole extraction material such as PEDOT:PSS. Since there are already strategies of functionalizing organic molecules with TIPS groups such as TIPS-tetracene and TIPS-pentacene, a solution of singlet fission material and hole extraction layer that could be spin-coated is feasible. Similarly, a very thin singlet fission dye on a mesoporous substrate, as is used in dye-sensitized solar cells, could also overcome the absorption length problem.

As mentioned above, another route would be to add buried contacts on top of silicon but below the singlet fission layer that collects holes from both silicon and the singlet fission material. If the lateral distance to a contact would be smaller than the film thickness, this geometry would also allow for shorter hole transport distances. The lateral mobility in organic crystals can also be higher than the vertical mobility. However, the metal fingers used to collect charges on top of standard silicon solar cells would be unsuitable for this scheme since they are usually several millimeters apart. Metal grids with a pitch of $1\,\mu\mathrm{m}$ have been shown [59] and could be combined with a singlet fission charge transfer solar cell. In case of a degraded singlet fission layer, the direct collection of silicon holes at the silicon surface is also beneficial since the silicon solar cell continues to be operational with an inactive, then transparent singlet fission layer [55]. Despite the attractive efficiency potential, charge transfer from triplet excitons into silicon has been attempted but not yet experimentally shown to occur with high transfer efficiencies [76].

#### 3.3.2.4 Dexter transfer

Dexter energy transfer directly transfers the whole triplet exciton energy at once, by concurrently transferring the electron and hole into the silicon. Since triplet excitons are dark states, FRET or photon emission cannot occur directly, and Dexter transfer is the only accessible energy transfer mechanism. For efficient Dexter transfer the wavefunction overlap between the triplet exited state on a singlet fission molecule and the accepting material has to be large. In upconversion systems it has been shown that the triplet exciton states can be populated from electrons and holes occupying bands in inorganic semiconductors. A recent example is the sensitization of the rubrene triplet states by a lead halide perovskite film [86]. These examples show the potential for large wavefunction overlap between the excitonic states and the band-like states.

The first demonstration of Dexter transfer from triplet excitons, generated by singlet fission, into an inorganic semiconductor was from tetracene into PbS quantum dots [129] and from pentacene into PbSe quantum dots [125]. After a long search, triplet transfer from tetracene into silicon has finally been demonstrated in a recent set of experimental studies [20, 29], even though there is no conclusive evidence that the transfer mechanism was indeed Dexter transfer.

In our model we assume efficient transfer if the triplet energy is sufficient, meaning larger than the silicon bandgap. If the triplet energy is smaller than the silicon bandgap then we assume that the thermal energy can add to the total energy and allow the transfer. We implemented this by a higher-energy population of triplets following the Maxwell-Boltzmann distribution. At room temperature the energy of 25 meV is small compared to the exciton energy, so the efficiency for Dexter transfer still falls dramatically if the triplet energy is too small, as can be seen in Figure 3.5 by the steep decrease of efficiency at lower singlet energies. In practice the Dexter transfer solar cell would be very simple, just a single organic layer on top of a suitably prepared silicon solar cell. We assume no parasitic additional absorption since there are no additional extraction or disassociation layers, and as above, a quantum yield of 1.805 for the

singlet fission process, assuming an efficiency of 95 % for both the triplet generation and triplet transfer.

In comparison to charge transfer, Dexter transfer shows a higher efficiency for high singlet energies above 2.1 eV since the parasitic absorption is absent (Figure 3.5). The thick line in Figure 3.5 is calculated with an entropic gain of 100 meV, the dashed line assumes a 300 meV entropic gain. The additional entropic gain extends the possible singlet energies further to down to lower values for potential singlet fission materials, but shows the same abrupt decrease if the triplet energy is smaller than the silicon bandgap. We can see that the possible efficiencies are lower than in the charge transfer case, with a maximum of 32.9 % at 2.15 eV if 100 meV entropy gain is assumed and 35.1 % at 1.95 eV for 300 meV entropy gain. This transfer scheme, however, might be easier to realize than the charge transfer or FRET (see below) since there is no need for an additional top contacts or quantum dot layer.

For the practical implementation one needs to consider the silicon passivation. Efficient silicon solar cells are typically covered with a layer of thick $SiO_2$ or $Si_3N_4$ which acts both as a passivation layer and as an anti-reflection coating. For all transfer schemes the contact between the organic material and silicon needs to be close, thus one needs to remove the coating. While the low-index organic material would have some anti-reflection effect, the full performance would likely need to be restored by an additional anti-reflection layer on top of the organic layer. Also, the silicon layer would need to be passivated electronically. While some ultrathin layers have been developed (1.2 nm of $SiO_2$ [38] , 7 nm of $Al_2O_3$ [50], 15 nm of $HfO_2$ [147]), they may still be too thick to transmit triplet excitons. In that case, ideally, the singlet fission material would directly act as the passivation layer on silicon, for example by covalently attaching a singlet fission molecule on the silicon surface [19].

#### 3.3.2.5 *Förster resonant energy transfer*

Förster Resonant Energy Transfer (FRET) is the dominating transfer for singlet excitons in organic semiconductors. However, since triplet exciton states are dark states, they cannot undergo FRET directly. It is, however,

possible to transfer the excitons into an emissive material, for example quantum dots that have a large spin-orbit coupling so that triplet excitons can be converted into emissive excitons in these quantum dots. Then the exciton could be transferred into silicon via FRET. The main factor determining the efficiency of FRET between these quantum dots and the silicon acceptor is the very short Förster radius (distance at which transfer efficiency is 50 %), which means that the quantum dots have to be very close (1 nm) to the silicon surface [126]. The reason for the short Förster radius is the small overlap integral between the quantum dot emission at the silicon band-edge (1.2 eV) and the weak absorption cross section of silicon, an indirect-bandgap semiconductor. In an earlier work we have extended the FRET model that describes energy transfer between two dipoles to a more appropriate dipole-3D acceptor model, with a tunable energy PbS QD as the emitter and a slab of silicon as the acceptor. The distance dependence changes from a $\frac{1}{r^6}$ dependence of the dipole-dipole model to a $\frac{1}{r^3}$ dependence, making the transfer efficient for longer distances. The Förster radius in the 3D acceptor model for suitable quantum dots of 1.2 eV emission is 1.4 nm. In this work we place the dots directly at the interface, at a distance of 1 nm. The resulting transfer efficiency then depends on the wavelength of the emission since the overlap integral of the quantum dot PL and absorption changes. The PL emission wavelength is matched to the triplet energy of the singlet fission material plus the entropic gain described earlier. Thus, we assume no energetic losses from the triplet energy transfer into the quantum dot. We assume no Stokes shift. The Stokes shift in PbS QDs originates in the polydispersity of the ensemble [136], in our case the QDs can be very dilute and presumably monodisperse, leading to a small or no Stokes shift.

The triplet diffusion length can be short in this scheme since the QDs could be intermixed into the singlet fission layer. The transfer efficiency of triplets into the quantum dots is an additional loss channel and is assumed to be 90 % efficient, a realistic number for small singlet fission-QD distances [129], leading to an overall quantum yield of 1.71. In Figure 3.5 we show the efficiency as a function of singlet energy. The FRET curve follows the same general trend as the other transfer mechanisms, albeit

with lower efficiency of 28 % in the 100 meV entropy gain case, because of additional parasitic absorption, additional transfer losses and quickly decreasing FRET transfer efficiency at lower quantum dot emission energies. Additional entropy gains of 300 meV lead to a maximum efficiency of 30 % at a singlet energy of 2.1 eV, extending the singlet exciton energies with an efficiency gain to lower singlet energies, just as with the other two transfer mechanisms. In a realistic cell, this transfer scheme might be the easiest to manufacture, since it could be applied to any silicon solar cell with a thin passivation layer. However, for thick passivation layers that are currently the standard in silicon solar cells (for example a 80 nm $Si_3N_4$ passivation and antireflection layer) the FRET efficiency would effectively be zero and one would have to rely on the photon emission and absorption by the quantum dots, which necessitates new ways of directing the light downwards toward silicon. We calculate the efficiency potential of such a "photon multiplier" scheme elsewhere [34].

### 3.3.3 Influence of the underlying silicon solar cell

The transfer efficiencies that have been discussed so far have been calculated with a record silicon solar cell of 26.7 % efficiency [41]. This is, however, not what is currently available commercially, so how does the performance change if the base cell is less efficient?

To explore the efficiency potential on a broad range of silicon base cells we used the same diode model as above but now with recombination constants and resistance values that fit the IV curves for these less efficient silicon solar cells. This approach is based on work of Futscher et al. [33, 34]. The models for different silicon solar cells allow us to run the same calculations as before and observe the change with silicon cell efficiency. Figure 3.8 shows the results, with the optimal singlet energy for each transfer scheme and an entropy gain of 100 meV and other parameters as described above. As a comparison we have also included the results of an earlier calculation of an optimistic case for a perovskite-silicon two terminal tandem solar cell [34]. In this optimistic tandem cell the perovskite top cell is as optimized in terms of non-radiative recombination

and resistances as the current silicon record cell. We can see that the improvement in singlet fission-silicon solar cell efficiency is larger for more efficient base cells. This is in stark contrast to the behavior of the perovskite tandem cell, where the efficiency improvement decreases with more efficient base cells. The main reason for this difference is that we do not have to change the base cell at all. The energetics and voltage matching stays the same, we simply inject additional current. Thus, to first order, the efficiency is increased by a certain percentage of the silicon efficiency, which leads to higher absolute efficiency gains for more efficient silicon cells. In the tandem solar cell, both cells have to be electrically connected and the electrical properties of the full cell are limited by each of the subcells, so it is easy to degrade the highly optimized record silicon solar cells. Therefore, the largest relative gains in efficiency with singlet fission can be found in already efficient base cells, where they are otherwise most difficult to achieve and most valuable.

## 3.4 CONCLUSION

Singlet fission can lead to large absolute efficiency gains for silicon solar cells. While the best silicon solar cells are now very difficult to improve, with sub-percent level improvements celebrated as great successes, singlet fission can potentially increase the efficiency of a record silicon solar cell from 26.7 % to 37.6 %. Such a huge efficiency improvement could be reached with charge transfer from the triplet state into silicon when all processes work well: The singlet fission material absorbs all light above its bandgap, the efficiency of singlet fission is 95 %, the triplet transfer is 95 % efficient, the entropic gain during singlet fission is 300 meV and the additional resistance and optical losses in the silicon cell are small (doubled series resistance and 3 % parasitic absorption). With the exception of charge transfer from the triplet state into silicon, each of these quantities has been demonstrated individually, but the combination will still be a significant challenge to achieve. Yet, even somewhat less optimistic assumptions can lead to massive efficiency gains. We have shown that all

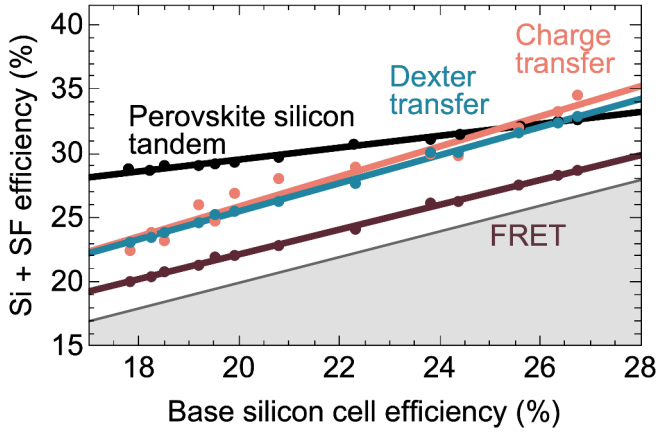


**Figure 3.8:** Calculated efficiency potential of singlet fission-silicon solar cells for charge transfer, Dexter transfer and FRET, compared with the efficiency potential of perovskite-silicon tandem solar cells as a function of base silicon cell efficiency. Lines are a linear fit to the datapoints. The grey line is the base silicon solar cell. The efficiency gain grows for better silicon base cells in the case of singlet fission cells, and *vice versa* for tandem solar cells.

transfer mechanisms can improve on the efficiency of silicon solar cells. Maybe most surprising is that the charge transfer route of triplet disassociation and subsequent hole and electron collection is most efficient and most forgiving in terms of the viable singlet energies. The voltage penalty is partially offset by the larger portion of light absorbed in the organic material such that the efficiency gain is less dramatically affected than naïvely assumed. Dexter energy transfer is simpler to implement but the energetics of the process restricts the potential singlet fission materials. FRET transfer is also somewhat promising, but the additional transfer step has to be efficient and the parasitic absorption has to be low. The distance between quantum dots and silicon also has to be small since the Förster distance is small. All transfer schemes share the requirement of direct access to the silicon surface which will require the use of new passivation and anti-reflection coatings. A conventional 80 nm silicon nitride coating would not be compatible with these kinds of transfer schemes. A good surface passivation is also crucial, otherwise the additional gains from singlet fission are lost via recombination at the silicon surface, an especially important aspect in the case Dexter and FRET transfer, as most charge carriers in the silicon will be generated close to the surface. It is thus of great importance for these singlet fission-silicon solar cells to find thin ($< 1$ nm) passivation layers that lead to very low surface passivation. Recent developments with metal oxides [29] and molecular monolayers [134] show promise. Alternatively, schemes where the singlet fission material injects the triplet energy at point contacts and the remainder of the surface is well-passivated with a thick insulator could work with existing passivation materials. Our work shows that the search for new singlet fission materials can be potentially less strict on the triplet energy requirements if charge transfer schemes were adopted, but that the entropic gain is hugely important for the potential efficiency gain, and should hence get more attention in the design of the molecules and the crystal stacking thereof. A major benefit of singlet fission-silicon solar cells is that it will be easier to improve on already efficient silicon solar cells, which is most important for lowering the cost of solar energy. In that sense singlet fission-silicon solar cells may form the next step after tandem solar cells have entered the market. They are easier

to fabricate and implement, or maybe even retrofitted, and benefit from highly efficient silicon base cells that are harder to improve in a tandem geometry.

# 4 A METHOD TO DETECT TRIPLET EXCITON TRANSFER FROM SINGLET FISSION INTO SILICON SOLAR CELLS: COMPARING DIFFERENT SURFACE TREATMENTS

This chapter is based on the following publication:

Benjamin Daiber, Sidharam P Pujari, Steven Verboom, Stefan L Luxembourg, Stefan W Tabernig, Moritz H Futscher, Jumin Lee, Han Zuilhof, and Bruno Ehrler. "A Method to Detect Triplet Exciton Transfer from Singlet Fission Materials into Silicon Solar Cells: Comparing Different Surface Treatments" In: *The Journal of Chemical Physics* (2020)

Singlet fission is one of the most promising routes to overcoming the single-junction efficiency limit for solar cells. Singlet fission-enhanced silicon solar cells are the most desirable implementation, but transfer of triplet excitons, the product of singlet fission, into silicon solar cells has proved very challenging. Here we report on an all optical measurement technique for the detection of triplet exciton quenching at semiconductor interfaces, a necessary requirement for triplet exciton or charge transfer. The method relies on growth of individual, single-crystal islands of the singlet fission material on the silicon surface. The islands have different heights, and we correlate these heights to the quenching efficiency of triplet excitons. The quenching efficiency is measured by spatially-

resolved delayed fluorescence and compared to a diffusion-quenching model. Using silicon capped with a blocking thermal oxide and aromatic monolayers, we demonstrate that this technique can quickly screen different silicon surface treatments for triplet exciton quenching.

## 4.1 INTRODUCTION

The efficiency of silicon solar cells is already very close to its theoretical limit [99], which drives the search for new concepts to increase power conversion efficiency. Next to tandem solar cells, singlet fission has emerged as a promising route to allow for higher efficiency [47], with comparably simple implementation in solar cell devices, and spectral stability in changing environmental conditions [34].

Singlet fission is the conversion of one singlet exciton in an organic semiconductor into two triplet excitons of roughly half the energy [100, 118]. Triplet excitons are dark states that cannot transfer energy radiatively or *via* a Förster type process, only Dexter type transfer or charge disassociation and subsequent charge transfer is possible. For an increase in power conversion efficiency these triplet excitons need to be transferred into a lower-bandgap semiconductor cell to generate additional current. One implementation where singlet fission enhances the current of a silicon solar cell (in a narrow spectral range) relies on a tandem cell configuration. Two separate cells are optically connected in series and electrically connected in parallel [69, 91]. Fabrication of these tandem solar cells would be equally as involved as conventional tandem solar cells. It would be more elegant to directly transfer triplet excitons into silicon which would not require any changes to the contacts of a conventional silicon solar cell.

In contrast, if the triplet excitons could be directly transferred into the low-bandgap semiconductor via charge or energy transfer, a very simple device implementation would be possible. Such transfer has successfully been shown for purely organic solar cells [68], into quantum dots [28, 125, 129], and silicon using a hafnium oxynitride ($HfO_xN_y$) interlayer [29]. In

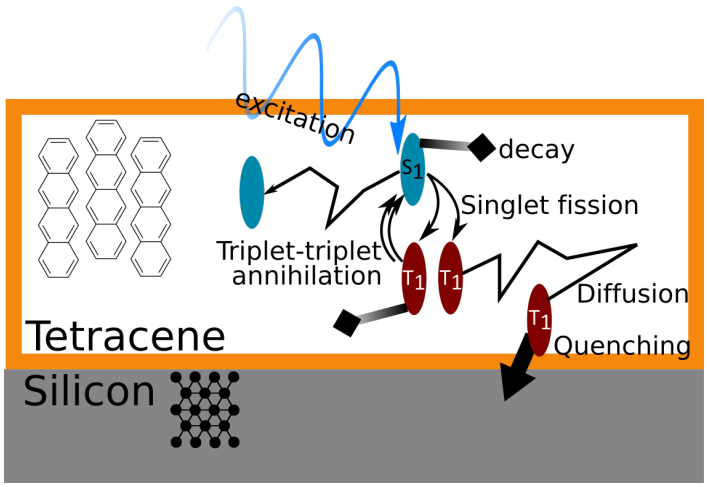


**Figure 4.1:** Schematics of the processes included in the simulation. Excitation with a short laser pulse is followed by singlet fission in tetracene and diffusion of both singlet and triplet excitons. Singlet and triplet excitons have various non-radiative decay mechanisms that can be summarized with one decay rate. Quenching at the interface is assumed to be only present for triplets. The simulations allow us to calculate the density of singlet and triplet excitons over time. The singlet exciton density is proportional to the emitted photons, which is the observable in our experiment.

the last example, a single layer of singlet fission material on top of the silicon cell absorbs the high-energy part of the spectrum, generates up to two triplet excitons per photon, and injects the energy of the excitons into silicon with an, as of yet, unspecified pathway; the injection has to proceed either via direct Dexter energy transfer [24], where both the electron and hole are concurrently transferred into silicon, or the transfer of a single charge at the heterojunction interface. Dexter transfer is observed for triplet transfer from pentacene into PbSe quantum dots [125], from tetracene into PbS quantum dots [129] and from tetracene into silicon [29]. Charge transfer has been observed at multiple organic/organic interfaces [17, 144], at the organic/quantum dot interface [27, 53, 145] at the organic/a-Si interface with a quantum dot interlayer [26]. Several attempts to show direct transfer of excitons or charges into crystalline silicon remained unsuccessful or inconclusive [76, 95], and only recently current enhancement of a silicon solar cell using a $HfO_xN_y$ interlayer between tetracene and silicon has been demonstrated [29].

One major hurdle in the path towards the triplet exciton transfer into silicon is the detection method of such transfer. Triplet excitons are "dark states", meaning that they do not emit or absorb light in the absence of strong spin-orbit coupling. The only direct optical measurement is therefore transient absorption spectroscopy, which has been employed to measure the charge separation dynamics at the pentacene/$C_{60}$ interface [105]. Transient absorption at the silicon interface is considerably more challenging because the features in silicon are comparably unspecific, and the absorption in the silicon solar cell reduces the signal. Further, spatially resolved studies are even more difficult [143], and excitation densities are typically orders of magnitude above those relevant in solar cells which makes it difficult to draw conclusions from these studies for solar cell operation.

A popular method to detect the contribution of triplet excitons to the photocurrent of a solar cells is to measure the photocurrent as a function of an externally applied magnetic field [144]. The field changes the ratio of singlet excitons to triplet excitons generated from photons absorbed in the singlet fission materials. At high external fields (100 mT), the ratio of singlets to triplets increases [79]. Thus, the photocurrent contribution

from triplets decreases. This method is very accurate, but it requires fabricating a solar cell, and the magnetic field measurement on a full solar cell device requires careful separation of magnetic field effects from the singlet fission contribution and form other layers in the solar cell stack. It is also a measurement that is typically done on bulk films which means that each variation in the materials parameters requires the fabrication of a separate solar cell.

Similarly, to the magnetic field measurement of the photocurrent of a solar cell, one can use the photoluminescence of the low bandgap semiconductor as an indication for energy transfer. If excitons are injected into silicon, then the photoluminescence (PL) of silicon can be used to measure triplet and singlet exciton injection [29]. The change of PL with magnetic field allows one to distinguish between triplet and singlet exciton injection. However, for example for silicon the photoluminescence quantum yield of silicon is weak, and normal silicon detectors cannot be used which complicates the measurement. Since a green laser beam excitation will also be absorbed in the silicon, the change of total PL from exciton injection is small, especially for thin singlet fission layers.

Recently, the external quantum efficiency has been used to study the photocurrent contribution from singlet fission materials [29, 76]. If all triplet excitons are utilized for photocurrent, the internal quantum efficiency of the singlet fission materials would be close to 2, which would increase the external quantum efficiency of the silicon solar cell. So far, however, the contributions from triplet excitons could only clearly be distinguished from the noise for very efficient transfer of triplet excitons [29]. The noise level and therefore the error is comparably high because the method relies on accurate optical modeling of the full solar cell stack and the comparison with a reference cell. Again, this method also requires solar cell fabrication, which adds fabrication complications and additional potential for errors.

A necessary requirement for the transfer of triplet exciton energy or charge is the quenching of the triplet exciton at the organic/silicon interface. This effect was used to study exciton transfer by Piland and co-workers [95]. They deposited tetracene layers of varying thicknesses, with and without an insulating spacer layer. They used quenching of the

delayed luminescence lifetime to detect any transfer of triplet excitons at the tetracene/silicon interface. Again, no clear sign of transfer was detected. This method relies on a material that shows delayed fluorescence, originating from the recombination of two triplet excitons into an emissive singlet exciton. It also requires separate samples for each thickness, and is a bulk method, without spatial resolution, while tetracene forms an intricate microstructure [83] which influences singlet fission rates [5].

Here we measure the quenching of the delayed fluorescence with high spatial resolution on a silicon sample covered in many single-crystal tetracene islands of different thickness. We therefore can measure the lifetime quenching for hundreds of different thicknesses in a single measurement on a single sample under the very same conditions (deposition, interface, light excitation and collection). We use this rapid and accurate method to study triplet transfer on tetracene/silicon samples with different interfacial surface treatments, and compare the result to a model of exciton diffusion and transfer. Despite very thin interfacial layers on silicon, and comparable passivation across surface treatments, we find no evidence for transfer of either charge or excitons into silicon. We speculate about the possible reasons and suggest a path towards efficient transfer.

## 4.2 RESULTS AND DISCUSSION

### 4.2.1 Quenching on the Interface as a Function of Thickness

A necessary requirement for triplet energy transfer is the change in the delayed fluorescence as a function of distance to the interface. The photoluminescence of singlet fission materials such as tetracene commonly shows two decay components in the polycrystalline thin films, prompt and delayed fluorescence [11]. The prompt fluorescence is due to the quenching of singlet exciton recombination by singlet fission, while the delayed fluorescence stems from the recombination of two triplet excitons to form an emissive singlet state. If the triplet excitons transfer across the interface, then the excitons that experience the interface during their lifetime are quenched (Figure 4.2). Thus, for efficient triplet (singlet)

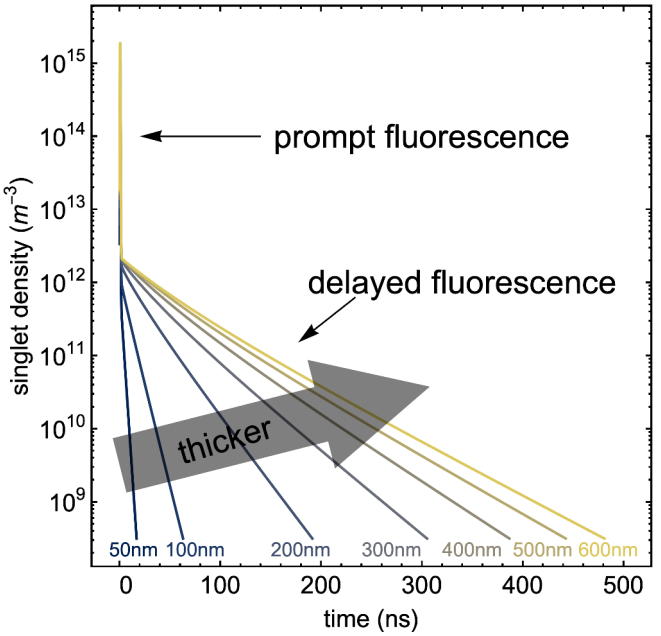


**Figure 4.2:** Simulation of the singlet density (proportional to the PL intensity) as a function of time. Different colors represent different thicknesses of the tetracene slab. The delayed fluorescence slows down with thicker tetracene layers.

transfer, thinner films will show a shorter delayed (prompt) fluorescence compared to thicker films [95].

To simulate the effect of surface quenching on the photoluminescence we modeled the generation, diffusion and extinction of singlet and triplet excitons. The singlet exciton density profile follows the absorption in tetracene, described by the Beer-Lambert law. Interference effects only have a small effect on the absorption profile, as shown by transfer matrix modeling in the Appendix. We follow Piland et al. [95] to model the generation and recombination of singlet and triplet excitons and add a 1D-diffusion term for singlet and triplet excitons. The quenching (e.g. by transfer into silicon) of triplet excitons is modeled *via* different boundary conditions at the tetracene silicon interface. We initially assume full

quenching but the model also allows to use different quenching efficiencies (surface recombination velocities), as described in the Appendix. The photoluminescence intensity is proportional to the singlet exciton density, which allows us to predict the photoluminescence transients for tetracene islands with different thicknesses. The model shows how the delayed lifetime depends on the film thickness when assuming perfect transfer (Figure 4.2). The model is described by the following differential equations for singlet density (S) and triplet density (T):

$$\frac{\partial S(z,t)}{\partial t} = -k_{SD} S(z,t) + k_{TS} T(z,t)^2 + \\ + excitation(t)\, e^{-\frac{z}{z_0}} + Diff_S \frac{\partial^2 S(z,t)}{\partial z^2}$$

$$\frac{\partial T(z,t)}{\partial t} = -k_{TD} T(z,t) - k_{TS} T(z,t)^2 - k_{TT} T(z,t)^2 \\ + (k_{ISC} + 2k_{fiss})\, S(z,t) + Diff_T \frac{\partial^2 T(z,t)}{\partial z^2}$$

The rates $k_{SD}$ and $k_{TD}$ are the sum of all singlet and triplet decay mechanisms respectively, $k_{TS}$ the triplet to singlet decay rate. $excitation(t)$ is the excitation laser profile with time, multiplied with the exponential decrease of the light intensity according to the Beer-Lambert law inside the slab. $Diff_S$and $Diff_T$are the average diffusion constants for singlets and triplet excitons. $k_{TT}$ is the triplet-triplet annihilation rate. $k_{ISC}$ is the intersystem crossing rate and $k_{fiss}$ is the singlet fission rate. All constants are taken from literature and are shown in the Appendix.

The prompt fluorescence lifetime is only determined by the singlet fission rate, which does not change with tetracene thickness. The delayed fluorescence becomes slower with thicker tetracene layers and levels off after 500 nm (Figure 4.4).

Using our diffusion model, we find that the delayed lifetime should in fact depend on the distance to the interface, while the prompt fluorescence lifetime should be independent of that distance (Figure 4.11 in

Appendix). Note that the length-scales involved here are shorter than the length-scales at which we expect a change in optical coupling into the Si from the refractive index difference and Purcell enhancement of the lifetime because of an enhanced local optical density of states close to a semiconductor interface.

Tetracene, the prototypical singlet fission material, grows in islands on the silicon surface for nominally thin films. These presumably single-crystal islands show a range of thicknesses and can hence be used to distinguish the change in delayed lifetime for a range of distances to the surface. We note that when observing a large area of different islands, any effect of different island heights will be averaged out. Thus, here we probe the lifetime of the islands individually by microscopically-resolved photoluminescence lifetime, and correlate the delayed lifetime of each island to its height. It has been shown that morphology has an influence on singlet fission efficiency [31, 93] and that the growth mode of tetracene changes from 3D to 2D growth with increasing deposition rates above a few Å/s [83]. The tetracene islands in this experiment are grown with a deposition rate of 1 Å/s for all samples, so we can assume that the growth mode stays constant between islands and between samples.

A well-performing silicon solar cell needs a good surface passivation, usually accomplished by amorphous silicon layers, highly doped layers or $SiN_x$ passivation layers. All these layers do not allow for free access to the front side of the silicon that is necessary for direct energy transfer from tetracene into silicon. The close distance needed between tetracene and silicon precludes a thick passivation layer, we therefore probe the transfer on thinner passivating layers. One such passivating interlayer is a short organic molecule that is covalently bound the top layer of silicon atoms. It has been shown that such organic passivation layers can reach a surface recombination velocity comparable to that of good inorganic passivation layers [116]. This layer of organic molecules can also prevent the growth of a native oxide layer between tetracene and silicon. In addition to the passivation and close distance to the surface, the organic molecules could also be used to control the tetracene growth, and therefore its orientation. The orientation of the tetracene molecules on the silicon surface determines the degree of wavefunction overlap

between the triplet exciton and silicon; a larger wavefunction overlap integral leads to a more efficient exciton transfer.

The alignment of the tetracene molecules at the surface depends both on the deposition conditions and on the surface energies, which can be tuned with different capping layers of the organic passivation. We have attached molecules consisting of four benzene rings (pyrene) as interlayers, designed to facilitate the transfer of triplet excitons, and we compare them to our reference sample of thin 2.4 nm thermally grown layers of silicon oxide, which will block the short range ($< 1$ nm [88]) Dexter type transfer. The Appendix contains the details of the surface modification procedure of aromatic alkynes (phenyl acetylene, 2-ethynylnaphtalene, 1-ethynylpyrene) on hydrogen terminated silicon surface and their characterization. We use ellipsometry and XPS to measure their thickness to be between 1 nm and 1.4 nm; water contact angles to assess their quality and AFM to measure film roughness (see Appendix).

### 4.2.2 AFM and TCSPC overlay

To measure the delayed fluorescence lifetime as a function of island height, we mark a spot on our substrate and measure both the height of the islands using AFM, and the lifetime using time-correlated single photon counting (TCSPC) microscopy. We then use an automated algorithm overlap the measurements, find the individual islands, and compare the height and lifetime of each of the islands (Figure 4.3)

We combine all pixels that make up an island in the TCPSC data to calculate the lifetime average over that island. From the AFM data of each island we choose to use the mean of the highest 25 % of pixels as a measure for the height of an island. Using the mean of all pixels yields similar results (see Figure 4.16 in Appendix).

Fitting the TCSPC data of the PL decay presents a unique set of challenges. We measure the islands microscopically, therefore we only collect few counts in the delayed fluorescence decay, on the order of 100 photons per island in total. The decay is not mono-exponential, a fact we can already see in our model and the raw decay trace data. We found that

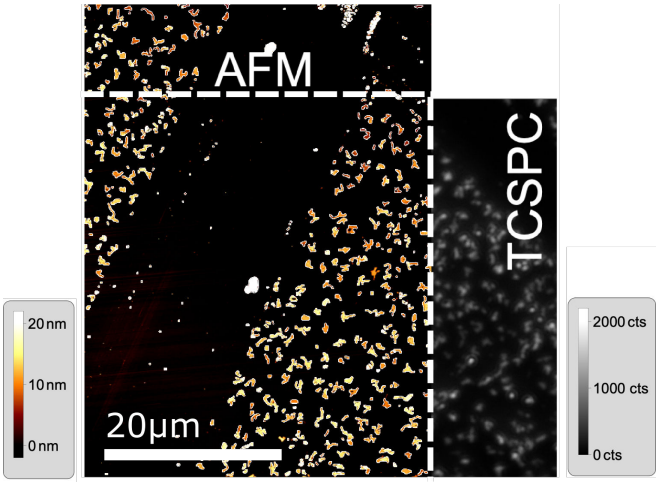


**Figure 4.3:** Visualization of algorithm that overlays AFM and TCSPC data and identifies islands in both data sets.

the proper accounting of the Poissonian distribution of photons in the low count regime and the choice of a simple fitting model are critical to extract the correct correlation between lifetime and height. Fitting the decay traces with an unsuitable method, for example assuming Gaussian noise, can lead to correlations that are an artifact of the assumption and not the data. More insight into the lifetime fitting and a link to our fitting script can be found in the Appendix.

### 4.2.3 Comparing the diffusion model with two surface functionalizations

Plotting the delayed lifetime of each island against the height of each island allows us to detect correlations between the two. If there was efficient transfer of triplet excitons, we would expect longer delayed lifetimes at large islands, leading to a positive slope. The results for the samples with oxide grown between the Si and the tetracene are shown in Figure 4.5. The delayed lifetime is related to the slowest timescale fitted, $\tau_3$. For the thermal blocking oxide, we find a slope of $(-3.3 \pm 3.8) \cdot 10^{-2} \frac{\mathrm{ns}}{\mathrm{nm}}$ . The pyrene passivation in Figure 4.6 shows a slope of $(-3 \pm 2) \cdot$

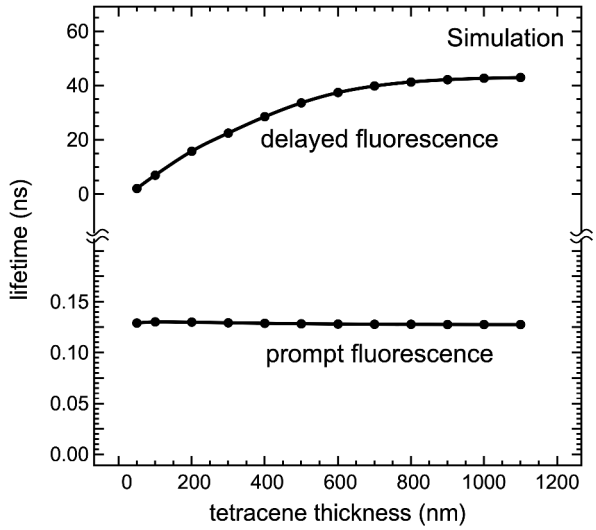


**Figure 4.4:** Simulation of the lifetimes of a tetracene slab on top of a quenching silicon surface. The values are extracted from Figure 4.2 with a double exponential fit. The delayed fluorescence describes the triplet lifetime and can be used to identify a quenching surface. After a certain thickness the quenching surface does not influence the triplets anymore and the lifetime levels off. The prompt fluorescence is not affected by the quenching surface and stays constant.

$10^{-2}\,\frac{\mathrm{ns}}{\mathrm{nm}}$, both compatible with the absence of any correlation between island height and delayed fluorescence lifetime. The absence of a slope with the pyrene surface passivation techniques in Figure 4.6 shows that there is either no or only very inefficient transfer of triplet excitons.

Different silicon treatments can lead to different tetracene growth modes and interface trap densities which could affect the triplet lifetime. However, the tetracene islands of one sample experience the same surface and environment, which allows us to compare these islands and observe quenching for each surface.

The model we have described above allows us to simulate different quenching efficiencies, from the simulations we can estimate that the

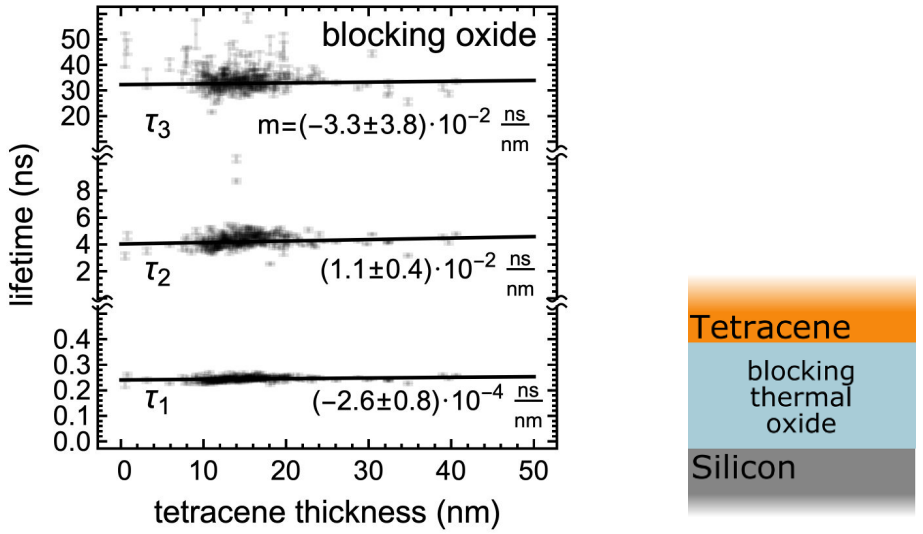


**Figure 4.5:** The results of the lifetime fitting for the blocking thermal oxide layer. Each data point represents one island. All three exponential functions needed to fit the data do not show a slope within the error, which excludes quenching effects at the interface.

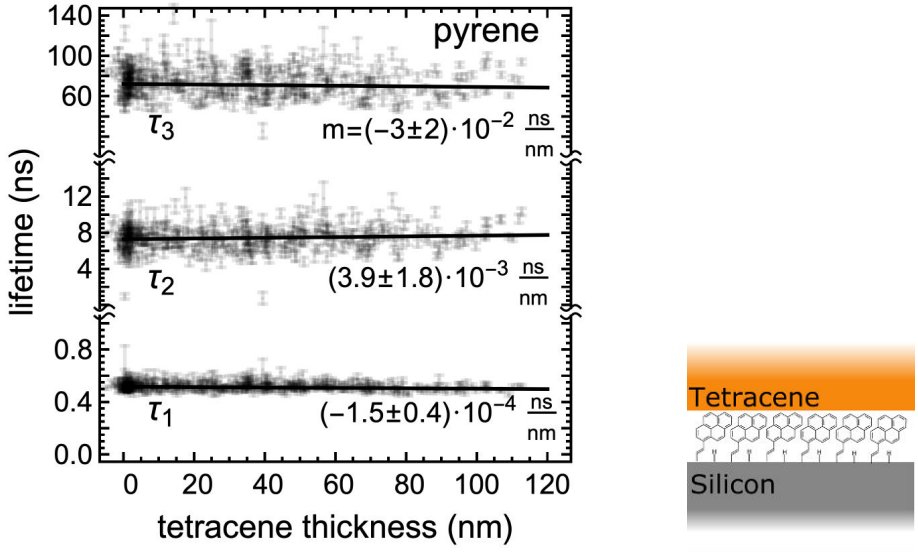


**Figure 4.6:** Lifetimes of islands on the pyrene treated silicon surface. All three lifetime components show no slope so they are in agreement with no quenching at the surface.

surface quenching in these samples is smaller than 20 $^{cm}/_{s}$ (Figure 4.13 in the Appendix).

We note that our method cannot distinguish between the presence of quenching at the interface by triplet transfer and quenching by charge transfer, surface traps etc.. There are large differences in the silicon surface treatments and presumably trap state density. We measured the surface recombination velocity for all the surface passivation methods described above to study the influence of trapping on triplet exciton lifetime. We find no significant difference in the recombination velocity between samples. This measurement suggests that the triplets are reflected at the interface for all surface treatments, independent of any differences in trap state density.

## 4.3 CONCLUSION

Any transfer of excitons would lead to a difference in recombination velocity, independent of the transfer mechanism. Therefore, our method cannot be used to distinguish between different mechanisms. However, the mechanism for triplet exciton transfer must be charge transfer or Dexter transfer, because Förster transfer is spin-forbidden. Dexter transfer is the correlated transfer of two electrons where an excited-state electron from the donor transfers into the excited state of the acceptor, and a ground-state electron from the acceptor transfers into the ground state of the donor. Alternatively, the triplet excitons could be quenched by the transfer of just one charge. Any charge transfer, including Dexter energy transfer requires the overlap of the triplet exciton wavefunction of tetracene with the acceptor wavefunction in silicon. Wavefunctions in excitonic materials typically attenuate exponentially with distance, so that close proximity between donor and acceptor is important. All our surface passivation layers are very thin ($\sim 1\,nm$), ensuring close contact between tetracene and silicon. Another important requirement for efficient transfer is the alignment of the triplet exciton wavefunction in relation to the silicon surface. The triplet exciton in tetracene is formed

mostly by the pi-orbitals, which reside on the face of the molecule. Thus, overlap of these wavefunctions would be most efficiently facilitated by horizontal growth where the long axis of the molecule is perpendicular to the silicon interface. We do not have a direct measurement of alignment of the first tetracene molecules on the silicon surface. Different surface passivation layers likely have different formation energies, leading to different alignments of the first crucial tetracene molecules, however we observe absence of quenching in all cases, indicating absence of wavefunction overlap. We note that the exciton wavefunction on tetracene is very localized [6] (the triplet exciton wavefunction has a theoretically calculated root mean square size of 0.35nm [97], experimentally measured to be 0.38 nm [6]) and therefore different in nature from the delocalized Bloch-waves that form the silicon band structure. This difference might introduce additional inefficiencies into the transformation process between the two.

The energy of the triplet exciton (1.25 eV) is larger than the silicon bandgap (1.1 eV) but this is not the only requirement for triplet exciton transfer; the energy levels of triplet exciton in tetracene and the bands in silicon have to align with respect to vacuum. This alignment should be fulfilled in HF-etched silicon [76] but they may misalign with our different surface passivation layers.

Since any of the bottlenecks discussed above can block the transfer of energy, it is important to develop microscopic models and measurements to investigate the rich physical system of the organic-inorganic interface. In this paper we have described a method for sensitive quenching detection at an interface between tetracene and silicon by only using a TCSPC lifetime map and AFM height data. Correlating the delayed fluorescence and the thickness of islands with different heights allows us to detect quenching of triplet excitons. Quenching is the necessary requirement for triplet exciton transfer, which would be technologically interesting for applications in singlet fission solar cells.

# APPENDIX

## SAMPLE FABRICATION

### Aromatic Monolayer Formation

#### *Hydrogen terminated surface preparation*

1 × 1 cm pieces of n-Si (111) were consecutively sonicated for 10 minutes in: acetone, ethanol and DCM. Subsequently the wafers were dried by a stream of argon and placed in Harrick plasma cleaner connected to a Harrick PlasmaFlo for plasma treatment. Followed by a purging of the chamber with Argon for 5 minutes. After 10 minutes of plasma treatment the samples were swiftly transported into a Nitrogen filled glovebox, where upon the samples were placed in an Argon saturated 40 % ammonium fluoride solution, to etch for 15 minutes. Next, the etched samples were rinsed with argon-saturated milli-Q-water and blown dry by a stream of argon [101].

### *Surface Modification Aromatics*

The freshly etched and rinsed surfaces were then submerged in 2 mL neat phenyl acetylene or a 20 % v/v mesitylene (in case of 2-ethtnyl naphthalene and 1-ethynyl-pyrene) solution of the desired solution which had been placed under high vacuum (10 mbar) for at least 1 h prior to submergence. The submerged samples were then kept at 80 °C overnight as was described in previous surface modification literature [116] after which the surfaces were washed with DCM within the glovebox and prior to storage again sonicated for 10 min in DCM.

### Monolayer Characterization

Static Contact Angle (SCA): Static water angle measurements were made with an automated Krüss DSA 100 goniometer. Depending on the size of the modified surfaces 2-3 droplets were dispensed on the surface and the contact angles were determined using a Tangent 2 fitting model. The standard error in the determined contact angles is approximately 1°.

### Ellipsometry

The elipsometric thicknesses of the samples were assessed by using a Sentech Instruments type SE-400 ellipsometer, operating at 623.8 nm (He-Ne laser), and an angle of incidence of 70°. The optical constants of a freshly etched hydrogen-terminated Si(111) surface were taken as $n = 3.821$ and $k = 0.057$. The reported values are the result of a planar three layered (ambient, monolayer, substrate) model with the assumed refractive indices of 1.00 and 1.46 for the ambient and monolayer respectively. All the reported values are averages of at least 10 measurements and the error is approximately 0.2 nm.

### X-ray Photoelectron Spectroscopy (XPS)

X-ray photoelectron spectroscopy (XPS) spectra were attained on a JPS-9200 photoelectron spectrometer (JEOL,Japan). The analysis was performed under ultra-high vacuum conditions using a monochromatic $Al\,K-\alpha$ X-rays $(h\nu = 1486.7eV)$ at 12 kV and 20 mA and an analyzer pass energy of 10 eV. A take-off angle $\varphi$ of 80° was used. All the XPS spectra were processed with Casa XPS software (2.3.18) and the binding energies were calibrated on the hydrocarbon ($CH_2$) peak with a binding energy of285.0 eV.

### Atomic Force Microscopy (AFM) of aromatic monolayers

Atomic Force Microscopy measurements were obtained by means of an Asylum MFP-3D Atomic Force Microscope which was equipped with a 100-micron closed-loop XY-stage which allows for AFM imaging as well as precise sample positioning. A minimum of two scans per modified surface at 20 x 20, 5 x 5 and 1 x 1 μm were made in standard ACAirTopography mode. After the measurements, a height and roughness profile was produced using the AFM Analysis tool in Igor Pro 6 with a third order flattening.

### Interlayer Characterization

In this section we will be further discussing the obtained results of the various aromatic organic monolayers on Si(111). The polyacene like monolayers are also referred to as the aromatic surfaces.

#### Silicon functionalized with aromatic surfaces

All the aromatic functionalized silicon surfaces summarized in Figure 4.7: silicon modified with phenylacetylene (Si-Ph) and silicon modified with 2-ethynyl-napthalene(Si-Naph), silicon modified with 1-ethynyl pyrene (Si-Pyr), silicon modified with 1-ethynyl pyrene and backfilled with 1-pentyne and respectively all three aromatic surfaces covered with a layer of tetracene (Si-Ar-tetracene) are all functionalized with two aims in mind. First, to prevent the oxidation of hydrogen-terminated silicon and second to enable or enhance the previously explained Dexter energy transfer into the silicon bulk. The following paragraphs will further elaborate as to how these aromatic monolayers were characterized.

### Characterization of the aromatic surfaces

After the aforementioned sample preparation and modification and prior to any characterization, three samples of each batch were measured by ellipsometry for a first indication of the quality of the desired monolayer.

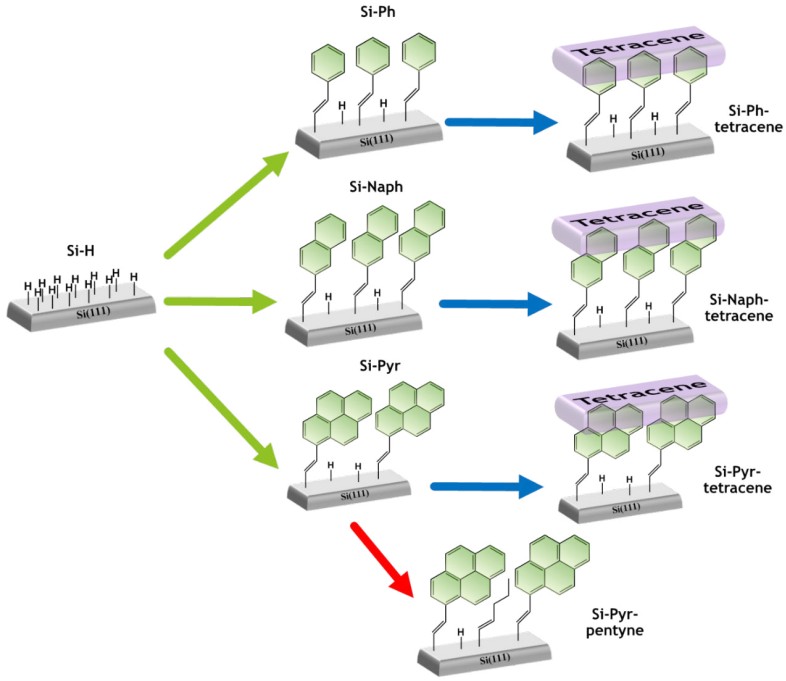


**Figure 4.7:** Overview of the different modifications of the various aromatic surfaces. First Si-H is modified with different SAMs to either Si-Ph, Si-Naph or Si-Pyr. These surfaces then have 4-40 nm tetracene deposited onto them resulting in Si-Ph-tetracene, Si-Naph-tetracene and Si-Pyr-tetracene. Alternatively, to prevent the rapid oxidation of Si-Pyr one can backfill surfaces with pentyne to counteract immediate oxidation resulting in Si-Pyr-pentyne for example.

| Mono layer | Theoretical (Chem 3D, Å) | Measured (Ellip, Å) (±2 Å) | C:Si (XPS, %) (±2 %) | Measured (XPS, Å) (±2 Å) |
|---|---|---|---|---|
| Phenyl acetylene | 6.5 | 10 | 23.3:75.5 | 9.2 |
| 2-ethynyl naphtal. | 8.5 | 12 | 25.9:68.0 | 11.0 |
| 1-ethynyl pyrene | 10.6 | 14 | 28.5/71.5 | 14.5 |

**Table 4.1:** Overview over the different heights per surface. The theoretical column is found measuring the differences of the top and bottom carbon in Chem3D, the measured column represents the averages of ellipsometry measurements, the C:Si ratio is obtained by the XPS wide scans and lastly the calculated column logically follows from using the previously found C:Si ratio in Equation 1.

The theoretical length of the monomer was assessed by using a model of the completely stretched out monomer in Chem3D. This would give an adequate upper-limit to what a completely sterile modified surface would look like. Table 4.1 accordingly summarizes the findings across several batches and several surfaces, note that the reported values are averages of all the measurements. Additionally, the thickness of the layer was also calculated by means of using the carbon: silicon ratio supplied by the XPS wide scans and the following equation:

$$Th_{xps} = \lambda_M^{Si} \sin(\varphi) \ln\left(1 + \frac{C}{Si}\right)$$

with $\lambda_M^{Si} = 38.5\text{Å}$ and $\varphi = 80°$, where $Th_{xps}$ represents the thickness from using the C:Si ratio found by the XPS wide-scan, $\lambda_M^{Si}$ being the attenuation length of the Si 2p photoelectron and $\varphi$ representing the angle between the surface plane and the detector.

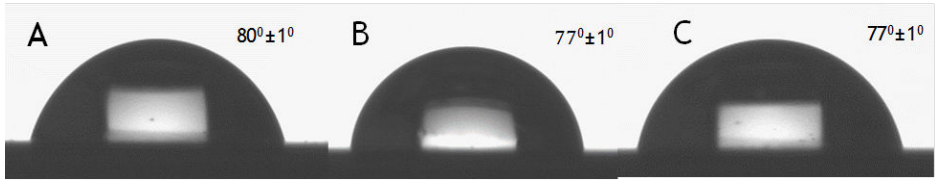


**Figure 4.8:** A) Snapshot of Si-Ph surface with a Mili-Q-water droplet with an SCA angle of 80°. B) A picture of Si-Naph with a Mili-Q-water droplet with an accordingly SCA of 77° and lastly C) is the same as A and B but now with a Si-Pyr surface also with a SCA of 77°.

Interestingly, both the measured and calculated heights of the functionalized surfaces exceed the theoretical upper limit of the completely stretched out molecule. The differences between the measured and theoretical values may be due to the uncertainty associated with the ellipsometry measurements (index of refraction, cleanliness of the silicon etc.) [3, 127]; however, Jakubowicz et al. have similar ellipsometric data when comparing p-nitrobenzenethiol monolayers on gold surfaces [54]. The ellipsometry data here can only serve as a qualitative support of the "monolayer" nature of the adsorbed film and thus the interpretation should be regarded with some degree of reservation until more evidence is available. Nonetheless, several anstrom differences by ellipsometry and an overestimation based on the carbon to silicon ratio by XPS also seem to point that there is some physio-absorption. To counter this the surfaces post modification are sonicated in DCM and toluene but the heights still exceed the upper limit found by Chem3D.

After checking the initial quality of the batch several other experiments were conducted to further assess the quality of the aromatic surfaces. Amongst these tests is the static water contact angle. On every surface a minimum of three drops were placed and for all three surfaces a minimum of two different batches were measured. Comparing the SCA findings (Figure 4.8) to those previously reported[3, 63] for Si-Ph it becomes apparent that the static contact angles are smaller than reported by Kondo et al.[63]. This difference could either be attributed to local impurities or a not perfectly homogeneous monolayer. Additionally, the

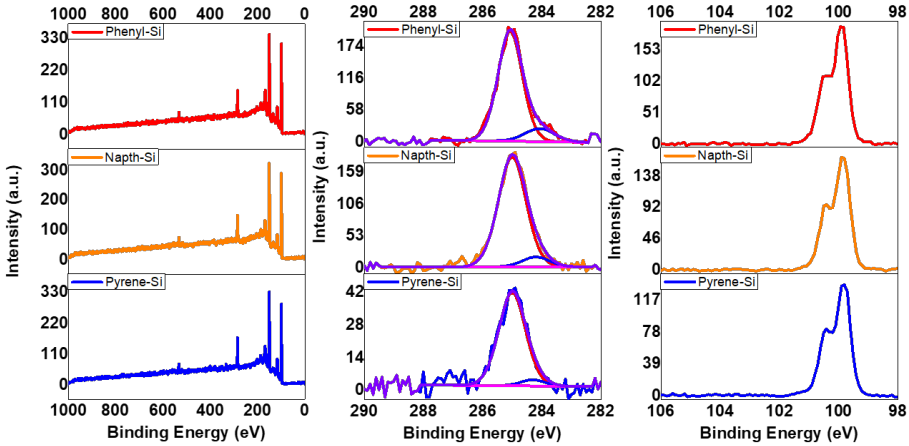


**Figure 4.9:** XPS data of different surfaces. Top row is the wide scan, the carbon narrow scan and the silicon narrow scan of a Si-Ph surface. Middle row is the wide scan, the carbon narrow scan and the silicon narrow scan of a Si-Naph surface. Bottom row is the wide scan, the carbon narrow scan and the silicon narrow scan of a Si-Pyr surface.

difference in SCA between Si-Ph, Si-Naph and Si-Pyr is hypothesized to be due to the lower density of these SAMs. These surfaces would more readily oxidize and therefore also show lower SCA values.

Having completed a first assessment of the various aromatic functionalized silicon surfaces, to either deem a batch successful or not, two samples were submitted for further XPS analysis. Figure 4.9gives an overview of the carbon and silicon narrow scans of Si-Ph, Si-Naph and Si-Pyr. In the Si narrow scans the emission peaks of 99.5 eV and 100.1 eV correspond to the $Si2p_{3/2}$ and $Si2p_{1/2}$ respectively (see Figure 4.9 right side column). More importantly a flat baseline around 103 eV is present in all surfaces; this is indicative of the absence of a silicon oxide ($SiO_x$) layer. This is of vital importance to the overall functioning of the proposed cascade outlined in the theory section as the oxide would act as a pacifying layer and thus the absence of it is key. Additionally, the absence of any other distinguishable peaks aside from the characteristic C-C peak (285 eV) in

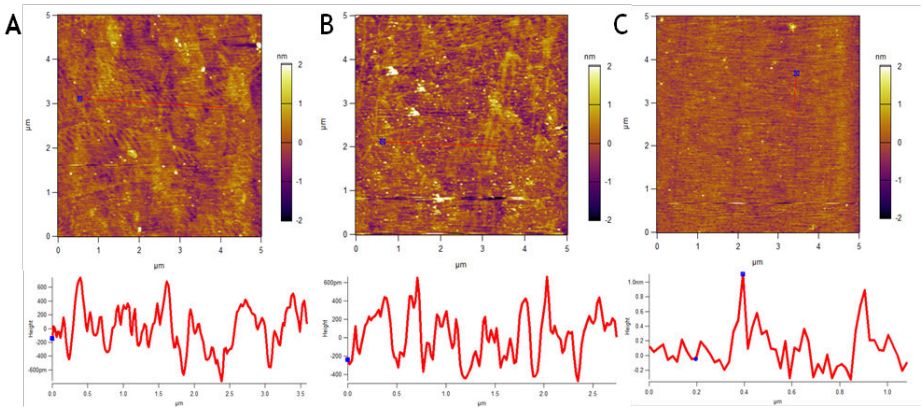


**Figure 4.10:** AFM and height profiles of A) Si-Ph (RMS = 0.4 ±0.2 nm), Si-Naph (RMS= 0.5 ±0.2 nm) and Si-Pyr (RMS= 0.3 ±0.2 nm)

the carbon narrow scan is a good indication that no carbons are bound to other heterogeneous elements (see Figure 4.9, middle column) and at 284 eV which corresponds to the Si-C=C- peak.

Lastly, AFM measurements were taken of a minimum of two surfaces at (at least) two different spots on the respective surface. Figure 4.10 shows the 5 µm areas of the Si-Ph, Si-Naph and the Si-Pyr modified surfaces, below each respective surface are profile plots to give an indication of the roughness of the surface. In the case of Si-Ph the upper and lower limit vary between −400 to600 pm or approximately 1 nm. Similarly, for Si-Naph the upper and lower limit are between −300 to 600 pm, and lastly with Si-Pyr the limits range from approximately −0.1 nm to 1 nm. The respective RMS values are 0.4,0.5 and 0.3 ± 0.2 nm for Si-Ph, Si-Naph and Si-Pyr respectively.

Together, the acquired data suggests that various aromatic surfaces were modified successfully and are oxygen free. The thicknesses range from $9 - 16$ Å which is within the typical Dexter Energy transfer range of $6 - 20$ Å. Similar results were obtained by Garg et al.[35] especially with respect to the SCA, ellipsometry and $1 \times 1$ µm AFM measurements. The key difference is that in their research they were modifying hydrogen-

terminated silicon with longer alkyl chains whereas in this research exclusively ethynyl substituted polyacenes were used.

## Thermal blocking oxide

For the samples with a thermal blocking oxide the silicon wafer was first HF etched (2 % HF aquous solution) for 3 minutes to remove the native oxide. The samples were then transferred into a rapid thermal annealing chamber and were heated under constant nitrogen flow of 1 l/min to 775 °C and kept at that temperature for 10 s under an $O_2$ flow of 1.5 l/min. The resulting $SiO_2$ film thickness was characterized with Ellipsometry to be 1.9 nm and XPS to be 2.4 nm following Lu et al. [74].

## Tetracene evaporation

Sample Preparation: Tetracene was evaporated inside an Angstrom Engineering thermal evaporation chamber at room temperature below $7 \times 10^{-7}$ mbar. Tetracene was bought from Sigma-Aldrich in 99.99 % purity and used as is. The nominal evaporation thickness was 2 nm at an evaporation speed of 1 Å/s. The samples were encapsulated in nitrogen atmosphere using two glass slides and a rubber gasket. We use a sharp needle to scratch a cross into the tetracene layer that serves as a reference to find the same area in the AFM and the TCSPC setup and facilitates the data overlay.

### AFM measurement of tetracene islands

AFM was measured with a Bruker Instruments Dimension Icon atomic force microscope in PeakForce tapping mode with Scan Asyst.

### TCPSC measurement

We performed all experiments in a home built TCPSC setup, using a PicoQuant LDH-D-C 485 nm laser, fiber coupled into a Nikon 60x water immersion objective (PlanAPO VC 60x A/1.2 WI). The same objective is collecting the photoluminescence. The excitation light is filtered with a 488 nm notch filter and a 500 nm longpass filter in the detection path. The detectors used are silicon-single photon avalanche detectors (Micro Photon Devices, MPD-5CTD). The detectors are connected to a PicoQuant HydraHarp 400 event timer with a repetition rate of 0.7 MHz. The TCPSC lifetime map is created by scanning a PI piezo stage. Control of the laser, piezo stage and detectors is handled by PicoQuant SymphoTime software. The average excitation density over time is estimated to be $80\frac{W}{cm^2}$.

## DIFFUSION MODEL

The Diffusion model uses the model of Piland et al. [95] as a starting point and. Piland and coworkers use a coupled differential rate equation for the density of singlets and triplets over time. We then add the 1D diffusion of both triplet and singlet excitons to the differential equation by using Fick's second law, resulting in the equations used in the main text.

The excitation source is modeled as a normal function with a variance of 150 ps which is also a realistic value for our experiment. The excitation function is also visible in light blue in Figure 4.11. We solve the differential equations for each time after the initial excitation.

The following constants have been used: $\mathrm{Diff_S} = 2.8\mathrm{cm^2/s}$ and $\mathrm{Diff_T} = 0.0023\mathrm{cm^2/s}$ taken from Wan et al. [137]. $\mathrm{kRad} = 8 \times 10^7\,1/\mathrm{s}$, $k_{IC} = 0$, $k_{ISC} = 0$, $k_{fiss} = 8.3 \times 10^9\,1/\mathrm{s}$, $k_{ee} = 1 \times 10^{-8}\mathrm{cm^3/s}$,

$k_{SD} = k_{RadS} + k_{IC} + k_{ISC} + k_{fiss} + k_{ee}$, $\mathrm{kTriplet} = 6.7 \times 10^6\,1/\mathrm{s}$, $\mathrm{kTS} = 0.5 \times 10^{-10}\mathrm{cm^3/s}$, $\mathrm{kTT} = 2 \times 10^{-10}\mathrm{cm^3/s}$, and $\mathrm{Excitation} = 30 \times 10^3\,\mu\mathrm{m}^{-3}$.

The boundary conditions for the singlet exciton density are as follows: $S(z, t = 0) = 0$ meaning there are no singlet excitons present before excitation. At the interface $\frac{dS(z,t)}{dz} = 0$ at $z = 0$, so that there is no flux of

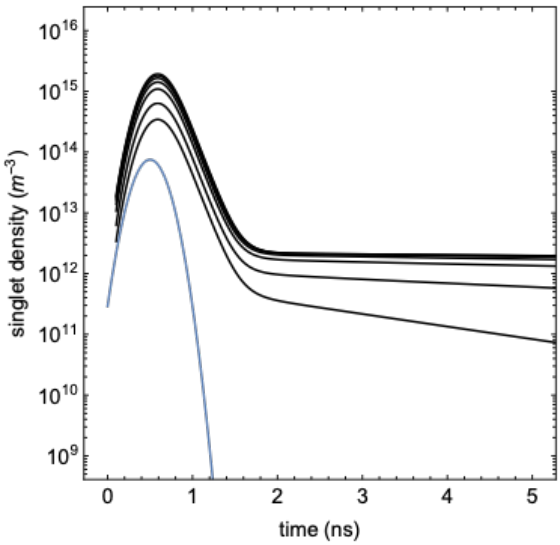


**Figure 4.11:** Simulation of Singlet decay upon excitation pulse (light blue) for different thicknesses of tetracene. The prompt fluorescence is not affected by the thickness. The blue curve indicates the excitation rate (in $m^{-3}ns^{-1}$).

singlets at the boundary of tetracene and silicon. The flux at the top of the tetracene slab is also set to zero (at z = thickness).

The boundary conditions for the triplet excitons are set so that there are no triplet excitons at time zero. At the top of the tetracene there is no outward flux of triplet excitons, just as with the singlet excitons. A crucial difference between singlet and triplet excitons in our model is the behavior at the tetracene-silicon interface, for triplets we set the density to zero at all times, which simulates perfect quenching at this interface.

We can also simulate a different quenching efficiency of the triplets in tetracene for a wide range of thicknesses. We implement this by replacing the boundary condition at the interface between tetracene and silicon. Before the triplet exciton density was set to zero at the interface - a perfect quenching scenario. Now we set the density the interface to a quenching rate which is the y-axis in Figure 4.12. From this plot it

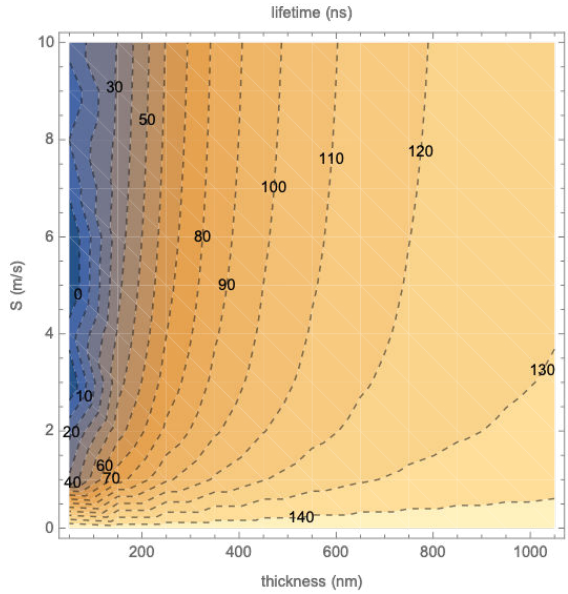


**Figure 4.12:** Plot of the delayed fluorescence as a function of the quenching speed, expressed in a surface recombination rate (m/s). The numbers in the plot are the delayed fluorescence lifetimes, with their corresponding contour lines. The quenching rate levels off for higher quenching rates.

becomes evident that below a certain quenching rate, here represented by a surface recombination velocity of 1 m/s, the lifetime change with thickness becomes shallower. This would mean that it would be harder to detect in the experiment, and the trend is also not linear any more.

We can use this plot to estimate a lower bound for the quenching rate that we observe in our experiment. A crosscut along Figure 4.12 in the horizontal axis (S, quenching rate) and for low quenching rates $< 1$ m/s shows at which quenching rates we should expect a slope of delayed lifetime vs thickness in our experiment. Even at 20 cm/s there is a significant slope, so we can safely conclude that our quenching rate is below 20 cm/s for all surfaces in the experiment.

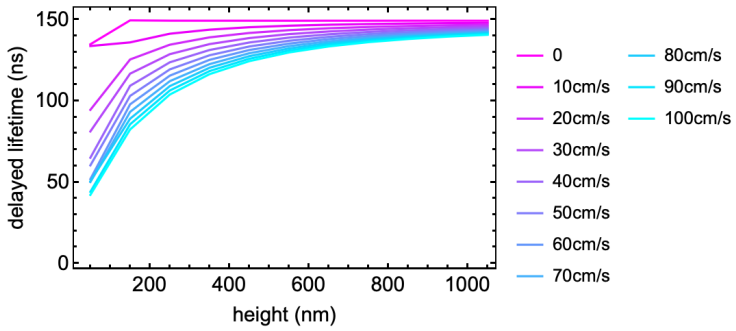


**Figure 4.13:** Horizontal cross cuts through Figure 4.12 in the low quenching regime for specific quenching rates. Even at 20 $cm/s$ there is still a considerable delayed lifetime slope that should be observable in the experiment.

## Transfer Matrix modeling of absorption in tetracene

We calculated the absorption of laser light with a transfer matrix model to investigate whether interference effects influence the absorption modelling in our diffusion model. In the diffusion model the absorption is assumed to follow the Lambert-Beer law.

The software used to perform the transfer matrix simulations is the Python implementation of a transfer matrix model developed at the McGehee group in Stanford [12]. The model assumes that the layers are flat and indefinitely large, which is not necessarily the case in the island structures we have on our samples.

We use the complex refractive index of air, tetracene and crystalline silicon to set up the simulation. The incoming light is a laser beam at 485 $nm$, orthogonal to the substrate, with a FWHM of 7 $nm$ and a power of 100 $mW/cm^2$, which corresponds to a current density of 40 $mW/cm^2$ (assuming an IQE of 100 %).

The absorption in the active material, tetracene, is calculated as a function of the thickness.

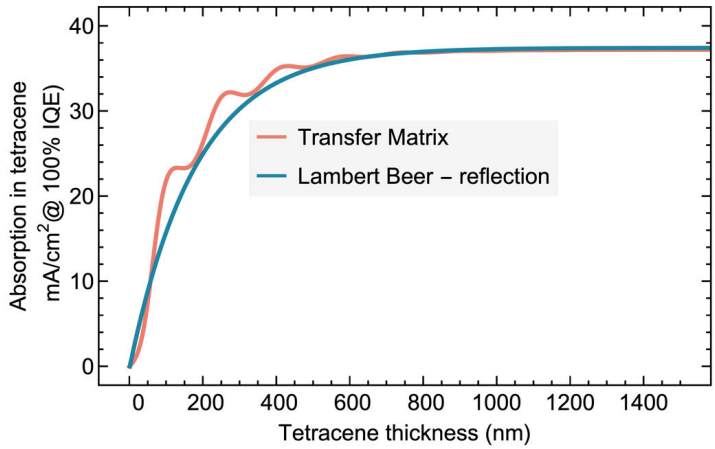


**Figure 4.14:** Comparison of the Lambert-Beer law of absorption and the transfer matrix calculations. The Lambert-Beer law is corrected for the reflection at the interface between air and tetracene. The oscillations on top of the lambert-beer absorption is due to interference effects included in the transfer matrix model.

Interference effects on the absorption are included in the transfer matrix calculations which leads to oscillations in the absorption as a function of thickness, visible in Figure 4.14.

These are secondary effects are neglected in the diffusion simulation, since the only change is in the initial charge carrier distribution inside the tetracene slab. Small differences here would not result in drastically different triplet distributions, and we have therefore chosen to use the simpler Lambert-Beer profile. For samples where the cavity effects are more severe one might chose to use transfer matrix modeling to determine the initial singlet exciton profile.

In addition to the absorption changes from the cavity effect, the singlet exciton can also change its lifetime close to a reflecting surface (Purcell enhancement [4]). We note, however, that the delayed fluorescence lifetime is determined by the slow triplet-triplet annihilation rate and not the singlet decay rate, so lifetime enhancement effects of a dipole emission

close to a dielectric surface can be neglected if the singlet fission rate is much larger than the singlet exciton emission rate, as is the case in tetracene.

### IDENTIFICATION OF ISLANDS

Procedure to identify islands in AFM and TCSCP data: In order to identify the islands in the AFM data we first import the raw AFM data and convert it into a grey scale image. This image as well as the TCSPC image is then converted into a black and white image. Since the background is changing slightly it is important to use a binarization function that only takes the immediate surroundings into account. The binarized image of fore- and background then allows us to dissect each island. The linear transformation between both AFM and TCPSC picture can be used to identify each island that are the same in each dataset. Figure 4.15 shows the quality of the overlap.

### HEIGHT DETERMINATION

The height of an island is defined by the mean of the top 25% of pixels. This measure is more robust to outliers than taking the maximum but still representative of the maximum height of the island. Figure 4.16 shows the difference between different ways of measuring the height of a tetracene island for one example island.

### FITTING OF TCSPC DATA

By summing up the TCSPC data for each island we can fit the very low intensity PL decay of the delayed fluorescence. Since the delayed fluorescence is several magnitudes less intense than the prompt fluorescence the

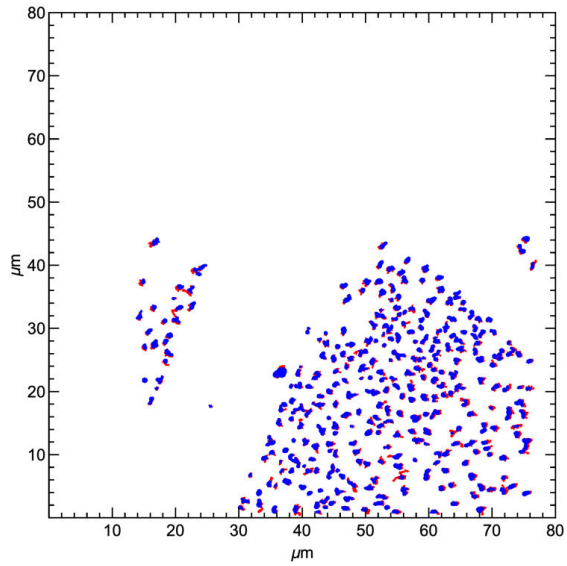


**Figure 4.15:** Blue is TCSPC and Red is AFM data. The overlay of islands is good, which allows us to compare AFM and TCSPC data on an island to island basis.

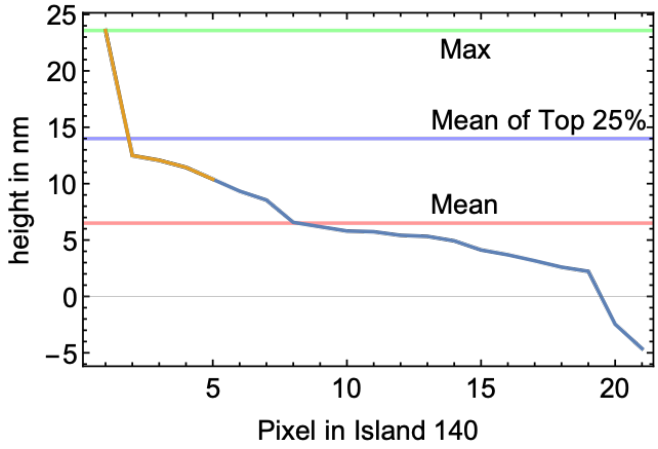


**Figure 4.16:** All height values of one typical island sorted by height. Green: maximum value. Blue: mean of top 25 %. Red: mean of all pixels. The line in orange are the largest 25 % of the pixels, used to calculate the blue line.

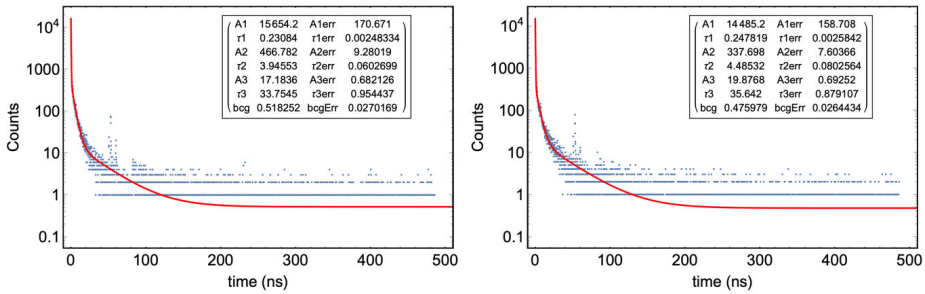


**Figure 4.17:** Fit of two example islands of the oxide sample for the three-exponential function with the MLE fitting algorithm. Resulting parameter estimates and errors are shown in the inset.

number of photons in the delayed fluorescence is low and each photon is important for the noise level.

We need three exponentials to properly describe the data. One for the prompt fluorescence, one for the intermediate region and one for the delayed fluorescence. This can only be seen as a representation of the data and cannot be used to rationalize an underlying rate-equation model. It is however sufficient to quantify the changes in each lifetime with a change in height.

Since the we only have a few photons in the low intensity region of the PL decay traces, fitting with an algorithm that uses the sum of the least-squares is no longer valid. The least-squares fitting assumes the noise of the data to be distributed like a normal distribution. In our case though the proper noise distribution is poissonian since we count individual photons. In most cases this difference is not important since the normal distribution approximates the poissonian distribution well if the mean is larger than 15. In our experiment the number of photons per bin is regularly below 10, so we cannot use the least squares fit. The proper cost function to minimize to find the best fit is the so-called Maximum-Likelihood-Estimation. With this method we can define the correct Poissonian noise distribution. We have implemented this algorithm in MATHEMATICA 12. Two example fits can be seen in Figure 4.16.

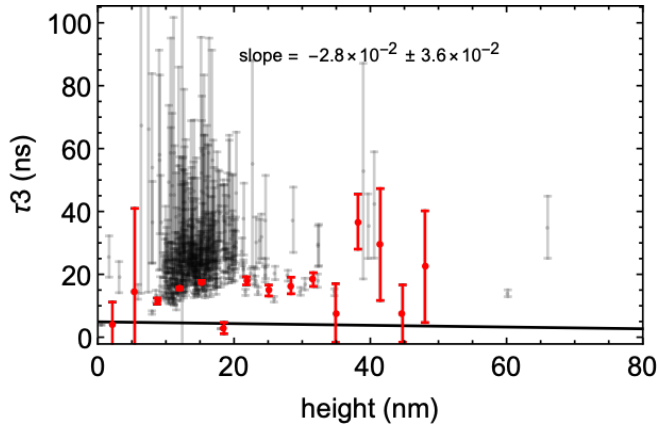


**Figure 4.18:** Fitting of thermal oxide islands fitted with the standard least-squares algorithm. The error bars are extremely large and the mean value does not correspond with the MLE fitting result. Each grey point represents one tetracene island, the red points are averages of the grey points in a certain height range.

The need for the proper account of the noise can also be seen if we attempt to fit the data with the standard least-squares fitting as implemented in the MATHEMATICA function NonLinearmodelFit. The error bars are much larger and the mean value of the long lifetime is also far from the real value retrieved by the MLE fitting. This is shown in Figure 4.18.

It has also been suggested in literature [95] to only fit the end of the decay with one exponential as a way to measure the delayed fluorescence lifetime. This however is heavily dependent on the starting point of where we fit the data. In Figure 4.19 we can see that the slope of lifetime vs. height we get from the tetracene-oxide sample is positive, negative, or zero depending on the start value of the fit, eg. how many data points are considered to be part of the delayed fluorescence. We therefore deem this fitting procedure unreliable for our dataset.

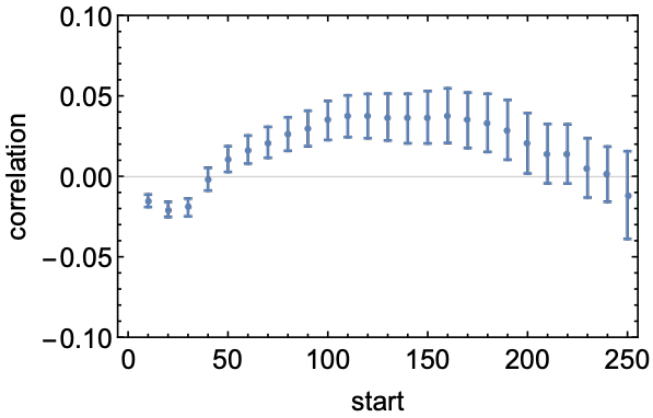


**Figure 4.19:** Slope of delayed lifetime vs. height for the tetracene-oxide sample as a function of the start value of a mono-exponential fit. The value of the slope and therefore the indication of quenching is highly dependent on the start point.

## SURFACE PASSIVATION MEASUREMENT USING PHOTOCONDUCTANCE

Microwave photoconductance decay (μPCD) measurements were performed on a Semilab WT-2000 tool. After illumination of the sample with a 200 ns laser pulse (904 nm, $1.2 \times 10^{12}$ photons/pulse), photoconductance decay is determined from the reflected microwave intensity (at 10.3 GHz), which is a measure of the free carrier concentration in the sample. The carrier lifetime is then extracted from the recorded transient. Lifetime maps were recorded with a 1 $mm^2$ laser spot and 125 or 250 μm step size. We can see in Figure 4.20 that the free carrier lifetime does not differ significantly between the different functionalized samples and bare silicon, indicating a poor surface passivation effect of the functionalized samples.

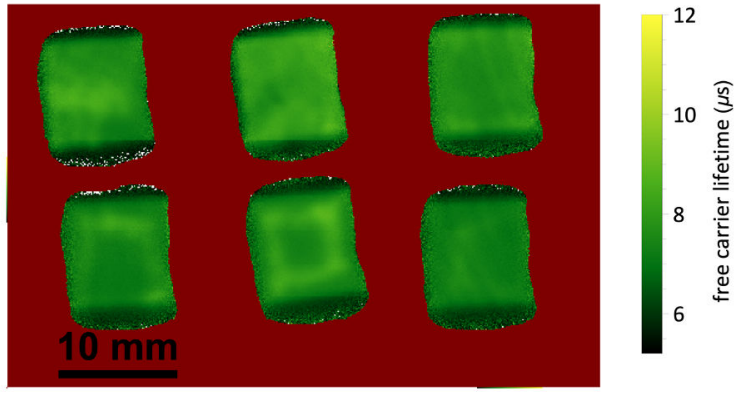


**Figure 4.20:** Free carrier lifetime in silicon for six different 10x10 mm silicon samples. The top row are the functionalized silicon samples, with Si-Ph, Si-Naph or Si-Pyr from left to right. The bottom row is bare n-doped silicon <111>. We can see that the passivation quality is comparable between all samples.

# 5 CHANGE IN TETRACENE POLYMORPHISM FACILITATES TRIPLET TRANSFER IN SINGLET FISSION-SENSITIZED SILICON SOLAR CELLS

This chapter is based on the following publication [20]:

Benjamin Daiber*, Sourav Maiti*, Silvia M Ferro, Joris Bodin,Alyssa FJ van den Boom, Stefan L Luxembourg, Sachin Kinge, Sidharam P Pujari,Han Zuilhof, Laurens DA Siebbeles, and Bruno Ehrler. "Change in Tetracene Polymorphism Facilitates Triplet Transfer in Singlet Fission-Sensitized Silicon Solar Cells" In: *The Journal of Physical Chemistry Letters* (2020)

Singlet fission in tetracene generates two triplet excitons per absorbed photon. If these triplet excitons can be effectively transferred into silicon (Si) then additional photocurrent can be generated from photons above the bandgap of Si. This could alleviate the thermalization loss and increase the efficiency of conventional Si solar cells. Here we show that a change in the polymorphism of tetracene deposited on Si due to air exposure, facilitates triplet transfer from tetracene into Si. Magnetic field-dependent photocurrent measurements confirm that triplet excitons contribute to the photocurrent. The decay of tetracene delayed photoluminescence was used to determine a transfer efficiency into Si of around 36 %. Our study suggests that control over the morphology of tetracene during the deposition will be of great importance to boost the triplet transfer yield further.

## 5.1 INTRODUCTION

Silicon is currently the dominating semiconductor material for solar cells, but suffers from several loss mechanisms that reduce its efficiency [103, 108]. The largest loss mechanism results from the inefficient utilization of high-energy photons. The additional energy between the Si band gap and the high-energy photons is lost to heat. Sensitizing Si solar cells with a top layer of singlet fission material can reduce this loss, and theoretically even overcome the detailed balance efficiency limit of ~ 31 % for a single-junction solar cell [7, 17, 30, 34, 37, 64, 84, 91, 104, 115, 119, 128].

Singlet fission is a spin-allowed process of creating two triplet excitons from one singlet exciton that can occur in certain organic semiconductor materials with delocalized $\pi$-orbitals [117–119, 124]. In this paper, we will focus on tetracene, which consists of four benzene rings that are annularly and linearly fused (Figure 5.1). Upon absorption of a high-energy photon ($> 2.4\,\mathrm{eV}$), a singlet exciton (bound electron-hole pair) is formed. This singlet exciton ($S_1$) can subsequently be split into two triplet excitons ($T_1$) with each roughly half the energy of the singlet exciton. This singlet fission process is mediated by a pair of spin-correlated triplets (TT), based on the kinetic model proposed by Johnson and Merrifield in 1970 [44, 56]:

$$S_0 + h\nu \Rightarrow S_1 \Rightarrow (TT) \Rightarrow T_1 + T_1$$

where $S_0$ is the singlet ground state, $h\nu$ the incoming photon energy, and $T_1 + T_1$ a pair of free triplets. In this model, the rate of singlet fission is determined by the coupling between the $S_1$ and TT states [80, 94]. Singlet fission competes with other processes (e.g. radiative and non-radiative recombination and excimer formation), such that some singlet excitons are lost and cannot undergo singlet fission. In tetracene, one absorbed photon leads to close to 2 triplet excitons, as singlet fission is very fast compared to other competing decay channels [11, 13].

In a solar cell architecture where the triplet exciton is transferred into Si, the bandgap of the Si cell has to be smaller than the energy of the triplet

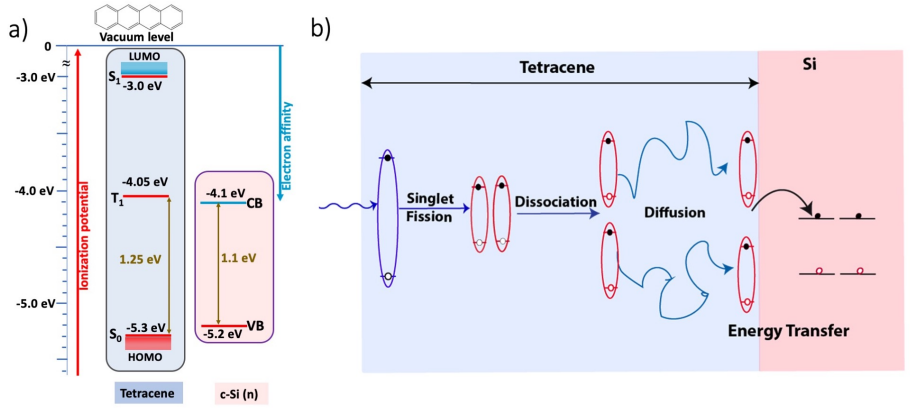


**Figure 5.1:** a) Energy alignment of tetracene in the ground state ($S_0$), triplet state ($T_1$), singlet state ($S_1$) and Si valence band (VB) and conduction band (CB) from the literature [13, 76, 131, 149]. The structure of tetracene is shown at the top. b) Schematic of a singlet fission-sensitized Si solar cell. Photons at or above the singlet energy of tetracene are absorbed and create one singlet exciton, which splits into two triplet excitons forming a correlated triplet pair (TT) via singlet fission. The TT dissociates into free triplets which can then independently diffuse to the tetracene-Si interface and transfer into Si to generate free charge carriers.

exciton state of the singlet fission material. In tetracene, the triplet energy is $\sim$ 1.25 eV which exceeds the Si bandgap of 1.1 eV, allowing triplet exciton transfer [13, 76, 109, 131]. The $V_{oc}$ is determined by the low-bandgap semiconductor Si and the photocurrent from the high-energy photons can be doubled due to singlet fission that eventually generates two electron-hole pairs from the high-energy photons of energy $> 2.4$ eV.

Triplet transfer to Si can happen through energy transfer or charge transfer. In the case of energy transfer, both electrons and holes arrive in Si concurrently. However, if either electrons or holes are transferred into Si via charge transfer, the remaining countercharges in tetracene have to be extracted by an additional contact [76]. Hence, if triplet energy transfer into Si could be realized the resulting tetracene-Si solar cell would not need an additional charge extracting electrode on top of the tetracene

layer. Therefore, energy transfer could in principle enable a simpler solar cell architecture and less added cost to silicon solar cell manufacturing. As the tetracene triplet energy is higher than the Si band gap, transfer into Si is energetically allowed. Figure 5.1 a) shows the ionization energy of the tetracene exciton states and the position of the Si bands. The absolute energy level of the triplet exciton ionization energy with respect to the vacuum level is reported to be in the range of −4.0 eV to −4.3 eV [13, 76]. Figure 5.1 b) shows a schematic of the processes involved in the operation of a singlet fission-sensitized Si solar cell, singlet generation, singlet fission, triplet diffusion, and triplet transfer.

To date, the transfer of triplet excitons from the singlet fission layer to the underlying low-bandgap semiconductor has proven to be the bottleneck for real-world applications. The extraction of triplets directly from tetracene into Si has been investigated by several research groups. Piland et al. did not find any evidence of triplet transfer from tetracene into Si upon direct deposition and with a LiF spacer [95]. MacQueen et al. reported a small contribution of triplets to the photocurrent upon direct deposition of tetracene on a Si solar cell [76]. The reasons for inefficient triplet transfer could be related to insufficient passivation of the Si surface and the weak coupling between the triplet exciton molecular orbitals and the electronic states in Si. Recently, Einzinger et al. unambiguously reported successful triplet transfer from tetracene into Si with 75% efficiency after passivating the Si with a thin (8 Å) dielectric layer of hafnium oxynitride ($HfO_xN_y$)grown through atomic layer deposition (ALD) [29]. The ALD-grown interlayer passivates the Si surface and is thin enough to allow the transfer of triplets from tetracene into Si. However, this system is very sensitive to the exact interlayer thickness and composition, and the effect of the tetracene structure remains unclear. The transfer mechanism is still under debate and additional self-passivation effects complicate the interpretation.

Here we report evidence for the triplet exciton transfer in a simpler system, from tetracene into bare Si, after exposure of the tetracene layer to ambient air. We find signatures of triplet exciton transfer in magnetic field-dependent photocurrent measurements and a faster decay of the delayed photoluminescence (PL) from tetracene, indicating triplet exciton

quenching. We correlate these changes to a change in tetracene morphology as seen in X-ray diffraction (XRD) spectra that show the conversion of polycrystalline tetracene from polymorph I (TCI) to polymorph II (TCII) [5, 112]. We propose that the change of tetracene polymorph is important for the observed triplet transfer into Si solar cells.

## 5.2 RESULTS

### 5.2.1 Triplet Signature in Photocurrent

Measuring the effect of triplet excitons on the photocurrent of a solar cell is the most direct way of measuring the transfer of triplet excitons, and is most relevant for the real-world application of a singlet fission-sensitized Si solar cell. The final goal is to increase the Si photocurrent from transferred triplet excitons. However, both singlet and triplet excitons can contribute to the photocurrent. Therefore, it is important to prove whether photocurrent originates from triplet versus singlet excitons. To distinguish between singlet and triplet exciton transfer we exploit the behavior of singlet fission under a magnetic field (see Figure 5.2). Under a magnetic field of 300 mT singlet fission in tetracene becomes less efficient, resulting in a lower triplet exciton population compared to the situation without the magnetic field [79]. The characteristic shape of the photocurrent change under a magnetic field can be unambiguously attributed to triplet excitons originating from singlet fission [29, 44, 144]. If the photocurrent from Si has the same magnetic field dependence as the triplet population (blue curve in Figure 5.2 a)) we conclude that there is transfer of triplet excitons into Si.

The photocurrent is caused prevalently by triplet transfer; the opposite magnetic field dependence (yellow curve in Figure 5.2 a) would indicate that the photocurrent is dominated by singlet transfer or radiative transfer. The relationship between magnetic field and singlet fission efficiency (or singlet/triplet populations) is not monotonic, below 50 mT there is a small dip in the opposite direction as described by Merrifield et al. (see also Figure 5.2 a) [79]. This characteristic curve also allows us to exclude

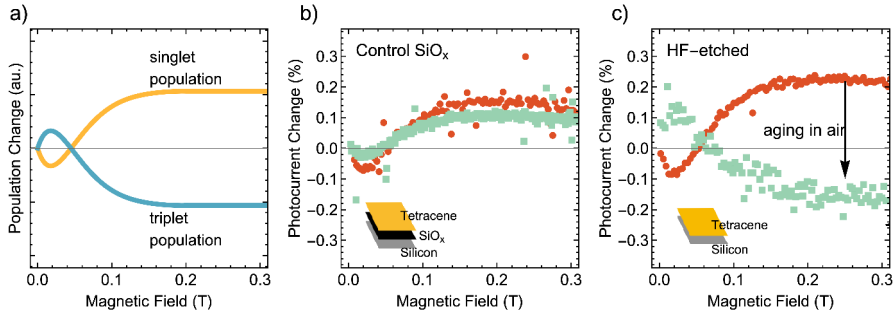


**Figure 5.2:** a) Schematic for the behavior of singlet and triplet population in tetracene for photocurrent as a function of the magnetic field. b/c) Magnetic field-dependent photocurrent measurements for b) $Si/SiO_x$/tetracene (control), and c) HF-Si/tetracene, both before (red curve) and after (green curve) exposure to air. For both samples b) and c) the positive change in photocurrent can be attributed to the dominant contribution of singlets. Aging the HF-etched sample in air flips the curve and leads to a triplet curve, indicating that triplets are transferred and contributing to the Si photocurrent.

any other effects that the magnetic field could have on the photocurrent, like a displacement of the sample, induced currents at the contacts, or sample degradation over time.

We fabricated Si solar cells with an additional tetracene singlet fission top layer. The solar cells are heterostructure with intrinsic thin (HIT) layer solar cells with an interdigitated back contact (IBC). This means that contacts are on the back, which allows free access to the front surface. The solar cells are then encapsulated in an inert $N_2$ atmosphere between two glass slides to keep oxygen and moisture out. Between the tetracene layer and the Si solar cell we used different interlayers for reference measurements and to gain insight into the transfer mechanism. We then measured the photocurrent as a function of an externally applied magnetic field as described above. Figure 5.2 b) shows the magnetic field dependent photocurrent of solar cells with an insulating interlayer of $\sim 2\,\text{nm}$ $SiO_x$, which shows no signature of triplet exciton transfer. A thick ($\sim 80\,\text{nm}$) $Si_3N_4$ (SiN) interlayer shows the same blocking behavior, as

shown in Figure 5.6 a) in the Appendix. The photocurrent follows the curve we would expect for singlet excitons, indicating that the singlet excitons contribute to the photocurrent. Utilizing a HF-etch to remove the blocking layer and enabling direct contact between tetracene and Si (HF-Si/tetracene) does not change this behavior, as seen in Figure 5.2 c) (red curve), which is in line with earlier reports [95]. The photocurrent still follows the singlet exciton population, and no evidence for triplet transfer is observed.

Si/$SiO_x$/tetracene and HF-Si/tetracene samples were then stored in the air under ambient conditions in the lab for five days and re-measured (Figure 5.2 b) and c)). The magnetic-field dependence of the photocurrent curve for the HF-Si/tetracene solar cell, shown in Figure 5.2 c), reverses for the air-exposed sample, closely following the characteristic shape for a triplet exciton population, which is strong evidence for triplet exciton transfer. If we encapsulate the solar cell and store it in air, we also observe the triplet curve, although its emergence is then much slower, i.e. after six weeks, as shown in Figure 5.6 b) (see Appendix), indicating that eventually, air enters the encapsulation. If the HF-Si/tetracene solar cell is stored under a dry nitrogen atmosphere in the glovebox ($< 10\,\mathrm{ppm}\,O_2; < 1\,\mathrm{ppm}\,H_2O$), we instead observed the singlet curve, which was retained after six weeks (Figure 5.6 c), Appendix). The strong difference in magnetic-field photocurrent behavior between the air-exposed and nitrogen-stored samples indicates that air-exposure plays a crucial role in enabling successful triplet transfer to Si. In Figure 5.2 c) the decrease in photocurrent at high field is around 0.2%, which is comparable to silicon-tetracene solar cells with $HfO_xN_y$ interlayers [29]. In that study the self-passivation in Si, due to improved surface screening by charge carriers at the Si interface, caused an increased photocurrent [29]. This self-passivation can lead to an overestimation of the contribution of triplet exciton injection, and the effects of triplet excitons and self-passivation were separated by a strong background illumination. We performed similar experiments to investigate the self-passivation of Si in our samples by using a strong (100 W) xenon light source with red light below the absorption onset of tetracene but above the absorption onset of Si. This allows us to inject charge carriers directly in Si that

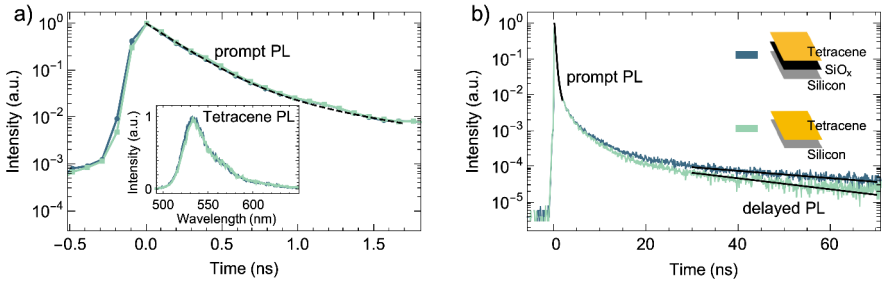


**Figure 5.3:** The PL decay traces in Si/$SiO_x$/tetracene and HF-Si/tetracene solar cells. Both samples have been aged in the air under similar conditions. The dotted black line represents the output from the kinetic model; a) short-time (prompt) PL shows no difference in singlet fission time and efficiency between samples; b) long time (delayed) PL shows faster decay for the HF-Si/tetracene solar cell, which we attribute to triplet transfer into Si. The inset in a) shows the PL spectra of both samples.

cannot have originated in tetracene. We did not see an influence of this additional light on the photocurrent change under the magnetic field after correcting for the additional bias current, so we can exclude large influences from self-passivation in the Si solar cell (see Figure 5.7, Appendix). Therefore, we can conclude that exposure to air leads to triplet transfer from tetracene into Si. We also measured the external quantum efficiency (EQE) of the HF-etched solar cell and the same solar cell before and after aging (Figure 5.8, Appendix). After accounting for measurement position variation, we saw a small increase in EQE over the region of tetracene absorption, an increase likely within the noise level of our measurement. The tetracene layer is thicker than the triplet exciton diffusion length, and charge carriers are injected near the interface where the passivation is poor, leading to little additional photocurrent from triplet excitons [2]. The following experiments will offer additional evidence for triplet exciton transfer and insight into the dynamics and mechanism.

### 5.2.2 Quenching of delayed photoluminescence

To investigate the mechanism, timescale, and yield of the transfer process of triplets into Si, we measured the tetracene PL decay both in the solar cells and tetracene deposited on Si wafers. The inset in Figure 5.3 a), compares the PL spectra of Si/$SiO_x$/tetracene and HF-Si/tetracene solar cells after exposure to air, showing the characteristic tetracene 0-0 emission peak at 535 nm with a shoulder at 580 nm due to the 0-1 transition, and a broad defect emission around 615 nm. This defect emission arises from structural defects in tetracene during the vacuum evaporation process [93, 135]. The PL spectra are the same for both the samples upon air exposure, thus the PL spectra show no evidence of additional trap states from the aging process in samples with and without the $SiO_x$. The PL in tetracene originates from singlet exciton emission. The PL decay shows a fast initial component due to singlet fission at short times ($<$ 1 ns, prompt PL) and a long-lived delayed PL arising from the triplet-triplet annihilation to singlet excitons at later times ($>$ 40 ns, delayed PL). The prompt PL decay is identical for the aged samples with and without the $SiO_x$ blocking layer, showing that the singlet fission rate is not affected by the blocking layer (Figure 5.3 a). However, the delayed PL component was faster in the HF-Si/tetracene solar cell upon air exposure, which provides additional evidence for the depopulation of triplets in tetracene caused by triplet transfer into Si (Figure 5.3 b). Since triplet excitons disappear from tetracene because they are transferred into Si, triplet-triplet annihilation is reduced which in turn reduces the delayed PL intensity. The PL lifetime measurements have been reproduced with solar cell samples having a SiN blocking layer (Figure 5.9, Appendix) showing no evidence for triplet transfer, just like in the $SiO_x$ samples. The samples with and without the blocking layer in Figure 5.3 b) and Figure 5.9 have been aged under similar conditions, the tetracene layer was exposed to air in all cases but we only see delayed PL quenching in the sample without the interlayer. We can, therefore, exclude that oxygen quenching of the triplets leads to the faster delayed PL. The samples with the SiN blocking layer and HF-Si have been measured at different spots of the solar cell (Figure 5.10, Appendix), and showed no dependence on the measurement position on

the samples. To reconfirm the results PL decay measurements were performed in tetracene deposited on Si wafers (i.e., not a full solar cell) with and without the $SiO_x$ blocking layer, and similar results were obtained (see Figure 5.11, Appendix). This ensures that the observed PL dynamics are a characteristic of the HF-Si/tetracene interface, and that it is not influenced by the presence of other solar cell components. Together with the magnetic field-dependent photocurrent measurements, we correlate the faster decay in the delayed PL to triplet quenching to the triplet transfer process from tetracene into Si.

### 5.2.3 Tetracene Polymorphism

What is the mechanism of activating triplet transfer in the HF-Si/tetracene samples after aging in the air? The activation could originate from either a change in the tetracene or of the HF-Si interface or both. We deployed X-Ray diffraction (XRD) to detect changes in the tetracene morphology and X-ray Photoemission Spectroscopy (XPS) to investigate changes on the HF-Si surface.

Two different polymorphs, created by heated (TCI) or cooled (TCII) substrates can form during tetracene deposition.

The TCII polymorph has different packing with increased distance along the c-axis compared to TCI, resulting in a lower diffraction angle in XRD along the (00c) diffraction [112]. Before air exposure, the XRD spectra show the presence of both polymorphs with slightly more TCI ($2\Theta = 7.3$) compared to TCII ($2\Theta = 6.9$) as seen in Figure 5.4. However, after air exposure, the ratio reversed with more TCII compared to TCI, suggesting a change in polymorphism in tetracene. The two polymorphs have different intermolecular coupling strengths due to a difference in molecular orientations that leads to a faster singlet fission rate in TCII compared to TCI as reported by Arias et al [5]. The transition between both polymorphs is smooth (Figure 5.12, Appendix) and is not triggered when storing the samples in nitrogen for seven months (Figure 5.13, Appendix). We also observe a change in singlet fission rate, as the prompt PL decay of tetracene deposited on quartz becomes faster after air exposure

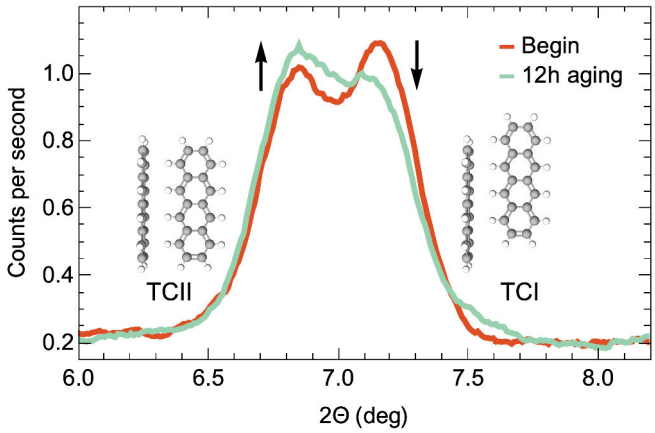


**Figure 5.4:** XRD of tetracene deposited on fresh HF-Si/tetracene and after 12 h of air exposure. We observe a conversion of TCI to TCII.

(Figure 5.14, Appendix). To confirm that the change responsible for triplet transfer is the aging of tetracene and not the aging of the HF-Si surface we exposed HF-Si samples to air for different amounts of time, to grow a $SiO_x$ layer with various thicknesses. We measured XPS to confirm the growth of this $SiO_x$ overlay by monitoring the Si-$O_x$ peak in the Si 2p photoelectron emission narrow scan (Figure 5.15 a) and b), Appendix). On these samples, we deposited fresh tetracene and measured the PL-decay. Triplet transfer was not observed in these samples (Figure 5.15 c), Appendix) confirming that triplet transfer is not associated with the growth of a $SiO_x$ layer, and the aging and subsequent change in the polymorphism of tetracene is related to the triplet transfer. Triplet transfer via a direct Dexter-type mechanism is dependent on the overlap between the triplet exciton wavefunction of tetracene and of the electron and hole wavefunctions at the Si surface [24]. This coupling will change depending on the distance and orientation of the tetracene molecules with respect to the Si surface. Therefore, the change in the orbital coupling in going from TCI to TCII and its effect on the triplet transfer efficiency is likely crucial and needs to be investigated further theoretically. A recent report by Niederhausen et al. that deployed near-edge X-ray absorption fine

structure (NEXAFS), XPS, and density functional theory (DFT) calculations also suggests that different orientations at the interface exist and could lead to a change in transfer efficiency [85].

### 5.2.4 Triplet Transfer Efficiency

To extract the triplet transfer rate and transfer efficiency we model the PL decay data considering the singlet fission process as depicted in Figure 5.5 a) [5, 95, 141]. The singlet fission process in tetracene (with rate: $k_{SF}$) competes with the radiative decay ($k_{Rad}$) through the formation of triplet pairs, which can then dissociate ($k_{Diss}$) to form free triplets or fuse back ($k_{TT}$) to create an excited singlet state. The free triplets can decay with the triplet lifetime ($k_{Trip}$), or regenerate the triplet pair state through triplet-triplet annihilation ($k_{TTA}$). TTA results in the delayed PL from tetracene and determines the triplet lifetime [10, 43, 95]. The populations of the $S_1$, TT and T states can be determined by solving the coupled differential equations as detailed in the Appendix. The $S_1$ population is plotted against the measured PL decay traces in Figure 5.3 (dotted lines) for the prompt and delayed PL. The rate constants described above were determined by solving the differential equation for HF-Si/tetracene before and after exposure to air and using a least-squares algorithm to fit the data as described in the Appendix. The rate constants obtained are in agreement with the literature as shown in Table 1, Appendix. The singlet fission time constant was determined to be $220 \pm 1$ ps, which is in good agreement with reported values of $\sim 75 - 200$ ps depending on the crystallinity, grain size and preparation conditions [5, 10, 93, 95, 141, 148]. The faster decay of the delayed PL can be reproduced with the kinetic model by incorporating an additional triplet transfer process to Si without changing the other rate constants. The model based on these kinetic equations reproduces the data for prompt (until 1.7 ns) and delayed PL ($> 30$ ns) well, but fails to describe the decay at intermediate times between prompt and delayed PL. This is most likely due to additional effects of triplet pair diffusion, which have been explained by modeling that leads to a $t^{-\frac{3}{2}}$ dependence of the PL decay [113]. Our

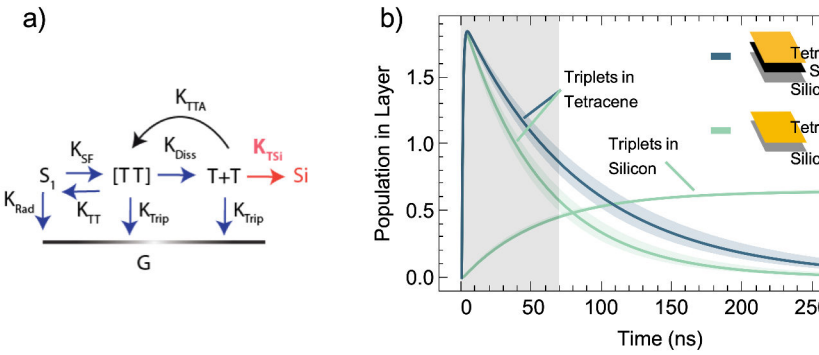


**Figure 5.5:** a) Schematic representation of the kinetic model used to determine the triplet transfer efficiency b) the triplet population in $Si/SiO_x$/tetracene (control), HF-Si/tetracene and in HF-Si after air exposure predicted from our model as a function of time. The grey area shows our experimental range of the PL decay measurements (70 ns). Transparent bands are 95 % confidence intervals of the fitting parameters.

intermediate PL decay data is also described by this function (Figure 5.16, Appendix) [113].

From the kinetic model, the triplet lifetime is 85 ± 6 ns in both samples and the triplet transfer time into Si is 169 ± 8 ns in the aged sample. Figure 5.5 b) shows how the triplet population varies with time with a faster decay of the triplet population in HF-Si due to triplet transfer into Si. The growth of the triplet population in HF-Si corresponds to 35.7 % ± 0.9 % of triplet transfer. Our model is robust against sample-to-sample variation, aging of tetracene on its own, and between wafers and solar cell (see Appendix Figure 5.9, Figure 5.10, Figure 5.11, Figure 5.14). Our findings show that efficient triplet transfer can be obtained when the percentage of TCII is increased. Thus, to achieve even higher triplet transfer yield into HF-Si, control over the morphology appears to be crucial, so that TCII becomes the predominant polymorph. This also suggests that apart from the complex $HfO_xN_y$ interlayers used before,

we can also exploit the tetracene orientation itself for efficient triplet transfer [29].

## 5.3 CONCLUSION

In summary, we have shown that a change in the dominant tetracene polymorph by air exposure facilitates triplet transfer from tetracene into Si. The triplet transfer process is confirmed through magnetic field-dependent photocurrent measurements, and the timescale of triplet transfer is obtained from delayed PL decay measurements. We find that the transition from the tetracene polymorph TCI to TCII is essential for efficient triplet transfer. This suggests that the orientation (w.r.t. the surface), and the packing of the singlet fission molecule is crucial for an efficient triplet transfer process. Future research should focus on an optimal alignment of tetracene molecules by preparing a pure TCII polymorph on Si and potential combinations of both interlayers and polymorph control, which could lead to the optimal triplet transfer efficiency. This could then enable the cheap manufacturing of singlet fission-sensitized Si solar cells.

## 5.4 EXPERIMENTAL DETAILS

### Solar cells

The solar cells are Interdigitated Back Contact (IBC) silicon solar cells with a silicon pyramid antireflection layer and a $\sim 80\,\text{nm}$ SiN passivation and antireflection layer. We cut the $4\,\text{cm} \times 4\,\text{cm}$ solar cells in three stripes with a laser cutter. We use a wire bonder to contact the back-side contacts to contact pads for the photocurrent measurements.

### Silicon Wafers

Silicon Wafers were purchased from Siegert Wafer GmbH. We used <111> FZ-silicon, n-doped (Ph) with a resistivity of $1-5\,\Omega\,\mathrm{cm}$, Double side polished with a thickness of 0.28 mm. We dice the wafers using a laser cutter.

### HF etching of solar cells

We dripped concentrated hydrofluoric acid (HF) solution (40 %, Sigma-Aldrich, as received) onto the top surface of the silicon solar cell with a pipette. In this way the HF solution does not contact the metallic back contacts. After 10 min of etching the wettability decreases dramatically, meaning that at this point we have etched away the SiN which has a lower contact angle than the bare Si surface. We then removed any of the remaining HF solution from the surface by dipping the samples sequentially twice in deionized water baths. Immediately afterwards, the sample was transferred into a nitrogen-filled glovebox.

### Tetracene deposition

We deposited 200 nm of tetracene onto the silicon solar cells, and either 35 nm or 200 nm onto the bare silicon samples. The evaporation was done inside a thermal evaporator (Angstrom Engineering Inc.), at a base pressure below $7\cdot10^{-7}$ mbar. Tetracene was purchased from Sigma-aldrich (99.99 % purity) and used as is. The deposition rate was $1\,\frac{\text{Å}}{\text{s}}$ in all cases. Encapsulation was also done inside the nitrogen-filled glove box, using two glass slides, a rubber gasket and silicone glue. None of the samples were exposed to UV light during storage and measurement.

#### *Magnetic-field dependent photocurrent measurements*

We measured the magnetic-field dependent photocurrent using a home-built setup. The magnetic field is applied by an electromagnet, made up by two Helmholtz coils and calibrated using a Hall effect sensor. The

magnetic field is applied by sending a current of up to 5 A of current through the coils, resulting in a magnetic field of up to 0.35 T. The field is oriented parallel to the sample surface. The excitation source is a 520 nm diode laser, installed in a Thorlabs temperature-controlled laser housing. The cw laser power is around 10 mW with a laser spot size of approximately 1 mm. The photocurrent is measured with a Keithly 2636A source-measure unit. After each measurement at a certain magnetic field we perform a reference measurement at zero magnetic field. For the self-passivation measurements we added a 100 W xenon lamp with a 550 nm longpass filter, to only excite the silicon substrate.

### Photoluminescence studies

Photoluminescence (PL) spectra and decay kinetics were monitored in Lifespec-ps (Edinburgh Instruments) upon 404 nm laser pulse (pulse width ~ 100 ps) excitation with a repetition rate of 200 kHz. The tetracene-deposited substrates were encapsulated inside a custom-made sample holder inside a glovebox prior to the measurement. Afterwards, the samples were exposed to air and encapsulated again inside the glovebox to investigate the effect of air exposure on PL decay.

### X-Ray diffraction

XRD was measured on a Bruker D2 Phaser using a Cu Tube with 1.54 Å at 10 mA and 30 kV as a source. We used a Lynxeye detector in 2Theta mode with a scan speed of 420 s per measurement. Each 7 min we measure the diffraction spectra once. The sample was rotating at 10 per min and kept inside the instrument during the whole measurement. We use a moving average over 21 points to smooth the diffraction curve. After tetracene deposition the devices were stored in a nitrogen-filled glovebox before the XRD measurement. The storage time inside the glovebox was 1 month for the sample in the main text and 7 months in the sample described in the Appendix.

### X-Ray Photoelectron spectroscopy

XPS measurements were performed with a JEOL JPS-9200 photoelectron spectrometer, using a 12 kV and 20 mA monochromatic Al K$\alpha$ source. The analyzer pass energy was 10 eV, and the take-off angle between sample and detector was set at 10°. Data was analyzed using the CasaXPS program, version 2.3.18PR1.0. To measure the samples, the silicon surfaces with tetracene layer were transferred in an air-tight container from a glovebox $O_2 < 0.01$ ppm, $H_2O < 0.01$ ppm to the XPS, to minimize air exposure during transfer. In the XPS, a first dummy measurement taking ~100 min was performed, to heat up the sample stage. This, in combination with the high vacuum in the measurement chamber $10^{-5} - 10^{-6}$ mbar, led to the sublimation of tetracene from the sample, leaving the bare silicon surface behind. The level of silicon surface oxidation was then assessed by performing narrow scans on the silicon 2p peak. The relative surface area of the Si 2p peak at ~ 103 eV was taken as a measure for surface oxidation.

## 5.5 APPENDIX

### ADDITIONAL MAGNETIC-FIELD DEPENDENT PHOTOCURRENT REFERENCE MEASUREMENTS

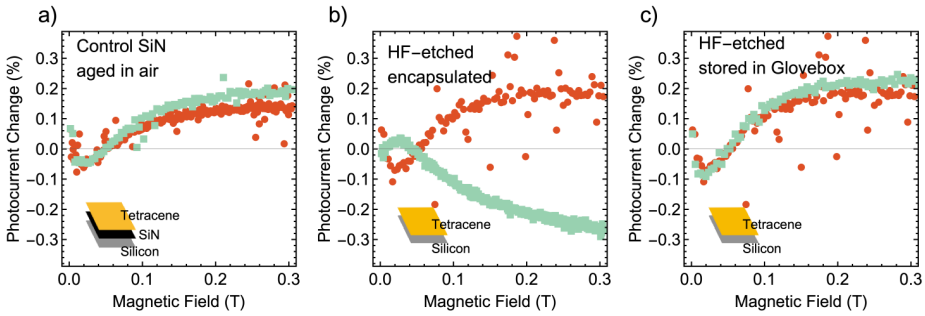


**Figure 5.6:** . Magnetic field-dependent photocurrent in a) Si/SiN/tetracene solar cell before (green curve) and after aging (red curve) in air with no change in triplet transfer behavior. b) Encapsulated HF-Si/tetracene silicon solar cell stored in air for six weeks. The photocurrent change flips from singlet to triplet curve, and c) HF-Si/tetracene solar cell stored under nitrogen atmosphere in the glovebox for six weeks without changes to the triplet transfer.

## ABSENCE OF SELF PASSIVATION EFFECT

To investigate whether the self-passivation of additional charge carriers in silicon can lead to an overestimation of the magnetic field effect, we add an additional red light with energy below the tetracene bandgap so that the light is only absorbed in the silicon layer. The change in photocurrent with magnetic field can be written as $\Delta I(B) = (I(B) - I(B = 0))/I(B)$ . If we add different light sources, each light source will add current that can also be dependent on the magnetic field. In our experiment we added red light (leading to current $I_{Red}(B)$) to the green laser (current $I_{Green}(B)$). The change in photocurrent then becomes

$$\begin{aligned}\Delta I(B) = {} & I^{Tc}_{Red}(B) + I^{Si}_{Red}(B) + I^{Tc}_{Green}(B) + I^{Si}_{Green}(B) \\ & - I^{Tc}_{Red}(B = 0) - I^{Si}_{Red}(0) - I^{Tc}_{Green}(0) - I^{Si}_{Green}(0)\end{aligned}$$

Since tetracene does not absorb in the red, we set $I^{Tc}_{Red}(B) = 0$. The current generated in silicon directly does not depend on the magnetic field, leading to $I^{Si}(B) = I^{Si}(0)$, leaving us with:

$$\Delta I(B) = \frac{I^{Tc}_{Green}(B) - I^{Tc}_{Green}(0)}{I_{Green}(0) + I_{Red}(0)}$$

We measure the current from only the red light at zero field and then correct the magnetic field curve with the formula above.

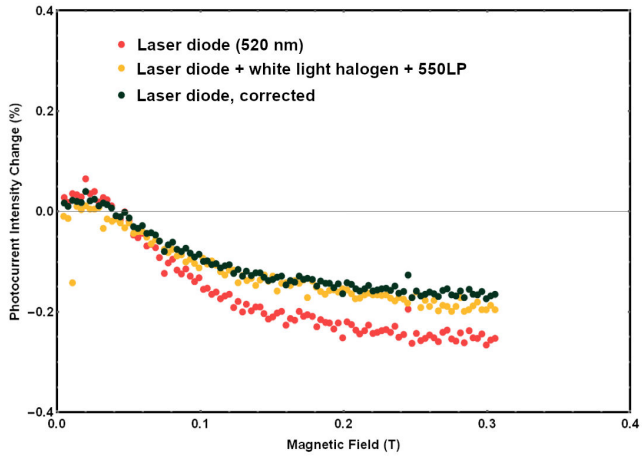


**Figure 5.7:** Change in photocurrent of HF-Si/tetracene solar cell under magnetic field with different light sources. Illumination with the green laser (red curve), illumination with green laser and red light (yellow), and correcting the red curve with the formula described below. If accounted for the additional charge carriers, both curves are on top of each other and we can conclude that there is a negligible effect of self passivation from the additional charge carriers in silicon.

## EXTERNAL QUANTUM EFFICIENCY

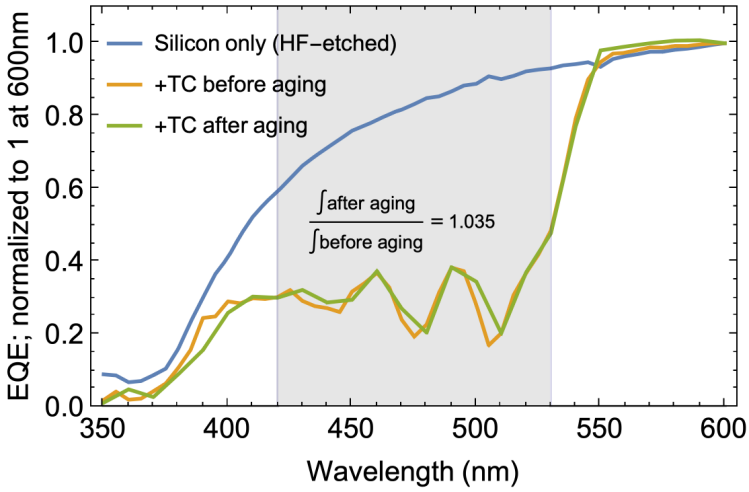


**Figure 5.8:** Normalized EQE of the silicon only, silicon/tetracene and silicon/tetracene (aged) solar cells in the region of tetracene absorption. These cells correspond to the magnetic-field dependent measurements presented in Figure 5.2 of the main text. The EQE is normalized to 1 at 600 nm to account for variability between measurement positions. The integral over the shaded area of 420 nm to 530 nm increases by 3.5 % upon aging, a small number most likely within the measurement error. The poor surface passivation and therefore lack of charge collection at the interface, and the transport of triplet excitons to the interfaces are the most likely reasons for this small absolute gain in EQE.

## SOLAR CELL WITH SIN LAYER PHOTOLUMINESCENCE DECAY AND MODELING

We model the PL decay from the solar cell with a SiN interlayer. The data with the fit is shown in 5.9 c) with the resulting triplet densities in Figure 5.9 d). From the fit we observe a triplet transfer efficiency of 34.5 % ± 0.01 %, comparable to the 35.7 % in the main text with the $SiO_x$ interlayer. The error is dominated by the fitting error of the triplet transfer rate, which is small. The kinetic parameters extracted from the model for Si/SiN/tetracene (aged) are $k_{sf} = (258.6 \pm 0.9\,ps)^{-1}$; $k_{rad} = (12.5\,ns)^{-1}$ (kept constant); $k_{TT} = (10360 \pm 750\,ps)^{-1}$; $k_{Diss} = (1337 \pm 137\,ps)^{-1}$;$k_{TTA} = (9.6 \pm 0.9) \cdot 10^{-11} cm^3 s^{-1}$; $k_{Trip} = (78 \pm 5\,ns)^{-1}$. For HF-Si/tetracene (aged) a triplet transfer rate of $k_{T\rightarrow Si} = (171 \pm 11\,ns)^{-1}$ and $k_{sf} = (217.2 \pm 0.5\,ps)^{-1}$ was fitted.

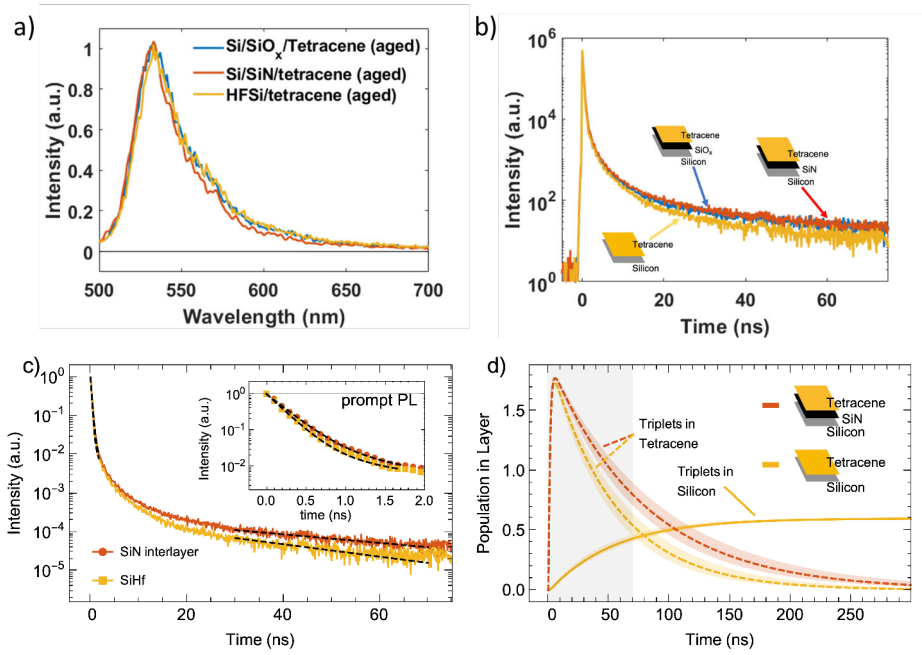


**Figure 5.9:** a) PL spectra of tetracene show the absence of degradation and additional trap states, and b) decay traces for tetracene deposited on Si/$SiO_x$, Si/SiN and HF-Si solar cells, showing no difference between slope of the long-time decay for the SiN and $SiO_x$ blocking layers and triplet quenching in fresh HF-Si. c) kinetic modeling of the SiN vs the SiHF (aged) solar cell to investigate the influence of the interlayer on transfer efficiency. d) Triplet population in tetracene and silicon derived from the kinetic modeling shown in Figure 5.9 c). The bands around the model in Figure 5.9 d) are 95% confidence intervals.

## SOLAR CELL PHOTOLUMINESCENCE IN DIFFERENT SPOTS

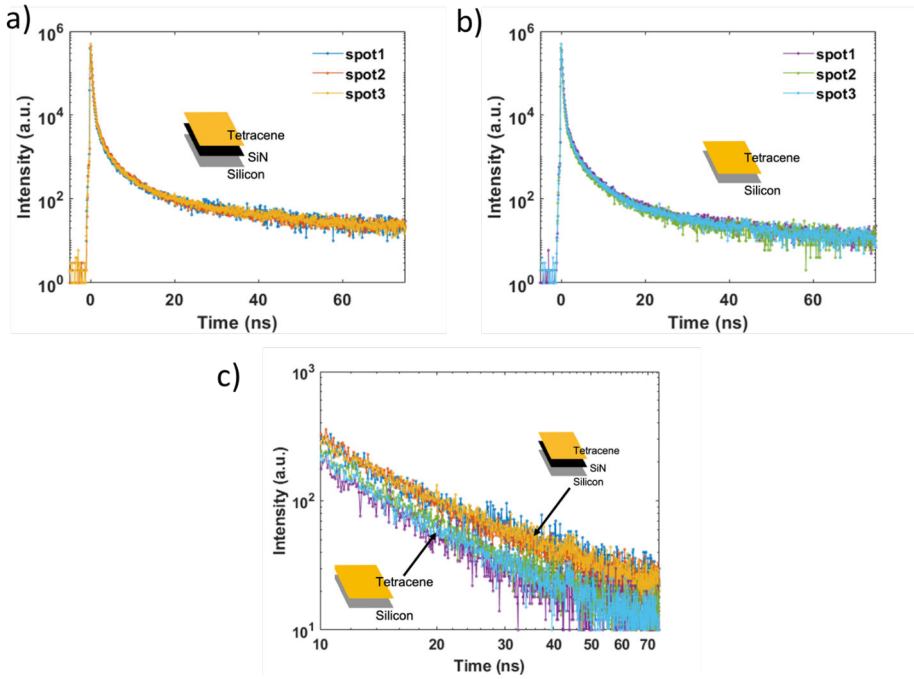


**Figure 5.10:** PL decay traces for a) Si/SiN and b) HF-Si solar cells sensitized with tetracene excited on different spots on the solar cell surface. c) Comparison of decay traces in a) and b) together to show the reproducibility of the data in different spots and measurements. We performed the kinetic modeling described on all nine combinations of reference (SiN) and quenching (HF-Si) samples and get a mean efficiency of 27.8% with a standard error of the mean of 2.0% and a standard deviation of 5.8% which corresponds to the sample-to-sample variation.

## WAFER PHOTOLUMINESCENCE DECAY AND MODELING

We also fabricated silicon wafers, deposited tetracene and aged them. The PL spectrum (Figure 5.11 a)) shows some difference in the defect emission around 620 nm upon exposure to air, contrary to the solar cells samples. The decay dynamics show a similar behavior as the solar cell samples. The initial singlet decay becomes equally faster upon air exposure in both $Si/SiO_x$ and HF-Si, implying a faster SF rate due to the increased concentration of TCII.

We applied the same kinetic model for tetracene on silicon *wafers* as for the solar cell samples and the outputs are shown as dotted black lines in Figure 5.11 c), together with the PL decay data. The efficiency of triplet transfer is 48.3 % ± 1.8 %, higher compared to the solar cell transfer efficiencies. The kinetic parameters extracted from the model for $Si/SiO_x$/tetracene (aged) are $k_{sf} = (235 \pm 1\,ps)^{-1}$; $k_{rad} = (12.5\,ns)^{-1}$ (kept constant); $k_{TT} = (3407 \pm 158\,ps)^{-1}$; $k_{Diss} = (655 \pm 24\,ps)^{-1}$; $k_{T}TA = (15.9 \pm 0.7) \cdot 10^{-11} cm^3 s^{-1}$; $k_{T}rip = (141 \pm 8.7\,ns)^{-1}$. For HF-Si/tetracene (aged) a triplet transfer rate of $k_{T\rightarrow Si} = (165.1 \pm 4.4\,ns)^{-1}$ and $k_{s}f = (226.8 \pm 0.4\,ps)^{-1}$ was fitted. The kinetic parameters are slightly different for these tetracene samples prepared on Si wafers which can be due to different sample preparation conditions and batch-to-batch variability.

To quantify the error introduced by different reference samples we use a fresh, not aged sample as a reference and perform the same model as before, seen in Figure 5.11 e) and f). The triplet transfer efficiency with this combination is 58.7 % ± 3 %, around 10 % higher than with the aged sample as a reference. This apparent 10 % higher transfer efficiency is the effect of aging of tetracene. The kinetic parameters extracted from the model for $Si/SiO_x$/tetracene (aged) are $k_{s}f = (255 \pm 1\,ps)^{-1}$; $k_{rad} = (12.5\,ns)^{-1}$ (kept constant); $k_{TT} = (3109 \pm 137\,ps)^{-1}$; $k_{Diss} = (724 \pm 27\,ps)^{-1}$; $k_{TTA} = (10.8 \pm 0.5) \cdot 10^{-11} cm^3 s^{-1}$; $k_{Trip} = (213 \pm 18\,ns)^{-1}$. For HF-Si/tetracene (aged) a triplet transfer rate of $k_{T\rightarrow Si} = (164.8 \pm 5.5\,ns)^{-1}$and $k_{sf} = (219.9 \pm 0.5\,ps)^{-1}$ was fitted.

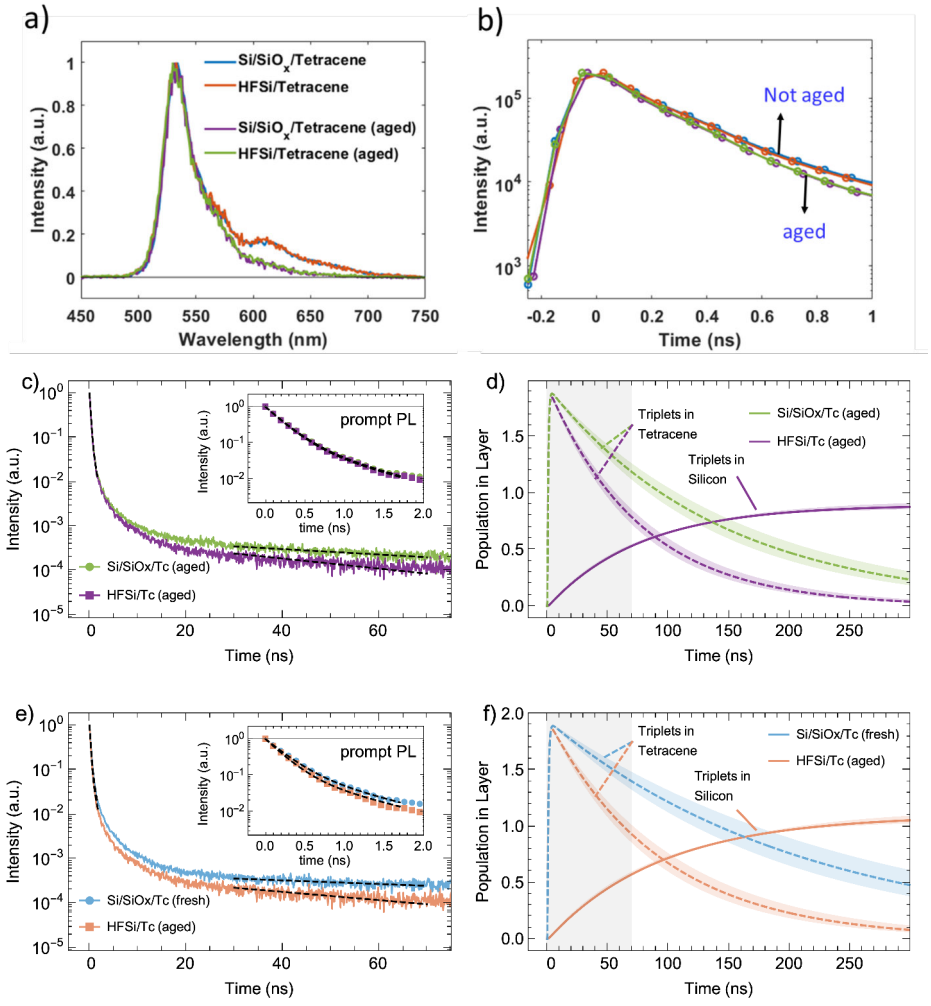


**Figure 5.11:** a) PL spectra, b) prompt, and c) delayed PL for tetracene deposited on Si/SiO$_x$ and HF-Si *wafers* (thus not solar cells as in the main text) with and without air exposure. The inset in c) shows the prompt PL decay. d) The triplet yield as a function of time as predicted from the model. The bands around the model are 95% confidence intervals. Panels e) and f) show kinetic modeling with a fresh Si/SiO$_x$/tetracene sample as reference sample, to quantify the influence of the aging of tetracene on top of the reference sample on the triplet efficiency of our model. The inset shows prompt PL and the different fit due the free fit parameter $k_{SF}$.

## X-RAY DIFFRACTION MEASUREMENT OVER TIME

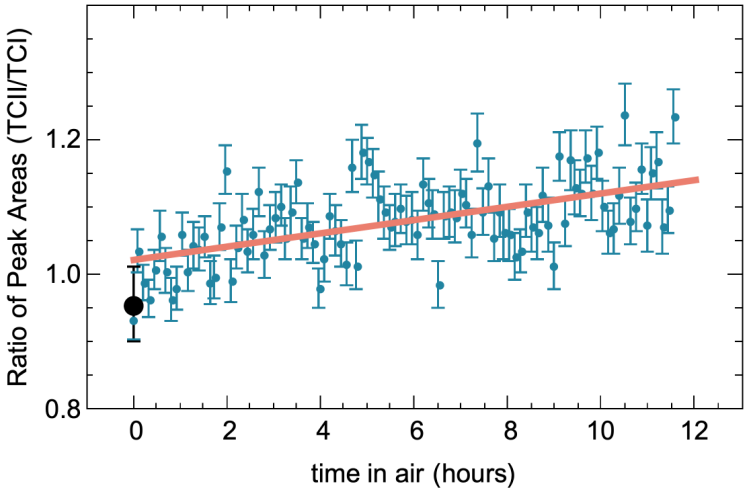


**Figure 5.12:** Ratio of peak areas of TCII/TCI determined from a fit of two normal functions to the XRD data, with a fixed position for TCI (7.2°) and TCII (6.8°) and free fit parameters of peak width and peak height. We observe a smooth transition between the polymorphs. The data in the main text (Figure 4) are the blue datapoints for 0 h and 12 h. In black is a measurement of a tetracene film on silicon of the same batch but stored in the glovebox for seven months (data in Figure 5.13).

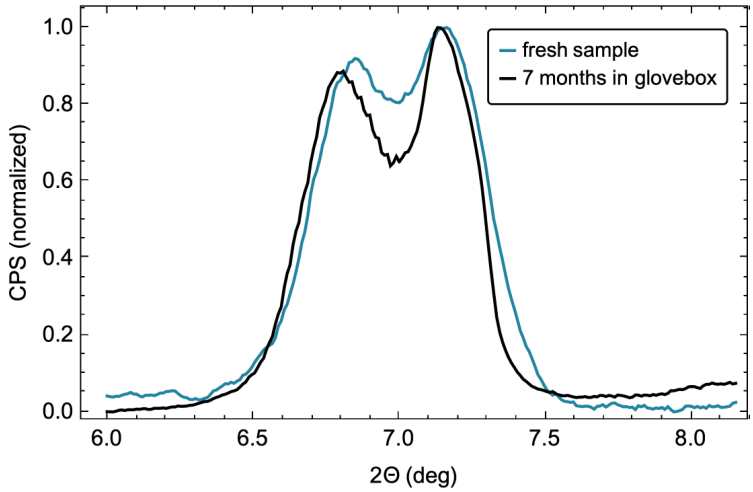


**Figure 5.13:** XRD measurement of tetracene films directly after removing them from the glovebox. Black when stored in glovebox for one month (data also in main text), blue when stored in the glovebox for seven months. We conclude that storage in nitrogen does not lead to a polymorphism change. Data is normalized to be between 0 and 1 and smoothed with a moving average function over 21 data points.

## TETRACENE PHOTOLUMINESCENCE AGING ON QUARTZ

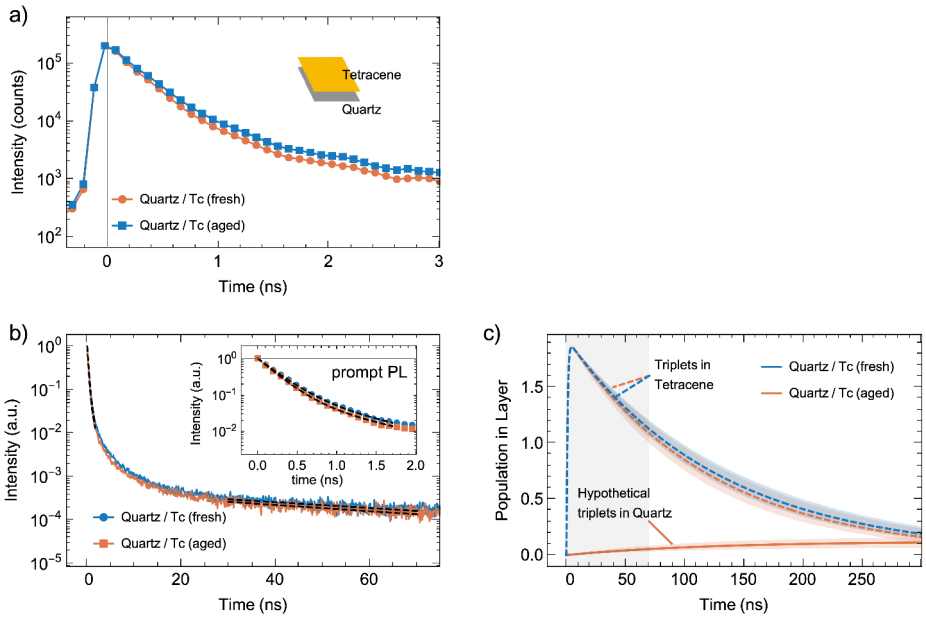


**Figure 5.14:** a) Prompt and b) delayed PL of tetracene deposited on quartz. The change in the initial fast decay after air exposure can be attributed to an interchange of TCI to TCII. The black lines represent the outputs from the kinetic model using the fresh tetracene sample as a reference and the aged tetracene sample as the quenched sample. We calculate this to quantify the influence of degradation of tetracene alone on our kinetic modeling. The triplet transfer efficiency obtained is 6.5 % $\pm$ 2.4 %, which means that the effect of tetracene aging alone on our model is much smaller than the transfer efficiency observed in the samples with HF-Si and aged tetracene. Panel c) shows the triplet populations as would be expected if the samples were on deposited on silicon. The bands around the model are 95 % confidence intervals.

## XPS MEASUREMENT ON HF-SI AND CHANGE OVER TIME

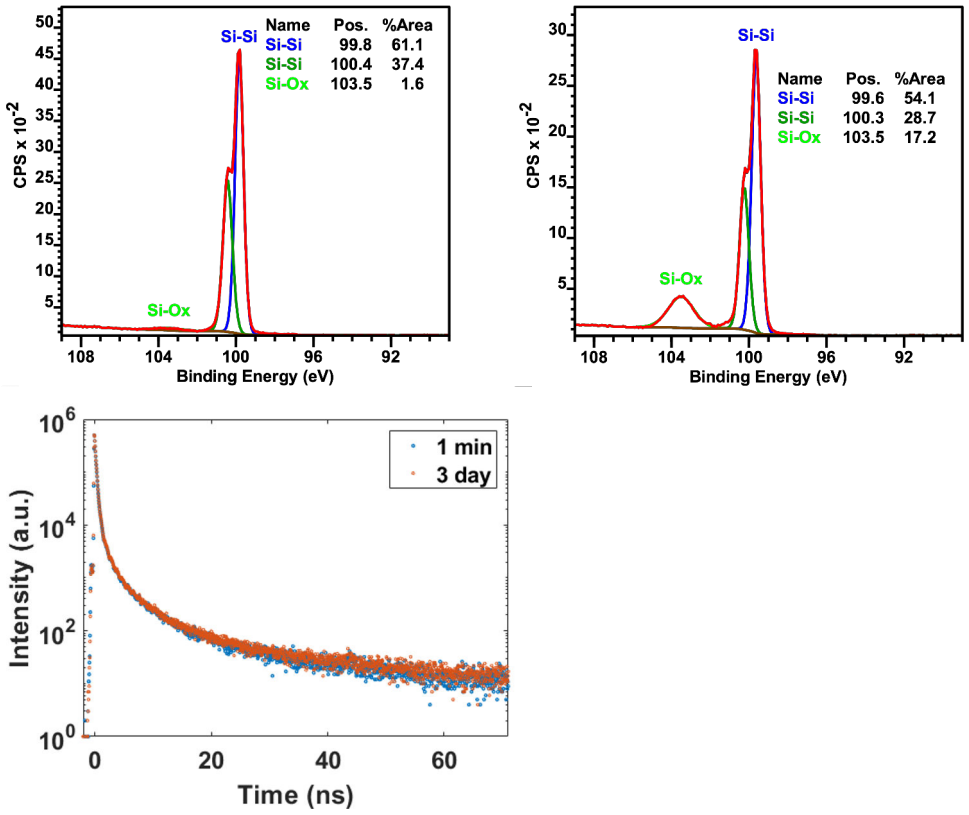


**Figure 5.15:** Si 2p XPS data of HF-Si sample exposed in air for a) 1 min, and b) 3 days. The difference shows the growth of $SiO_x$ upon longer exposure. Tetracene was deposited on these pre-exposed HF-Si substrates, and the PL lifetime of tetracene in panel c) is unchanged, suggesting exposure of HF-Si to air alone does not lead to triplet transfer.

## MODELING OF INTERMEDIATE PHOTOLUMINESCENCE DECAY

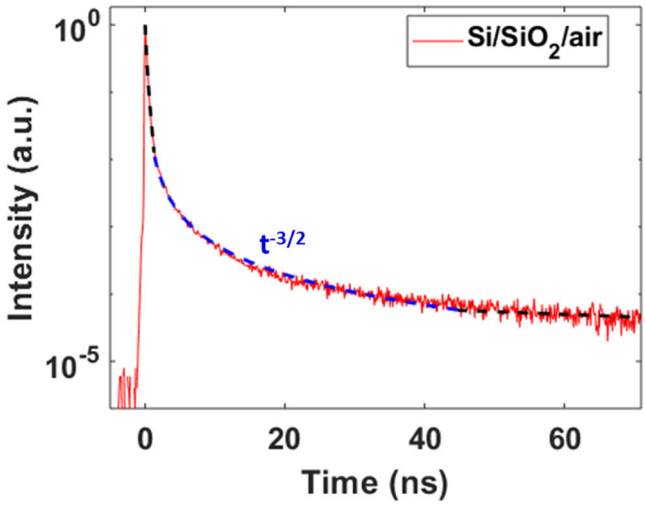


**Figure 5.16:** The kinetic model based on the solution of coupled differential equations reproduces the data for prompt and delayed PL (black dotted line) of tetracene deposited on $Si/SiO_x$. The intermediate-time region of the PL decay curve is dominated by diffusion of the triplet pair states, which follows a $t^{-\frac{3}{2}}$ dependence [113]. Here the $t^{-\frac{3}{2}}$ term was added manually to show the qualitative match with the data.

## KINETIC MODELING OF TRIPLET QUENCHING

### Differential equations

We set up the following set of coupled differential equations for all species present in an excited tetracene crystal *with* $SiO_2$interlayer:

$$\begin{aligned}
\frac{dS(t)}{dt} &= -(k_{SF} + k_{Rad})\,S(t) + k_{TT}TT(t) \\
\frac{dTT(t)}{dt} &= k_{SF}S(t) - k_{TT}TT(t) - k_{Diss}TT(t) \\
&\qquad + k_{TTA}T(t)^2 - k_{Trip}TT(t) \\
\frac{dT(t)}{dt} &= 2k_{Diss}TT(t) - 2k_{TTA}T(t)^2 - k_{Trip}T(t) \\
\frac{dG(t)}{dt} &= k_{Rad}S(t) + k_{Trip}TT(t) + k_{Trip}T(t)
\end{aligned}$$

The additional quenching in the samples *without* $SiO_2$ interlayer is modeled by an additional quenching term (**bold**) on the triplet density T:

$$\begin{aligned}
\frac{dS(t)}{dt} &= -(k_{SF} + k_{Rad})\,S(t) + k_{TT}TT(t) \\
\frac{dTT(t)}{dt} &= k_{SF}S(t) - k_{TT}TT(t) - k_{Diss}TT(t) \\
&\qquad + k_{TTA}T(t)^2 - k_{Trip}TT(t) \\
\frac{dT(t)}{dt} &= 2k_{Diss}TT(t) - 2k_{TTA}T(t)^2 - k_{Trip}T(t) - \mathbf{k_{T\to Si}T(t)} \\
\mathbf{\frac{dT_{Si}(t)}{dt}} &= \mathbf{k_{T\to Si}T(t)} \\
\frac{dG(t)}{dt} &= k_{Rad}S(t) + k_{Trip}TT(t) + k_{Trip}T(t)
\end{aligned}$$

The singlet ($S_1$) produces a triplet pair (TT) state through singlet fission ($k_{SF}$), which then dissociates ($k_{Diss}$) into free triplets (T). Both singlet, triplet and triplet pair can recombine to the ground state (G).

The radiative decay of the $S_1$ state has a lifetime of 12.5 ns (taken from literature, Table 1). The TT state decays back to a $S_1$ state with the rate $k_{TT}$. The free triplets can regenerate the TT state through triplet-triplet annihilation ($k_{TTA}$). The triplet state or triplet pair state decay non-radiatively ($k_{Trip}$) to the ground state. Upon air exposure, triplet transfer to Si also diminishes the triplet population through triplet transfer to Si $k_{T\rightarrow Si}$.

### Fitting procedure of differential equation to PL decay

We are solving the differential equations above using ParametricNDSolve and NonlinearModelFit functions in MATHEMATICA 12.1. The initial boundary conditions are $S(t=0) = 2 \cdot 10^{16}\,cm^{-3}$ (the laser power density), $T(t=0) = 0$, and $TT(t=0) = 0$. First, we fit the reference PL-decay to the prompt PL data between 0 ns and 1.7 ns and then delayed PL data between 30 ns to 70 ns to the singlet population of the differential equations above (the PL is proportional to the singlet population for excitonic PL). After 70 ns the afterpulsing of our single photon counter starts to affect the measurement. All parameters except for $k_{rad}$ are free, with literature values used as starting values. We use weights of $1/N_i$ for the fit ($N_i$ is the number of counts at each time $t_i$) to account for the Poisson counting error. We do not fit the intermediate part of the decay (1.7 ns to 30 ns) where the triplet diffusion dominates (see Figure 5.16). After fitting the reference sample we fit the data from the quenching sample to estimate the transfer efficiency. We use the reference rate constants and add a quenching term to the triplet state population. Since the tetracene is aged in both reference and quenching data the other rates are assumed to be constant, except for $k_{sf}$ which can vary slightly upon aging as seen from the SiN interlayer data shown in Figure 5.11 e). We calculate the 95% confidence bands for the triplet population by varying each rate by the confidence interval, which assumes that the parameters have negligible covariances. The triplet transfer efficiency is calculated from the triplet population in silicon at long times after saturation ($> 500$ ns) divided by the maximum of the triplet population in tetracene upon excitation.

| | Solar cell sample exposed to air | | Literature | | | |
|---|---|---|---|---|---|---|
| | $Si/SiO_2$ | HF-Si | fs-TA on single cryst. [5] | fs-TA polycryst. [148] | PL decay polycryst. [141] | Reference [95] |
| $k_{SF}$ | Fitted $(220 \pm 1\,ps)^{-1}$ | Fitted $(212 \pm 1\,ps)^{-1}$ | $(124\,ps)^{-1}$ | $(120\,ps)^{-1}$ | $(90\,ps)^{-1}$ | $(180\,ps)^{-1}$ |
| $k_{Rad}$ | Set to $(12.5\,ns)^{-1}$ | Set to $(12.\,ns)^{-1}$ | $(524ps)^{-1}$ | $(12.5ns)^{-1}$ | $(12.5ns)^{-1}$ | $(12.5ns)^{-1}$ |
| $k_{TT}$ | Fitted $(6303 \pm 304\,ps)^{-1}$ | Set to $(6303\,ps)^{-1}$ | $(360\,ps)^{-1}$ | $(1000\,ps)^{-1}$ | $(150\,ps)^{-1}$ | $(100\,ns)^{-1}$ [1] |
| $k_{Diss}$ | Fitted $(810 \pm 36\,ps)^{-1}$ | Set to $(810\,ps)^{-1}$ | $(439\,ps)^{-1}$ | $(500\,ps)^{-1}$ | $(600\,ps)^{-1}$ | – |
| $k_{TTA}$ | Fitted $(9.2 \pm 0.7) \cdot 10^{-11} \frac{cm^3}{s}$ | Set to $9.2 \cdot 10^{-11} \frac{cm^3}{s}$ | 0 | $1.7 \cdot 10^{-11} \frac{cm^3}{s}$ | 0 | |
| $k_{Trip}$ | Fitted $(85 \pm 6\,ns)^{-1}$ | Set to $(85\,ns)^{-1}$ | $(21.59\,ns)^{-1}$ | $(62.5\,\mu s)^{-1}$ | $(20\,ns)^{-1}$ | $(200\,ns)^{-1}$ |
| $k_{T \to Si}$ | Set to 0 | Fitted $(169 \pm 8\,ns)^{-1}$ | - | - | - | - |

**Table 5.1:** Comparison of rate constants determined from the above model with literature values for tetracene singlet fission process. TA = transient absorption; PL = photoluminescence

# 6 CONCLUSION AND OUTLOOK

In this work we set out to investigate the transfer of triplet excitons and demonstrate a singlet fission solar cell. Since the transfer of triplet excitons remains the main unaddressed challenge in the realization of singlet fission solar cells, any progress in this area is of great technological importance.

In Chapter 2 we saw quantum dots can be used to transfer triplet energy, but the requirement is a very close distance between quantum dots and a silicon surface. This distance requirement might be challenging if silicon is passivated by a thick passivation layer. The quantum dot itself can also have passivation shells that are thicker than the oleic acid groups we used. However, a main advantage of FRET compared to photon transfer is that we do not have to engineer any photon collection scheme in the singlet fission layer, potentially saving costs. It would be interesting to see an experimental demonstration of the predicted $r^{-3}$ distance dependency. This has been attempted in the Master Thesis of Stefan Tabernig but the data was unfortunately not sufficiently clear to distinguish different distance functions.

The different transfer schemes in Chapter 3 lead to different solar cell efficiencies. It will be interesting to see whether this calculation increases the efforts to search for singlet fission materials with lower exciton energy and high entropy gain, to be used in a charge transfer singlet fission-solar cell. The requirements for a singlet fission material that can be used to manufacture an efficient singlet fission-silicon solar cell are numerous. The absorption has to be strong and broadband at the right absorption onset, the singlet fission process has to be efficient, the entropy gain should be high, and the triplet and hole transport has to be efficient.

Different schemes have less strict requirements for each of these, but the challenge remains. Once a solar cell has been produced it should also be stable for 25 years, since this is the lifetime of the base silicon cell. It might therefore be wise to focus first on the easiest singlet fission-silicon solar cell implementations.

Another problem we discussed is the detection of triplet transfer in Chapter 4. It is often difficult to immediately produce a complete solar cell stack with a singlet fission layer for each idea of how to facilitate triplet transfer. Even if the triplet exciton is transferred it can still be lost subsequently due to poor charge collection. One might therefore discard interlayers or other harvesting schemes because the solar cell is inefficient. This is only exacerbated for small singlet fission injection currents that only slightly change the overall cell current. Our method addresses some of these issues since a whole solar cell is not required, which can speed up sample preparation and throughput. We compare the triplet quenching of many different tetracene islands on the same sample with the same deposition and measurement conditions. It is however necessary to collect light from the recombining triplets, which is not possible for singlet fission materials with ultrafast singlet fission, such as pentacene.

During our demonstration of a singlet fission-silicon solar cell in Chapter 5 we saw that the polymorphism of tetracene can facilitate triplet transfer into silicon. In future work it will be very interesting to see whether one can deliberately deposit one or the other polymorph to control the transfer efficiency. The orientation of molecules at the buried interface is not yet measured, which would give further insight into the transfer mechanism. To increase our theoretical understanding of triplet exciton transfer it will be worthwhile to develop a theoretical framework of molecule orbital overlap with the tetracene wavefunctions and the silicon bandstructure, which could be used to investigate the effects of different interlayers and orientations on the Dexter transfer efficiency.

At last, we have to ask whether singlet fission-silicon solar cells can be on the market fast enough to compete with perovskite tandems and contribute to the green energy transition. There has been good progress recently, but fundamental challenges remain and the focus of the organic solar cell community has shifted towards perovskite solar cells in the last years. The author hopes that the successful realizations of singlet fission-silicon solar cells lead to increased research interest.

# BIBLIOGRAPHY


[1] Gleb M. Akselrod, Mark C. Weidman, Ying Li, Christos Argyropoulos, William A. Tisdale, and Maiken H. Mikkelsen. "Efficient Nanosecond Photoluminescence from Infrared PbS Quantum Dots Coupled to Plasmonic Nanoantennas." In: *ACS Photonics* 3.10 (2016), pp. 1741–1746. DOI: 10.1021/acsphotonics.6b00357 (cit. on p. 22).

[2] Gleb M. Akselrod et al. "Visualization of Exciton Transport in Ordered and Disordered Molecular Solids." In: *Nature Communications* 5 (2014), p. 3646. DOI: 10.1038/ncomms4646 (cit. on pp. 22, 34, 45, 106).

[3] Hadas Alon et al. "Effect of Internal Heteroatoms on Level Alignment at Metal/Molecular Monolayer/Si Interfaces." In: *Journal of Physical Chemistry C* 122.6 (2018), pp. 3312–3325. DOI: 10.1021/acs.jpcc.7b09118 (cit. on p. 84).

[4] R. Amos and W. Barnes. "Modification of the Spontaneous Emission Rate of Ions Close to a Thin Metal Mirror." In: *Physical Review B - Condensed Matter and Materials Physics* 55.11 (1997), pp. 7249–7254. DOI: 10.1103/PhysRevB.55.7249 (cit. on p. 92).

[5] Dylan H. Arias, Joseph L. Ryerson, Jasper D. Cook, Niels H. Damrauer, and Justin C. Johnson. "Polymorphism influences singlet fission rates in tetracene thin films." In: *Chemical Science* 7.2 (2016), pp. 1185–1191. DOI: 10.1039/c5sc03535j (cit. on pp. 68, 103, 108, 110, 132).

[6] Sam L. Bayliss, Alexei D. Chepelianskii, Alessandro Sepe, Brian J. Walker, Bruno Ehrler, Matthew J. Bruzek, John E. Anthony, and Neil C. Greenham. "Geminate and Nongeminate Recombination of Triplet Excitons Formed by Singlet Fission." In: *Physical Review*

*Letters* 112.23 (2014), p. 238701. DOI: 10.1103/PhysRevLett.112.238701 (cit. on p. 78).

[7] Matthew C. Beard, Justin C. Johnson, Joseph M. Luther, and Arthur J. Nozik. "Multiple Exciton Generation in Quantum Dots Versus Singlet Fssion in Molecular Chromophores for Solar Photon Conversion." In: *Philosophical Transactions of the Royal Society A: Mathematical, Physical and Engineering Sciences* 373.2044 (2015). DOI: 10.1098/rsta.2014.0412 (cit. on p. 100).

[8] Ruirt Bosma. "MSc Physics Size-Dependent Open-Circuit Voltage in Lead Sulfide Colloidal Quantum Dot Solar Cells." PhD thesis. 2017 (cit. on p. 30).

[9] F. Bournel, J. J. Gallet, F. Rochet, J. Fujii, and G. Panaccione. "Adsorption of 2-Butyne on Si(0 0 1) at Room Temperature: A Valence Band Photoemission Study." In: *Surface Science* 601.18 (2007), pp. 3750–3754. DOI: 10.1016/j.susc.2007.04.099 (cit. on p. 30).

[10] Jonathan J. Burdett and Christopher J. Bardeen. *The dynamics of singlet fission in crystalline tetracene and covalent analogs*. June 2013. DOI: 10.1021/ar300191w (cit. on p. 110).

[11] Jonathan J. Burdett, Astrid M. Müller, David Gosztola, and Christopher J. Bardeen. "Excited State Dynamics in Solid and Monomeric Tetracene: The Roles of Superradiance and Exciton Fission." In: *Journal of Chemical Physics* 133.14 (2010), pp. 1–12. DOI: 10.1063/1.3495764 (cit. on pp. 68, 100).

[12] George F. Burkhard, Eric T. Hoke, and Michael D. McGehee. "Accounting for Interference, Scattering, and Electrode Absorption to Make Accurate Internal Quantum Efficiency Measurements in Organic and Other Thin Solar Cells." In: *Advanced Materials* 22.30 (2010), pp. 3293–3297. DOI: 10.1002/adma.201000883 (cit. on p. 91).

[13] Wai-Lun Lun Chan, Manuel Ligges, and X-Y. Y. Zhu. "The Energy Barrier in Singlet Fission Can Be Overcome Through Coherent Coupling and Entropic Gain." In: *Nature Chemistry* 4.10 (2012), pp. 840–845. DOI: 10.1038/nchem.1436 (cit. on pp. 100–102).

[14] R. R. Chance, A. Prock, and R. Silbey. "Molecular Fluorescence and Energy Transfer Near Interfaces." In: 2007, pp. 1–65. DOI: 10.1002/9780470142561.ch1 (cit. on p. 29).

[15] Kenny F. Chou and Allison M. Dennis. "Förster resonance energy transfer between quantum dot donors and quantum dot acceptors." In: *Sensors (Switzerland)* 15.6 (June 2015), pp. 13288–13325. DOI: 10.3390/s150613288 (cit. on p. 17).

[16] Stephen W. Clark, Jeffrey M. Harbold, and Frank W. Wise. "Resonant Energy Transfer in Pbs Quantum Dots." In: *Journal of Physical Chemistry C* 111.20 (2007), pp. 7302–7305. DOI: 10.1021/jp0713561 (cit. on pp. 17, 18, 22, 26).

[17] Daniel N. Congreve et al. "External Quantum Efficiency Above 100% in a Singlet-Exciton-Fission–Based Organic Photovoltaic Cell." In: *Science* 340.6130 (2013), pp. 334–337. DOI: 10.1126/science.1232994 (cit. on pp. 48, 66, 100).

[18] B. M. Craig. "Refractive indices of some saturated and monoethenoid fatty acids and methyl esters." In: *Canadian Journal of Chemistry* 31.5 (1953), pp. 499–504. DOI: 10.1139/v53-068 (cit. on p. 21).

[19] Benjamin Daiber et al. "A Method to Detect Triplet Exciton Transfer From Singlet Fission Into Silicon Solar Cells : Comparing Different Surface Treatments." In: *Journal of Chemical Physics* 152.11 (2020), pp. 1–23. DOI: 10.1063/1.5139486 (cit. on p. 56).

[20] Benjamin Daiber et al. "Change in Tetracene Polymorphism Facilitates Triplet Transfer in Singlet Fission-Sensitized Silicon Solar Cells." In: *The journal of physical chemistry letters* 11.20 (Oct. 2020), pp. 8703–8709. DOI: 10.1021/acs.jpclett.0c02163 (cit. on pp. 55, 99).

[21] Nathaniel J.L.K. Davis, Jesse R. Allardice, James Xiao, Anthony J. Petty, Neil C. Greenham, John E. Anthony, and Akshay Rao. "Singlet Fission and Triplet Transfer to PbS Quantum Dots in TIPS-Tetracene Carboxylic Acid Ligands." In: *Journal of Physical Chemistry Letters* 9.6 (2018), pp. 1454–1460. DOI: 10.1021/acs.jpclett.8b00099 (cit. on p. 12).

[22] A. De Vos. "Detailed Balance Limit of the Efficiency of Tandem Solar Cells." In: *Journal of Physics D: Applied Physics* 13.5 (1980), pp. 839–846. DOI: 10.1088/0022-3727/13/5/018 (cit. on pp. 11, 16).

[23] A. De Vos and H. Pauwels. "On the Thermodynamic Limit of Photovoltaic Energy Conversion." In: *Applied Physics* 25.2 (1981), pp. 119–125. DOI: 10.1007/BF00901283 (cit. on pp. 40, 42).

[24] D. L. Dexter. "A Theory of Sensitized Luminescence in Solids." In: *The Journal of Chemical Physics* 21.5 (1953), pp. 836–850. DOI: 10.1063/1.1699044 (cit. on pp. 18, 29, 66, 109).

[25] Samuel W. Eaton et al. "Singlet Exciton Fission in Polycrystalline Thin Films of a Slip-Stacked Perylenediimide." In: *Journal of the American Chemical Society* 135.39 (2013), pp. 14701–14712. DOI: 10.1021/ja4053174 (cit. on p. 41).

[26] Bruno Ehrler, Kevin P. Musselman, Marcus L. Böhm, Richard H. Friend, and Neil C. Greenham. "Hybrid pentacene/a-silicon solar cells utilizing multiple carrier generation via singlet exciton fission." In: *Applied Physics Letters* 101.15 (2012). DOI: 10.1063/1.4757612 (cit. on p. 66).

[27] Bruno Ehrler, Brian J. Walker, Marcus L. Böhm, Mark W.B. Wilson, Yana Vaynzof, Richard H. Friend, and Neil C. Greenham. "In Situ Measurement of Exciton Energy in Hybrid Singlet-Fission Solar Cells." In: *Nature Communications* 3.may (2012), p. 1019. DOI: 10.1038/ncomms2012 (cit. on p. 66).

[28] Bruno Ehrler, Mark W.B. Wilson, Akshay Rao, Richard H Friend, and Neil C Greenham. "Singlet Exciton Fission-Sensitized Infrared Quantum Dot Solar Cells." In: *Nano Letters* 12.2 (2012), pp. 1053–1057. DOI: 10.1021/nl204297u (cit. on pp. 12, 44, 64).

[29] Markus Einzinger et al. "Sensitization of Silicon by Singlet Exciton Fission in Tetracene." In: *Nature* 571.7763 (2019), pp. 90–94. DOI: 10.1038/s41586-019-1339-4 (cit. on pp. 13, 55, 61, 64, 66, 67, 102, 103, 105, 112).

[30] Kevin M. Felter and Ferdinand C. Grozema. "Singlet Fission in Crystalline Organic Materials: Recent Insights and Future Directions." In: *Journal of Physical Chemistry Letters* 10.22 (2019), pp. 7208–7214. DOI: 10.1021/acs.jpclett.9b00754 (cit. on p. 100).

[31] Xintian Feng, Anatoly B. Kolomeisky, and Anna I. Krylov. "Dissecting the Effect of Morphology on the Rates of Singlet Fission: Insights From Theory." In: *Journal of Physical Chemistry C* 118.34 (2014), pp. 19608–19617. DOI: 10.1021/jp505942k (cit. on p. 71).

[32] Th Forster. "Energiewanderung und Fluoreszenz." In: *Die Naturwissenschaften* 33.6 (1946), pp. 166–175. DOI: 10.1007/BF00585226 (cit. on p. 19).

[33] Moritz H. Futscher and Bruno Ehrler. "Efficiency Limit of Perovskite/Si Tandem Solar Cells." In: *ACS Energy Letters* 1.4 (2016), pp. 863–868. DOI: 10.1021/acsenergylett.6b00405 (cit. on pp. 40, 58).

[34] Moritz H. Futscher, Akshay Rao, and Bruno Ehrler. "The Potential of Singlet Fission Photon Multipliers as an Alternative to Silicon-Based Tandem Solar Cells." In: *ACS Energy Letters* 3.10 (2018), pp. 2587–2592. DOI: 10.1021/acsenergylett.8b01322 (cit. on pp. 58, 64, 100).

[35] Kavita Garg, Chiranjib Majumder, Sandip K. Nayak, Dinesh K. Aswal, Shiv K. Gupta, and Subrata Chattopadhyay. "Silicon-Pyrene/Perylene Hybrids as Molecular Rectifiers." In: *Physical Chemistry Chemical Physics* 17.3 (2015), pp. 1891–1899. DOI: 10.1039/c4cp04044a (cit. on p. 86).

[36] Elham M. Gholizadeh et al. "Photochemical Upconversion of Near-Infrared Light from Below the Silicon Bandgap." In: *Nature Photonics* 14.9 (2020), pp. 585–590. DOI: 10.1038/s41566-020-0664-3 (cit. on p. 13).

[37] Melissa K. Gish, Natalie A. Pace, Garry Rumbles, and Justin C. Johnson. "Emerging Design Principles for Enhanced Solar Energy Utilization With Singlet Fission." In: *Journal of Physical Chemistry*

*C* 123.7 (2019), pp. 3923–3934. DOI: 10.1021/acs.jpcc.8b10876 (cit. on p. 100).

[38] Stefan W. Glunz and Frank Feldmann. "SiO2 Surface Passivation Layers – a Key Technology for Silicon Solar Cells." In: *Solar Energy Materials and Solar Cells* 185 (2018), pp. 260–269. DOI: 10.1016/j.solmat.2018.04.029 (cit. on p. 56).

[39] M. Greben, A. Fucikova, and J. Valenta. "Photoluminescence Quantum Yield of Pbs Nanocrystals in Colloidal Suspensions." In: *Journal of Applied Physics* 117.14 (2015). DOI: 10.1063/1.4917388 (cit. on pp. 21, 22, 29).

[40] Martin A. Green. "How Did Solar Cells Get So Cheap?" In: *Joule* 3.3 (2019), pp. 631–633. DOI: 10.1016/j.joule.2019.02.010 (cit. on p. 3).

[41] Martin A. Green, Yoshihiro Hishikawa, Wilhelm Warta, Ewan D. Dunlop, Dean H. Levi, Jochen Hohl-Ebinger, and Anita W.H. Ho-Baillie. "Solar Cell Efficiency Tables (Version 50)." In: *Progress in Photovoltaics: Research and Applications* 25.7 (2017), pp. 668–676. DOI: 10.1002/pip.2909 (cit. on pp. 39, 41, 47, 58).

[42] Martin A. Green and Mark J. Keevers. "Optical Properties of Intrinsic Silicon at 300 K." In: *Progress in Photovoltaics: Research and Applications* 3.3 (1995), pp. 189–192. DOI: 10.1002/pip.4670030303 (cit. on pp. 21, 26).

[43] R. P. Groff, P. Avakian, and R. E. Merrifield. "Coexistence of Exciton Fission and Fusion in Tetracene Crystals." In: *Physical Review B* 1.2 (1970), pp. 815–817. DOI: 10.1103/PhysRevB.1.815 (cit. on p. 110).

[44] R. P. Groff, P. Avakian, and R. E. Merrifield. "Magnetic Field Dependence of Delayed Fluorescence From Tetracene Crystals." In: *Journal of Luminescence* 1-2.C (1970), pp. 218–223. DOI: 10.1016/0022-2313(70)90036-0 (cit. on pp. 100, 103).

[45] Alrun A. Günther, Johannes Widmer, Daniel Kasemann, and Karl Leo. "Hole Mobility in Thermally Evaporated Pentacene: Morphological and Directional Dependence." In: *Applied Physics Letters* 106.23 (2015), p. 233301. DOI: 10.1063/1.4922422 (cit. on p. 53).

[46] Nancy M. Haegel et al. "Terawatt-Scale Photovoltaics: Transform Global Energy Improving Costs and Scale Reflect Looming Opportunities." In: *Science* 364.6443 (2019), pp. 836–838. DOI: 10.1126/science.aaw1845 (cit. on p. 2).

[47] M. C. Hanna and A. J. Nozik. "Solar Conversion Efficiency of Photovoltaic and Photoelectrolysis Cells With Carrier Multiplication Absorbers." In: *Journal of Applied Physics* 100.7 (2006), p. 074510. DOI: 10.1063/1.2356795 (cit. on pp. 16, 64).

[48] Zeger Hens and Iwan Moreels. "Light Absorption by Colloidal Semiconductor Quantum Dots." In: *Journal of Materials Chemistry* 22.21 (2012), pp. 10406–10415. DOI: 10.1039/c2jm30760j (cit. on p. 34).

[49] Margaret A. Hines and Gregory D. Scholes. "Colloidal PbS Nanocrystals with Size-Tunable Near-Infrared Emission: Observation of Post-Synthesis Self-Narrowing of the Particle Size Distribution." In: *Advanced Materials* 15.21 (2003), pp. 1844–1849. DOI: 10.1002/adma.200305395 (cit. on p. 30).

[50] B. Hoex, J. Schmidt, P. Pohl, M. C.M. Van De Sanden, and W. M.M. Kessels. "Silicon Surface Passivation by Atomic Layer Deposited Al2O3." In: *Journal of Applied Physics* 104.4 (2008), p. 044903. DOI: 10.1063/1.2963707 (cit. on p. 56).

[51] Bo Hou, Yuljae Cho, Byung Sung Kim, John Hong, Jong Bae Park, Se Jin Ahn, Jung Inn Sohn, Seungnam Cha, and Jong Min Kim. "Highly Monodispersed PbS Quantum Dots for Outstanding Cascaded-Junction Solar Cells." In: *ACS Energy Letters* 1.4 (2016), pp. 834–839. DOI: 10.1021/acsenergylett.6b00294 (cit. on p. 29).

[52] ASTM International. "Terrestrial Reference Spectra for Photovoltaic Performance Evaluation ASTM G-173." In: *American Society for Testing Materials (ASTM) International: West Conshohocken* (2003).

URL: http://rredc.nrel.gov/solar/spectra/am1.5/ (cit. on p. 34).

[53] Priya J. Jadhav et al. "Triplet Exciton Dissociation in Singlet Exciton Fission Photovoltaics." In: *Advanced Materials* 24.46 (2012), pp. 6169–6174. DOI: 10.1002/adma.201202397 (cit. on p. 66).

[54] A. Jakubowicz, H. Jia, R. M. Wallace, and B. E. Gnade. "Adsorption Kinetics of P-Nitrobenzenethiol Self-Assembled Monolayers on a Gold Surface." In: *Langmuir* 21.3 (2005), pp. 950–955. DOI: 10.1021/la048308h (cit. on p. 84).

[55] Y. Jiang, M. P. Nielsen, A. J. Baldacchino, M. A. Green, D. R. McCamey, M. J. Y. Tayebjee, T. W. Schmidt, and N. J. Ekins-Daukes. "Singlet Fission and Tandem Solar Cells Reduce Thermal Degradation and Enhance Lifespan." In: ii (2020), pp. 1–16. arXiv: 2003.05565 (cit. on p. 54).

[56] R. C. Johnson and R. E. Merrifield. "Effects of Magnetic Fields on the Mutual Annihilation of Triplet Excitons in Anthracene Crystals." In: *Physical Review B* 1.2 (1970), pp. 896–902. DOI: 10.1103/PhysRevB.1.896 (cit. on p. 100).

[57] Inuk Kang and Frank W. Wise. "Electronic Structure and Optical Properties of PbS and PbSe Quantum Dots." In: *Journal of the Optical Society of America B* 14.7 (1997), p. 1632. DOI: 10.1364/josab.14.001632 (cit. on p. 16).

[58] Charles Kittel. *Introduction to Solid State Physics*. Vol. 8th editio. 2004, p. 704. DOI: citeulike-article-id:4202357 (cit. on p. 5).

[59] Mark W. Knight, Jorik van de Groep, Paula C.P. Bronsveld, Wim C. Sinke, and Albert Polman. "Soft Imprinted Ag Nanowire Hybrid Electrodes on Silicon Heterojunction Solar Cells." In: *Nano Energy* 30.October (2016), pp. 398–406. DOI: 10.1016/j.nanoen.2016.10.011 (cit. on p. 54).

[60] Anna Köhler and Heinz Bässler. "Charges and Excited States in Organic Semiconductors." In: *Electronic Processes in Organic Semiconductors* (2015), pp. 87–191. DOI: 10.1002/9783527685172.ch2 (cit. on p. 7).

[61] Anna Köhler and Heinz Bässler. "The Electronic Structure of Organic Semiconductors." In: *Electronic Processes in Organic Semiconductors* (2015), pp. 307–388. DOI: 10.1002/9783527685172.ch1 (cit. on pp. 39, 43).

[62] Anatoly B. Kolomeisky, Xintian Feng, and Anna I. Krylov. "A Simple Kinetic Model for Singlet Fission: A Role of Electronic and Entropic Contributions to Macroscopic Rates." In: *Journal of Physical Chemistry C* 118.10 (2014), pp. 5188–5195. DOI: 10.1021/jp4128176 (cit. on pp. 41, 51).

[63] Masakazu Kondo, Thomas E. Mates, Daniel A. Fischer, Fred Wudl, and Edward J. Kramer. "Bonding Structure of Phenylacetylene on Hydrogen-Terminated Si(111) and Si(100): Surface Photoelectron Spectroscopy Analysis and Ab Initio Calculations." In: *Langmuir* 26.22 (2010), pp. 17000–17012. DOI: 10.1021/la103208n (cit. on p. 84).

[64] Andreas Kunzmann, Marco Gruber, Rubén Casillas, Johannes Zirzlmeier, Melanie Stanzel, Wolfgang Peukert, Rik R. Tykwinski, and Dirk M. Guldi. "Singlet Fission for Photovoltaics with 130 % Injection Efficiency." In: *Angewandte Chemie - International Edition* 57.33 (2018), pp. 10742–10747. DOI: 10.1002/anie.201801041 (cit. on p. 100).

[65] Joseph R. Lakowicz. *Principles of Fluorescence Spectroscopy*. 2006. DOI: 10.1007/978-0-387-46312-4 (cit. on p. 23).

[66] Xinzheng Lan et al. "Passivation Using Molecular Halides Increases Quantum Dot Solar Cell Performance." In: *Advanced Materials* 28.2 (2016), pp. 299–304. DOI: 10.1002/adma.201503657 (cit. on p. 31).

[67] Lazard. *Levelized Cost of Energy - Version 14.0*. Tech. rep. 2020, p. 21. URL: https://www.lazard.com/perspective/levelized-cost-of-energy-and-levelized-cost-of-storage-2020/ (cit. on pp. 1, 2).

[68] Jiye Lee, Priya Jadhav, Philip D Reusswig, Shane R Yost, Nicholas J Thompson, Daniel N Congreve, Eric Hontz, Troy Van Voorhis, and Marc A Baldo. "Singlet Exciton Fission Photovoltaics." In: *Accounts of Chemical Research* 46.6 (2013), pp. 1300–1311. DOI: 10.1021/ar300288e (cit. on p. 64).

[69] Ju Min Lee, Moritz H. Futscher, Luis M. Pazos-Outón, and Bruno Ehrler. "Highly Transparent Singlet Fission Solar Cell With Multi-stacked Thin Metal Contacts for Tandem Applications." In: *Progress in Photovoltaics: Research and Applications* 25.11 (2017), pp. 936–941. DOI: 10.1002/pip.2919 (cit. on p. 64).

[70] Aleksandr P. Litvin, Anton A. Babaev, Peter S. Parfenov, Elena V. Ushakova, Mikhail A. Baranov, Olga V. Andreeva, Kevin Berwick, Anatoly V. Fedorov, and Alexander V. Baranov. "Photoluminescence of Lead Sulfide Quantum Dots of Different Sizes in a Nanoporous Silicate Glass Matrix." In: *Journal of Physical Chemistry C* 121.15 (2017), pp. 8645–8652. DOI: 10.1021/acs.jpcc.7b01952 (cit. on pp. 18, 22, 26).

[71] Alexander P. Litvin, Peter S. Parfenov, Elena V. Ushakova, Anatoly V. Fedorov, Mikhail V. Artemyev, Anatoly V. Prudnikau, Sergey A. Cherevkov, Ivan D. Rukhlenko, and Alexander V. Baranov. "Size-Dependent Room-Temperature Luminescence Decay From Pbs Quantum Dots." In: *Nanophotonics and Micro/Nano Optics* 8564 (2012), 85641Z. DOI: 10.1117/12.2001073 (cit. on pp. 20, 22).

[72] Atse Louwen, Wilfried Van Sark, Ruud Schropp, and André Faaij. "A Cost Roadmap for Silicon Heterojunction Solar Cells." In: *Solar Energy Materials and Solar Cells* 147 (2016), pp. 295–314. DOI: 10.1016/j.solmat.2015.12.026 (cit. on pp. 1, 3).

[73] Haipeng Lu, Xihan Chen, John E. Anthony, Justin C. Johnson, and Matthew C. Beard. "Sensitizing Singlet Fission with Perovskite Nanocrystals." In: *Journal of the American Chemical Society* 141.12 (Jan. 2019), pp. 4919–4927. DOI: 10.1021/jacs.8b13562 (cit. on p. 45).

[74] Z. H. Lu, J. P. McCaffrey, B. Brar, G. D. Wilk, R. M. Wallace, L. C. Feldman, and S. P. Tay. "SiO2 Film Thickness Metrology by X-Ray Photoelectron Spectroscopy." In: *Applied Physics Letters* 71.19 (1997), pp. 2764–2766. DOI: 10.1063/1.120438 (cit. on p. 87).

[75] Manuela Lunz, A. Louise Bradley, Valerie A. Gerard, Stephen J. Byrne, Yurii K. Gun'Ko, Vladimir Lesnyak, and Nikolai Gaponik. "Concentration Dependence of Förster Resonant Energy Transfer Between Donor and Acceptor Nanocrystal Quantum Dot Layers: Effect of Donor-Donor Interactions." In: *Physical Review B - Condensed Matter and Materials Physics* 83.11 (2011). DOI: 10.1103/PhysRevB.83.115423 (cit. on pp. 17, 23).

[76] Rowan W. Macqueen et al. "Crystalline Silicon Solar Cells With Tetracene Interlayers: The Path to Silicon-Singlet Fission Heterojunction Devices." In: *Materials Horizons* 5.6 (2018), pp. 1065–1075. DOI: 10.1039/c8mh00853a (cit. on pp. 13, 44, 54, 66, 67, 78, 101, 102).

[77] B. W. Van Der Meer, G. Coker Iii, and S.-Y. Simon Chen. *Resonance Energy Transfer: Theory and Data*. Wiley-VCH Verlag, 1994, p. 177 (cit. on pp. 19–21).

[78] *Mercaptoacetic acid | 68-11-1*. URL: https://www.chemicalbook.com/ (visited on 12/01/2020) (cit. on p. 21).

[79] R. E. Merrifield, P. Avakian, and R. P. Groff. "Fission of Singlet Excitons Into Pairs of Triplet Excitons in Tetracene Crystals." In: *Chemical Physics Letters* 3.3 (1969), pp. 155–157. DOI: 10.1016/0009-2614(69)80122-3 (cit. on pp. 66, 103).

[80] Kiyoshi Miyata, Felisa S. Conrad-Burton, Florian L. Geyer, and X. Y. Zhu. "Triplet Pair States in Singlet Fission." In: *Chemical Reviews* 119.6 (2019), pp. 4261–4292. DOI: 10.1021/acs.chemrev.8b00572 (cit. on p. 100).

[81] Iwan Moreels, Yolanda Justo, Bram De Geyter, Katrien Haustraete, José C. Martins, and Zeger Hens. "Size-Tunable, Bright, and Stable Pbs Quantum Dots: A Surface Chemistry Study." In: *ACS Nano*

5.3 (2011), pp. 2004–2012. DOI: 10.1021/nn103050w (cit. on pp. 20, 21).

[82] Iwan Moreels et al. "Size-Dependent Optical Properties of Colloidal Pbs Quantum Dots." In: *ACS Nano* 3.10 (2009), pp. 3023–3030. DOI: 10.1021/nn900863a (cit. on pp. 21, 22).

[83] R. K. Nahm and J. R. Engstrom. "Unexpected Effects of the Rate of Deposition on the Mode of Growth and Morphology of Thin Films of Tetracene Grown on SiO2." In: *Journal of Physical Chemistry C* 120.13 (2016), pp. 7183–7191. DOI: 10.1021/acs.jpcc.6b00963 (cit. on pp. 68, 71).

[84] Cory A. Nelson, Nicholas R. Monahan, and X. Y. Zhu. "Exceeding the Shockley-Queisser Limit in Solar Energy Conversion." In: *Energy and Environmental Science* 6.12 (2013), pp. 3508–3519. DOI: 10.1039/c3ee42098a (cit. on p. 100).

[85] Jens Niederhausen, Rowan W. MacQueen, Klaus Lips, Hazem Aldahhak, Wolf Gero Schmidt, and Uwe Gerstmann. "Tetracene Ultrathin Film Growth on Hydrogen-Passivated Silicon." In: *Langmuir* 36.31 (2020), pp. 9099–9113. DOI: 10.1021/acs.langmuir.0c01154 (cit. on p. 110).

[86] Lea Nienhaus et al. "Triplet-Sensitization by Lead Halide Perovskite Thin Films for Near-infrared-to-Visible Upconversion." In: *ACS Energy Letters* 4.4 (2019), pp. 888–895. DOI: 10.1021/acsenergylett.9b00283 (cit. on pp. 13, 55).

[87] NREL. *Best Research-Cell Efficiency Chart*. 2020. URL: https://www.nrel.gov/pv/cell-efficiency.html (visited on 11/04/2020) (cit. on p. 38).

[88] Alexandra Olaya-Castro and Gregory D. Scholes. "Energy Transfer From Förster-Dexter Theory to Quantum Coherent Light-Harvesting." In: *International Reviews in Physical Chemistry* 30.1 (2011), pp. 49–77. DOI: 10.1080/0144235X.2010.537060 (cit. on p. 72).

[89] U. Würfel P. Würfel. *Physics of Solar Cells: From Basic Principles to Advanced Concepts*. 2016, pp. 93–107 (cit. on p. 42).

[90] Alexandra F. Paterson et al. "Recent Progress in High-Mobility Organic Transistors: A Reality Check." In: *Advanced Materials* 30.36 (2018). DOI: 10.1002/adma.201801079 (cit. on p. 54).

[91] Luis M. Pazos-Outón, Ju Min Lee, Moritz H. Futscher, Anton Kirch, Maxim Tabachnyk, Richard H. Friend, and Bruno Ehrler. "A Silicon-Singlet Fission Tandem Solar Cell Exceeding 100% External Quantum Efficiency with High Spectral Stability." In: *ACS Energy Letters* 2.2 (Feb. 2017), pp. 476–480. DOI: 10.1021/acsenergylett.6b00678 (cit. on pp. 48, 64, 100).

[92] Simon Philipps. *Photovoltaics Report*. Tech. rep. September. Fraunhofer ISE, 2020. URL: https://www.ise.fraunhofer.de/en/publications/studies/photovoltaics-report.html (cit. on pp. 3, 4).

[93] Geoffrey B. Piland and Christopher J. Bardeen. "How Morphology Affects Singlet Fission in Crystalline Tetracene." In: *Journal of Physical Chemistry Letters* 6.10 (May 2015), pp. 1841–1846. DOI: 10.1021/acs.jpclett.5b00569 (cit. on pp. 71, 107, 110).

[94] Geoffrey B. Piland, Jonathan J. Burdett, Robert J. Dillon, and Christopher J. Bardeen. "Singlet Fission: From Coherences to Kinetics." In: *The Journal of Physical Chemistry Letters* 5.13 (2014), pp. 2312–2319. DOI: 10.1021/jz500676c (cit. on p. 100).

[95] Geoffrey B. Piland, Jonathan J. Burdett, Tzu Yao Hung, Po Hsun Chen, Chi Feng Lin, Tien Lung Chiu, Jiun Haw Lee, and Christopher J. Bardeen. "Dynamics of Molecular Excitons Near a Semiconductor Surface Studied by Fluorescence Quenching of Polycrystalline Tetracene on Silicon." In: *Chemical Physics Letters* 601 (2014), pp. 33–38. DOI: 10.1016/j.cplett.2014.03.075 (cit. on pp. 66, 67, 69, 88, 96, 102, 105, 110, 132).

[96] Robert Pirsig. *Zen and the Art of Motorcycle maintenance: An Inquiry into Values*. 1974 (cit. on p. 167).

[97] Felix Plasser, Stefanie A. Mewes, Andreas Dreuw, and Leticia González. "Detailed Wave Function Analysis for Multireference

Methods: Implementation in the Molcas Program Package and Applications to Tetracene." In: *Journal of Chemical Theory and Computation* 13.11 (2017), pp. 5343–5353. DOI: 10.1021/acs.jctc.7b00718 (cit. on p. 78).

[98] Andrey D. Poletayev, Jenny Clark, Mark W.B. Wilson, Akshay Rao, Yoshitaka Makino, Shu Hotta, and Richard H. Friend. "Triplet Dynamics in Pentacene Crystals: Applications to Fission-Sensitized Photovoltaics." In: *Advanced Materials* 26.6 (2014), pp. 919–924. DOI: 10.1002/adma.201302427 (cit. on pp. 44, 45).

[99] Albert Polman, Mark Knight, Erik C. Garnett, Bruno Ehrler, and Wim C. Sinke. "Photovoltaic materials: Present efficiencies and future challenges." In: *Science* 352.6283 (2016). DOI: 10.1126/science.aad4424 (cit. on p. 64).

[100] Martin Pope, Nicholas E. Geacintov, and Frank Vogel. "Singlet Exciton Fission and Triplet-Triplet Exciton Fusion in Crystalline Tetracene." In: *Molecular Crystals* 6.1 (Aug. 1969), pp. 83–104. DOI: 10.1080/15421406908082953 (cit. on p. 64).

[101] Sidharam P. Pujari, Alexei D. Filippov, Satesh Gangarapu, and Han Zuilhof. "High-Density modification of H-Terminated Si(111) surfaces using Short-Chain Alkynes." In: *Langmuir* 33.51 (Dec. 2017), pp. 14599–14607. DOI: 10.1021/acs.langmuir.7b03683 (cit. on p. 79).

[102] L.A. Meyer R.K. Pachauri and Core Writing Team. *Climate Change 2014: Synthesis Report. Contribution of Working Groups I, II and III to the Fifth Assessment Report of the Intergovernmental Panel on Climate Change*. Tech. rep. 2014, p. 151. arXiv: arXiv:1011.1669v3 (cit. on p. 1).

[103] Jeyakumar Ramanujam et al. "Inorganic Photovoltaics - Planar and Nanostructured Devices." In: *Progress in Materials Science* 82 (2016), pp. 294–404. DOI: 10.1016/j.pmatsci.2016.03.005 (cit. on p. 100).

[104] Akshay Rao and Richard H. Friend. "Harnessing Singlet Exciton Fission to Break the Shockley-Queisser Limit." In: *Nature Reviews Materials* 2 (2017). DOI: 10.1038/natrevmats.2017.63 (cit. on pp. 16, 18, 100).

[105] Akshay Rao, Mark W.B. Wilson, Justin M. Hodgkiss, Sebastian Albert-Seifried, Heinz Bässler, and Richard H. Friend. "Exciton Fission and Charge Generation via Triplet Excitons in Pentacene/C60 Bilayers." In: *Journal of the American Chemical Society* 132.36 (2010), pp. 12698–12703. DOI: 10.1021/ja1042462 (cit. on p. 66).

[106] Benjamin D. Ravetz, Andrew B. Pun, Emily M. Churchill, Daniel N. Congreve, Tomislav Rovis, and Luis M. Campos. "Photoredox Catalysis Using Infrared Light via Triplet Fusion Upconversion." In: *Nature* 565.7739 (2019), pp. 343–346. DOI: 10.1038/s41586-018-0835-2 (cit. on p. 13).

[107] Colin Reese, Wook Jin Chung, Mang Mang Ling, Mark Roberts, and Zhenan Bao. "High-Performance Microscale Single-Crystal Transistors by Lithography on an Elastomer Dielectric." In: *Applied Physics Letters* 89.20 (2006), p. 202108. DOI: 10.1063/1.2388151 (cit. on p. 53).

[108] Matthew O. Reese, Stephen Glynn, Michael D. Kempe, Deborah L. McGott, Matthew S. Dabney, Teresa M. Barnes, Samuel Booth, David Feldman, and Nancy M. Haegel. "Increasing Markets and Decreasing Package Weight for High-Specific-Power Photovoltaics." In: *Nature Energy* 3.11 (2018), pp. 1002–1012. DOI: 10.1038/s41560-018-0258-1 (cit. on p. 100).

[109] Sebastian Reineke and Marc A. Baldo. "Room Temperature Triplet State Spectroscopy of Organic Semiconductors." In: *Scientific reports* 4 (2014), p. 3797. DOI: 10.1038/srep03797 (cit. on p. 101).

[110] Chase C. Reinhart and Erik Johansson. "Colloidally Prepared 3-Mercaptopropionic Acid Capped Lead Sulfide Quantum Dots." In: *Chemistry of Materials* 27.21 (2015), pp. 7313–7320. DOI: 10.1021/acs.chemmater.5b02786 (cit. on p. 20).

[111] Armin Richter, Jan Benick, Martin Hermle, and Stefan W. Glunz. "Excellent Silicon Surface Passivation with 5 Å Thin ALD Al2O3 Layers: Influence of Different Thermal Post-Deposition Treatments." In: *Physica Status Solidi - Rapid Research Letters* 5.5-6 (2011), pp. 202–204. DOI: 10.1002/pssr.201105188 (cit. on p. 30).

[112] Bohdan Schatschneider, Stephen Monaco, Alexandre Tkatchenko, and Jian Jie Liang. "Understanding the Structure and Electronic Properties of Molecular Crystals Under Pressure: Application of Dispersion Corrected Dft to Oligoacenes." In: *Journal of Physical Chemistry A* 117.34 (2013), pp. 8323–8331. DOI: 10.1021/jp406573n (cit. on pp. 103, 108).

[113] Kazuhiko Seki, Yoriko Sonoda, and Ryuzi Katoh. "Diffusion-Mediated Delayed Fluorescence by Singlet Fission and Geminate Fusion of Correlated Triplets." In: *Journal of Physical Chemistry C* 122.22 (2018), pp. 11659–11670. DOI: 10.1021/acs.jpcc.8b02234 (cit. on pp. 110, 111, 129).

[114] Octavi E. Semonin, Justin C. Johnson, Joseph M. Luther, Aaron G. Midgett, Arthur J. Nozik, and Matthew C. Beard. "Absolute Photoluminescence Quantum Yields of IR-26 Dye, PbS, and PbSe Quantum Dots." In: *Journal of Physical Chemistry Letters* 1.16 (2010), pp. 2445–2450. DOI: 10.1021/jz100830r (cit. on p. 21).

[115] William Shockley and Hans J. Queisser. "Detailed Balance Limit of Efficiency of P-N Junction Solar Cells." In: *Journal of Applied Physics* 32.3 (1961), pp. 510–519. DOI: 10.1063/1.1736034 (cit. on pp. 4, 16, 100).

[116] Alexander B. Sieval, Vincent Vleeming, Han Zuilhof, and Ernst J.R. Sudhölter. "Improved Method for the Preparation of Organic Monolayers of 1-Alkenes on Hydrogen-Terminated Silicon Surfaces." In: *Langmuir* 15.23 (1999), pp. 8288–8291. DOI: 10.1021/la9904962 (cit. on pp. 71, 79).

[117] S. Singh, W. J. Jones, W. Siebrand, B. P. Stoicheff, and W. G. Schneider. "Laser Generation of Excitons and Fluorescence in Anthracene

Crystals." In: *The Journal of Chemical Physics* 42.1 (1965), pp. 330–342. DOI: 10.1063/1.1695695 (cit. on p. 100).

[118] Millicent B. Smith and Josef Michl. "Singlet Fission." In: *Chemical Reviews* 110.11 (2010), pp. 6891–6936. DOI: 10.1021/cr1002613 (cit. on pp. 39, 64, 100).

[119] Millicent B. Smith and Josef Michl. "Recent Advances in Singlet Fission." In: *Annual Review of Physical Chemistry* 64 (2013), pp. 361–386. DOI: 10.1146/annurev-physchem-040412-110130 (cit. on pp. 11, 100).

[120] Michael Stavola, David L. Dexter, and Robert S. Knox. "Electron-Hole Pair Excitation in Semiconductors via Energy Transfer From an External Sensitizer." In: *Physical Review B* 31.4 (1985), pp. 2277–2289. DOI: 10.1103/PhysRevB.31.2277 (cit. on p. 23).

[121] Hannah L. Stern et al. "Vibronically Coherent Ultrafast Triplet-Pair Formation and Subsequent Thermally Activated Dissociation Control Efficient Endothermic Singlet Fission." In: *Nature Chemistry* 9.12 (2017), pp. 1205–1212. DOI: 10.1038/nchem.2856 (cit. on p. 41).

[122] T. Suzuki, K. Yagyu, and H. Tochihara. "Initial Growth of Pentacene Thin Film on Si(001) Substrate." In: *Journal of Physical Chemistry C* 123.5 (2019), pp. 2996–3003. DOI: 10.1021/acs.jpcc.8b11238 (cit. on p. 53).

[123] Takayuki Suzuki, Kazuma Yagyu, and Hiroshi Tochihara. "Initial Growth of Pentacene on a Si(111)- Surface." In: *Physical Chemistry Chemical Physics* 22.26 (2020), pp. 14748–14755. DOI: 10.1039/d0cp01582b (cit. on p. 53).

[124] C. E. Swenberg and W. T. Stacy. "Bimolecular Radiationless Transitions in Crystalline Tetracene." In: *Chemical Physics Letters* 2.5 (1968), pp. 327–328. DOI: 10.1016/0009-2614(68)80087-9 (cit. on p. 100).

[125] Maxim Tabachnyk, Bruno Ehrler, Simon Gélinas, Marcus L Böhm, Brian J Walker, Kevin P Musselman, Neil C Greenham, Richard H Friend, and Akshay Rao. "Resonant Energy Transfer of Triplet Excitons From Pentacene to Pbse Nanocrystals." In: *Nature Materials* 13.11 (2014), pp. 1033–1038. DOI: 10.1038/NMAT4093 (cit. on pp. 17, 55, 64, 66).

[126] Stefan Wil Tabernig, Benjamin Daiber, Tianyi Wang, and Bruno Ehrler. "Enhancing Silicon Solar Cells With Singlet Fission: The Case for Förster Resonant Energy Transfer Using a Quantum Dot Intermediate." In: *Journal of Photonics for Energy* 8.02 (2018), p. 1. DOI: 10.1117/1.jpe.8.022008 (cit. on pp. 15, 57).

[127] Yu Tai Tao, Chien Ching Wu, Ji Yang Eu, Wen Ling Lin, Kwang Chen Wu, and Chun Hsien Chen. "Structure Evolution of Aromatic-Derivatized Thiol Monolayers on Evaporated Gold." In: *Langmuir* 13.15 (1997), pp. 4018–4023. DOI: 10.1021/la9700984 (cit. on p. 84).

[128] Murad J.Y. Tayebjee, Angus A. Gray-Weale, and Timothy W. Schmidt. "Thermodynamic Limit of Exciton Fission Solar Cell Efficiency." In: *Journal of Physical Chemistry Letters* 3.19 (2012), pp. 2749–2754. DOI: 10.1021/jz301069u (cit. on p. 100).

[129] Nicholas J Thompson et al. "Energy harvesting of non-emissive triplet excitons in tetracene by emissive PbS nanocrystals." In: *Nature Materials* 13 (2014), pp. 1039–1043. DOI: 10.1038/nmat4097 (cit. on pp. 16, 17, 23, 55, 57, 64, 66).

[130] Tom Tiedje, Eli Yablonovitch, George D. Cody, and Bonnie G. Brooks. "Limiting Efficiency of Silicon Solar Cells." In: *IEEE Transactions on Electron Devices* 31.5 (1984), pp. 711–716. DOI: 10.1109/T-ED.1984.21594 (cit. on pp. 3, 38, 40, 41).

[131] Y. Tomkiewicz, R. P. Groff, and P. Avakian. "Spectroscopic Approach to Energetics of Exciton Fission and Fusion in Tetracene Crystals." In: *The Journal of Chemical Physics* 54.10 (1971), pp. 4504–4507. DOI: 10.1063/1.1674702 (cit. on pp. 16, 101).

[132] US EIA. *Levelized Cost and Levelized Avoided Cost of New Generation Resources in the Annual Energy Outlook 2020*. Tech. rep. February. 2020, pp. 1–20 (cit. on p. 2).

[133] G. Vaubel and H. Kallmann. "Diffusion Length and Lifetime of Triplet Excitons and Crystal Absorption Coefficient in Tetracene Determined from Photocurrent Measurements." In: *Physica Status Solidi (B)* 35.2 (1969), pp. 789–792. DOI: 10.1002/pssb.19690350228 (cit. on pp. 22, 34).

[134] Janneke Veerbeek, Nienke J. Firet, Wouter Vijselaar, Rick Elbersen, Han Gardeniers, and Jurriaan Huskens. "Molecular Monolayers for Electrical Passivation and Functionalization of Silicon-Based Solar Energy Devices." In: *ACS Applied Materials and Interfaces* 9.1 (2017), pp. 413–421. DOI: 10.1021/acsami.6b12997 (cit. on p. 61).

[135] M. Voigt, A. Langner, P. Schouwink, J. M. Lupton, R. F. Mahrt, and M. Sokolowski. "Picosecond Time Resolved Photoluminescence Spectroscopy of a Tetracene Film on Highly Oriented Pyrolytic Graphite: Dynamical Relaxation, Trap Emission, and Superradiance." In: *Journal of Chemical Physics* 127.11 (2007). DOI: 10.1063/1.2766944 (cit. on p. 107).

[136] Oleksandr Voznyy et al. "Origins of Stokes Shift in PbS Nanocrystals." In: *Nano Letters* 17.12 (2017), pp. 7191–7195. DOI: 10.1021/acs.nanolett.7b01843 (cit. on pp. 43, 57).

[137] Yan Wan, Zhi Guo, Tong Zhu, Suxia Yan, Justin Johnson, and Libai Huang. "Cooperative Singlet and Triplet Exciton Transport in Tetracene Crystals Visualized by Ultrafast Microscopy." In: *Nature Chemistry* 7.10 (2015), pp. 785–792. DOI: 10.1038/nchem.2348 (cit. on p. 88).

[138] Chun Hsiung Wang, Chih Wei Chen, Chih Ming Wei, Yang Fang Chen, Chih Wei Lai, Mei Lin Ho, and Pi Tai Chou. "Resonant Energy Transfer Between Cdse/Zns Type I and Cdse/Znte Type II Quantum Dots." In: *Journal of Physical Chemistry C* 113.35 (2009), pp. 15548–15552. DOI: 10.1021/jp904361a (cit. on p. 17).

[139] T. H. Wang, T. F. Ciszek, C. R. Schwerdtfeger, H. Moutinho, and R. Matson. "Growth of Silicon Thin Layers on Cast MG-Si From Metal Solutions for Solar Cells." In: *Solar Energy Materials and Solar Cells* 41-42 (1996), pp. 19–30. DOI: 10.1016/0927-0248(95)00131-X (cit. on p. 5).

[140] Mark W.B. Wilson, Akshay Rao, Jenny Clark, R. Sai Santosh Kumar, Daniele Brida, Giulio Cerullo, and Richard H. Friend. "Ultrafast Dynamics of Exciton Fission in Polycrystalline Pentacene." In: *Journal of the American Chemical Society* 133.31 (2011), pp. 11830–11833. DOI: 10.1021/ja201688h (cit. on pp. 39, 41).

[141] Mark W.B. B Wilson, Akshay Rao, Kerr Johnson, Simon Gélinas, Riccardo Di Pietro, Jenny Clark, and Richard H. Friend. "Temperature-Independent Singlet Exciton Fission in Tetracene." In: *Journal of the American Chemical Society* 135.44 (2013), pp. 16680–16688. DOI: 10.1021/ja408854u (cit. on pp. 16, 110, 132).

[142] P. K. Wolber and B. S. Hudson. "An Analytic Solution to the Förster Energy Transfer Problem in Two Dimensions." In: *Biophysical Journal* 28.2 (1979), pp. 197–210. DOI: 10.1016/S0006-3495(79)85171-1 (cit. on p. 23).

[143] Cathy Y. Wong, Samuel B. Penwell, Benjamin L. Cotts, Rodrigo Noriega, Hao Wu, and Naomi S. Ginsberg. "Revealing Exciton Dynamics in a Small-Molecule Organic Semiconducting Film With Subdomain Transient Absorption Microscopy." In: *Journal of Physical Chemistry C* 117.42 (2013), pp. 22111–22122. DOI: 10.1021/jp407645k (cit. on p. 66).

[144] Tony C. Wu, Nicholas J. Thompson, Daniel N. Congreve, Eric Hontz, Shane R. Yost, Troy Van Voorhis, and Marc A. Baldo. "Singlet Fission Efficiency in Tetracene-Based Organic Solar Cells." In: *Applied Physics Letters* 104.19 (May 2014), p. 193901. DOI: 10.1063/1.4876600 (cit. on pp. 66, 103).

[145] Le Yang, Maxim Tabachnyk, Sam L. Bayliss, Marcus L. Böhm, Katharina Broch, Neil C. Greenham, Richard H. Friend, and Bruno Ehrler. "Solution-Processable Singlet Fission Photovoltaic

Devices." In: *Nano Letters* 15.1 (2015), pp. 354–358. DOI: 10.1021/nl503650a (cit. on p. 66).

[146] Aydan Yeltik, Burak Guzelturk, Pedro Ludwig Hernandez-Martinez, Alexander O. Govorov, and Hilmi Volkan Demir. "Phonon-Assisted Exciton Transfer Into Silicon Using Nanoemitters: The Role of Phonons and Temperature Effects in Förster Resonance Energy Transfer." In: *ACS Nano* 7.12 (2013), pp. 10492–10501. DOI: 10.1021/nn404627p (cit. on pp. 16, 17, 20).

[147] Xiao Ying Zhang et al. "Surface Passivation of Silicon Using HfO2 Thin Films Deposited by Remote Plasma Atomic Layer Deposition System." In: *Nanoscale Research Letters* 12.1 (2017), p. 324. DOI: 10.1186/s11671-017-2098-5 (cit. on p. 56).

[148] Tong Zhu, Yan Wan, Zhi Guo, Justin Johnson, and Libai Huang. "Two Birds with One Stone: Tailoring Singlet Fission for Both Triplet Yield and Exciton Diffusion Length." In: *Advanced Materials* 28.34 (2016), pp. 7539–7547. DOI: 10.1002/adma.201600968 (cit. on pp. 110, 132).

[149] X. Y. Zhu. "How to Draw Energy Level Diagrams in Excitonic Solar Cells." In: *Journal of Physical Chemistry Letters* 5.13 (2014), pp. 2283–2288. DOI: 10.1021/jz5008438 (cit. on p. 101).

# ABSTRACT

This thesis explores the theory and experimental design of singlet fission-silicon solar cells. Singlet fission is a process that can convert one high-energy photon into two excitons of roughly half the energy. When combined with a lower-bandgap material like silicon, singlet fission materials can increase the efficiency of solar cells by using the energy of blue and green part of the incoming light more efficiently. To enable this dream we have to then disassociate or transfer these triplet excitons so we can extract the additional energy in the singlet fission process and make it usable as a real-life electricity source. In this thesis we demonstrate several theoretical and experimental insights that can help with the development of useful singlet fission-solar cells.

**CHAPTER 1** introduces the singlet fission process and its application in solar cells. We discuss the difference between inorganic and organic semiconductors and how that difference presents special challenges when combining the two.

**CHAPTER 2** describes how a thin layer of quantum dots can help with transfer from a singlet fission material into silicon. We calculate the transfer efficiency for the Förster Resonant Energy Transfer (FRET) mechanism and find that, since silicon is an indirect bandgap semiconductor, the transfer can only be efficient if the quantum dot layer is very close to the silicon surface. We modify the standard FRET model to describe the transfer from a dipole donor (the quantum dot) into a bulk acceptor (the silicon) and find that the distance dependence weaker, predicting a higher transfer efficiency than expected from the standard model.

**CHAPTER 3** contains solar cell efficiency calculations for three different transfer mechanisms. One mechanism is FRET transfer for which we use

the FRET model from Chapter II to calculate a realistic but optimistic solar cell efficiency that is much higher than of just the silicon solar cell alone. Transfer can also happen by directly transferring the triplet exciton via Dexter transfer, for which we find an even higher efficiency, if the energy levels of the singlet fission material and silicon match well. The last transfer mechanism we discuss is via charge transfer, dissociating the triplet exciton at the silicon interface. This transfer mechanism has the highest efficiency gains of the three and puts the least constraints in the singlet exciton energies, but also adds experimental complexity.

**CHAPTER 4** discusses a new method of detecting evidence for triplet exciton transfer by quenching of the delayed photoluminescence of tetracene, a singlet fission material, on a silicon surface. Detecting quenching is necessary to determine if transfer occurs and we combined height maps and photoluminescence lifetime data of hundreds of small tetracene islands to correlate height and lifetime. We model photoluminescence in the islands with a diffusion model and find that we expect shorter lifetimes for thinner islands. We then apply this method to different silicon surface treatments and find that there is no quenching in these specific surface treatments.

**CHAPTER 5** demonstrates a singlet fission silicon solar cell with energy transfer of triplet excitons from tetracene into silicon. We detect the characteristic behavior of the solar cell current under a magnetic field and find evidence for triplet energy transfer if the protective layers of the silicon solar cell have been removed and the cell with tetracene has been exposed to air. We then use photoluminescence decay data and fit a differential equation describing the different species in tetracene that allows us to quantify the transfer efficiency. This solar cell is only the second demonstration of a singlet fission-silicon solar cell and works with a surprisingly simple geometry once the crystal packing of the singlet fission material is favorable for energy transfer.

# SAMENVATTING

van de proefschrift:

## Overdracht van Triplet Excitons in Singlet Splitsing-Siliciumzonnecellen

### Experimenten en Theorie Omtrent het Doorbreken van de Efficiëntielimiet van de Gedetailleerde Balans

Deze thesis onderzoekt de theorie en het ontwerp van singlet splitsing-silicium zonnecellen. Singlet splitsing is een proces waarbij één hoogenergetisch foton kan worden omgezet in twee excitonen met een lagere energie, elk met ruwweg de helft van de oorspronkelijke fotonenergie. Wanneer ze gecombineerd worden met een materiaal met lage bandkloof, zoals silicium, kunnen singlet splitsing materialen de efficiëntie van zonnecellen verhogen door de energie uit het blauwe en groene deel van inkomende licht efficiënter te gebruiken. Om deze droom te kunnen verwezenlijken moeten de triplet excitonen gedissocieerd danwel overgedragen worden zodat de toegevoegde energie van het singlet splitsingsproces kan worden geëxtraheerd en kan worden gebruikt als echte bron van elektriciteit. In deze thesis onderzoeken wij enkele theoretische en experimentele inzichten die kunnen helpen om de ontwikkeling van singlet splitsing zonnecellen realiteit te maken.

**HOOFDSTUK 1** introduceert het singlet splitsingsproces en zijn toepassing voor zonnecellen. We bediscussiëren het verschil tussen anorganische en organische halfgeleiders en hoe dit verschil uitdagingen vormt wanneer beiden gecombineerd worden.

**HOOFDSTUK 2** beschrijft hoe een dunne laag kwantumpunten kan helpen bij de overdracht van een singlet splitsing materiaal naar silicium. We berekenen de overdrachtsefficiëntie voor het Förster Resonant Energy Transfer-mechanisme en vinden dat, daar silicium en indirecte bandkloof heeft, de overdracht enkel efficiënt kan zijn als de kwantumpuntlaag zich zeer dichtbij het silicium bevindt. We modificeren het standaard FRET-model om de overdracht van een dipooldonor (het kwantumpunt) naar een bulk acceptor (het silicium) en vinden dat de afstandsafhankelijkheid zwakker is, waarmee we een hogere overdrachtsefficiëntie voorspellen dan verwacht kan worden op basis van het standaardmodel.

**HOOFDSTUK 3** bevat berekeningen voor de zonnecelefficiëntie op basis van drie verschillende overdrachtsmechanismes. Eén van deze mechanismen is FRET-overdracht waarvoor we het model van Hoofdstuk 2 gebruiken om een realistische, maar optimistische zonnecelefficiëntie te berekenen die een stuk hoger is dan de siliciumcel alleen. Overdracht kan ook plaatsvinden door directe overdracht van het triplet exciton via Dexteroverdracht, waarvoor we ook een toename in efficiëntie vinden, zolang de energieniveaus van het singlet splitsing materiaal goed overeenkomen met de energieniveaus van silicium. Het laatste overdrachtsmechanisme dat we bediscussiëren is ladingsoverdracht, waarbij het triplet exciton gescheiden wordt op het contactvlak met silicium. Dit mechanisme leidt tot de hoogste efficiëntie.

**HOOFDSTUK 4** bediscussieert een nieuwe methode voor het detecteren van de energieoverdracht van triplet excitonen vanuit tetraceen, een singlet splitsing materiaal, op silicium *via* de afname van de fotoluminescentie. Het detecteren van deze afname is een voorwaarde om te bepalen of tripletoverdracht plaatsvindt. We combineerden hoogtekaarten en de levensduur van het stralend verval van honderden kleine eilanden tetraceen om materiaaldikte en levensduur te correleren. We modeleren fotoluminescentie in de eilanden met een diffusiemodel en verwachten een kortere levensduur van het stralend verval in dunnere eilanden. We passen deze methode toe op siliciumoppervlakken met verschillende

oppervlaktebehandelingen en vinden dat er geen luminiscentie-afname plaatsvindt bij deze specifieke behandelde oppervlakken.

**HOOFDSTUK 5** beschrijft een daadwerkelijke singlet splitsing zonnecel met overdracht tussen tetraceen en silicium. Onder een magnetisch veld kunnen wij karakteristiek gedrag voor tripletexcitonoverdracht waarnemen in de zonnecelstroom. We vinden alleen bewijs voor deze overdracht als de beschermende lagen van de siliciumzonnecel zijn verwijderd en de cel met tetraceen is blootgesteld aan lucht. Vervolgens gebruiken we verval van fluorescentie en doen een regressie-analyse van een differentiaalvergelijking die de verschillende soorten excitonen in tetraceen beschrijft, waarmee we de overdrachtsefficiëntie kunnen bepalen. Deze zonnecel is slechts de tweede demonstratie van een singlet splitsing-silicium zonnecel en werkt met een verrassend eenvoudige geometrie zodra de kristalordening van het singlet-splitsing materiaal gunstig is voor de energieoverdracht.

# LIST OF PUBLICATIONS

The Chapters of this thesis are based on the following publications:

1. Stefan W Tabernig*, Benjamin Daiber*, Tianyi Wang, and Bruno Ehrler. "Enhancing Silicon Solar Cells with Singlet Fission: the Case for Förster Resonant Energy Transfer Using a Quantum Dot Intermediate" In: *Journal of Photonics for Energy* (2018)

2. Benjamin Daiber, Koen vd Hoven, Moritz H Futscher, and Bruno Ehrler. "Realistic Efficiency Limits for Singlet Fission Silicon Solar Cells" In: *In Preparation* (2020)

3. Benjamin Daiber, Sidharam P Pujari, Steven Verboom, Stefan L Luxembourg, Stefan W Tabernig, Moritz H Futscher, Jumin Lee, Han Zuilhof, and Bruno Ehrler. "A Method to Detect Triplet Exciton Transfer from Singlet Fission Materials into Silicon Solar Cells: Comparing Different Surface Treatments" In: *The Journal of Chemical Physics* (2020)

4. Benjamin Daiber*, Sourav Maiti*, Silvia M Ferro, Joris Bodin, Alyssa FJ van den Boom, Stefan L Luxembourg, Sachin Kinge, Sidharam P Pujari, Han Zuilhof, Laurens DA Siebbeles, and Bruno Ehrler. "Change in Tetracene Polymorphism Facilitates Triplet Transfer in Singlet Fission-Sensitized Silicon Solar Cells" In: *The Journal of Physical Chemistry Letters* (2020)

Other publications by the author:

5. Tianyi Wang*, Benjamin Daiber*, Jarvist M Frost, Sander A Mann, Erik C Garnett, Aron Walsh, and Bruno Ehrler. "Indirect to Direct Bandgap Transition in Methylammonium Lead Halide Perovskite" In: *Energy & Environmental Science* (2017)

6. Christian D Dieleman, Weiyi Ding, Lianjia Wu, Neha Thakur, Ivan Bespalov, Benjamin Daiber, Yasin Ekinci, Sonia Castellanos, and Bruno Ehrler "Universal Direct Patterning of Colloidal Quantum Dots by (Extreme) Ultraviolet and Electron Beam Lithography" In: *Nanoscale* (2020)

7. Jens Niederhausen, Rowan W. MacQueen, Engin Özkol, Clemens Gersmann, Moritz H. Futscher, Martin Liebhaber, Dennis Friedrich, Mario Borgwardt, Katherine A Mazzio, Patrick Amsalem, Minh Hai Nguyen, Benjamin Daiber, Mathias Mews, Jörg Rappich, Florian Ruske, Rainer Eichberger, Bruno Ehrler, and Klaus Lips. "Energy-level Alignment Tuning at Tetracene/c-Si Interfaces" In: *Journal of Physical Chemistry C* (2020)

*What's really been getting you stuck*
*is the running from the stuckness*
*through the cars of your train of knowledge*
*looking for a solution that is out in front of the train.*
*Stuckness shouldn't be avoided.*
*It's the psychic predecessor of all real understanding.*

— Robert M. Pirsig, Zen and the Art of Motorcycle Maintenance [96]

# ACKNOWLEDGMENTS

I have to thank many many people, I could only do this with your support and help.

Thank you to Dr. Esther Alarcón-Lladó for being my co-supervisor and Prof. Mark Wilson, Dr. Jenny Clark, Prof. Maria Loi, Prof. Maxim Pchenitchnikov, and Prof. Ferdinand Grozema for evaluating my work in this thesis.

I wholeheartedly thank Bruno Ehrler for the opportunity of doing a PhD, and putting his trust in me while building up a new research group. You were a great boss and I will miss the discussions that we had over coffee and lunch. Looking back it seems almost surreal that such a long time will end, I will miss it dearly and promise to bring all the things you taught me to good use. Now I would like to thank all the people in the Hybrid Solar Cells group that I met during my time here. In semi-random order: Thanks to Christian Dieleman for being a great officemate and friend for so many years, we also shared many great coffees through the ups and downs. Thanks to Moritz Futscher for the friendship, lively discussions and your enthusiasm in all things science, I wish you all the best in Zürich! (Thanks to you I bought one Tesla stock!) Tianyi Wang took me under his wings as a Master student, thank you for that! It was great working with you and learning how to be a scientist. Jumin Lee, you were so fun to be around, I also learned many things about Korea from you, thanks! Thanks also for your help during my project. Stefan

Tabernig, you were my first Master student of my own, thanks for the fun collaboration! I wish you all the best in your future endeavors. Joris Bodin, you were my second Master student, working with you has also been great, we did a lot in the time, and thanks to your knee we found the secret sauce! Emil Kensington, you were the third Master student, and even though you had to finish during the coronavirus pandemic, you did great. It was a pleasure working with you. I have been very blessed with three great Master students! Koen vd Hoven, working with you and Moritz was fun, best of luck during the PhD! Jouke Blum, with you I went on the voyage to new machine learning territories, we managed to arrive in a short time! Fabian Ecker, together we optimized the Magnetic Field setup and saw some interesting stuff, it was nice to see in how many things you dipped your toes in. Eline Hutter, it was a pleasure to have met you, I am sure you will have great success in you new position, congrats! Silvia Ferro, it was great to work with you and have coffees together, I wish you all the best and am looking forward to seeing great singlet fission solar cells! Lucie McGovern, thank you for the lively discussions and the good vibes. Loreta Muscarella, always fun to be around, especially in the vicinity of other Italians, all the best! Gianluca, thanks for your input during our meetings, it was always nice to hear your perspective. Imme Schuringa, I wish you all the best in the future! Marnix Akkermans, you did a great job with your project as well, it was fun to tinker with the optical setups together! David Langhorst, I hope you take good care of the office plants! Marc Duursma, thanks for the countless hours of helping with broken equipment and other organizational things, it would truly be impossible to do any research without you! Andrew Pun, it was a fun summer together, all the best! I also had the pleasure of meeting Merlijn Kersten, Merlinde Wobben, Linda van der Waart, Toon Maasen, Talia Martz-Oberlander, Mischa Hillenius, Ruirt Bosma, Andrea Pollastri, Arnoud Jongeling, Maria Mione, and Maarten Mennes. Thanks for the time together in the group.

Many people in the other Amolf groups also helped me. Mark Aarts, thanks for your help with the AFM! Parisa Khoram, it was a pleasure to talk to you and work for a short time on the TCSPC. Sarah Brittman, you

helped me first with the TCSPC setup. I hope I did take good care of it, we had to move it twice since! Giada La Gala, Annemarie Berkhout, and Remco Muller, thanks for being great office mates in my first months. Sven Askes, thanks for your help in the lab and proofreading. Lukas Helmbrecht, was a pleasure to meet you, great parties! And thanks for the ergonomic mouse, I will send you a post card in 30 years with an legible handwriting thanks to an intact wrist. Kevin Cognéé, was nice to have met you! Jian Yao Zheng, thanks for your help in the lab and sharing your intersting results with me! Susan Rigter, I hope you have success with the ball mill! Sebastian Öner, it was nice to meet you and thanks for the lab advice! Sander Mann, thanks for the discussions and our collaboration! Mark Knight, thanks for the discussion and being a good teacher in the AMEP courses. Benjamin Brenny, all the best, now there are zero Benjamins at Amolf, down from three! Verena Neder, thanks for being a great roommate during the Master, I wish you all the best! Tom Veeken, it was fun working with you. Our pillars did quench, and we took great TCSPC pictures together. Also the failed MPTMS functionalization was fun, we still learned a lot! Jenny Kontoleta, thanks for the great vibes, help in the lab and general pleasantness!

I would also like to thank the other group leaders I met at Amolf. Albert Polman for giving a great lecture that got me interested in solar cells and Amolf, Femius Koenderink also for a great lecture and fun conversations, also at the poster board. Esther Alarcón-Lladó for your enthusiasm about science and being my co-supervisor. Erik Garnett, for many piercing questions and the collaborations between our groups.

The Amolf support staff is also very important, countless designs have been thought of and produced, without them nothing would happen! Especially the team of the tekenkamer has been fun to work with and is always willing to entertain crazy ideas, together with the workshop they can build anything! So thanks Ricardo Struik, Henk-Jan Boluijt and Iliya Cerjak.

There are countless other people in Amolf that have made my time more pleasant, thank you for that, you know who you are!

Outside Amolf I would like to thank Arnon Lesage, for helping me with my AMEP project and giving an insight into the Ph.D. life. I wish

you all the best! Tom Gregorkiewcz, for the help during the Master and being my Master thesis co-supervisor, and great lecture about solar cells, you will always be remembered kindly.

My collaboration with the Wageningen University was also fun and fruitful. Thanks to Han Zuilhof for the opportunity, Sidharam Pujari for samples and help with chemistry, Alyssa vd Boom for XPS measurements, and Steven Verboom for the important functionalized surfaces.

At ECN I would like to thank Stefan Luxembourg for interesting and detailed discussions about the surface recombination velocity and the carrier lifetime measurements together with Petra Manshanden.

At TU Delft I would like to foremost thank Sourav Maiti, it was great working with you, we did a lot together. The one day coding together was probably the most effective I have ever been in my PhD, goes to show that together you can be better. I would like to thank Laurens Sibbeles for great discussions and his support. Kevin Felter for the collaboration and discussions. It was great to see your enthusiasm, together we measured changes in PL of only a few per mille! Ferdinand Grozema, for the discussions about the PDI's and singlet fission in general.

Outside of the Netherlands I would like to thank Jens Niederhausen at HZB Berlin, for the great insights into UPS/XPS and discussions during nanoGe. Rowan MacQueen, for the great time we had in the lab together. It was amazing to see your enthusiasm and it was fun to talk singlet fission with you. Onwards and upwards! Dan Congreve at the Rowland Institute for showing me around the lab, and the interesting discussions we had during conferences.

I would like to thank Diego Cohen, for being a great friend, for the political discussions and of course for the two crazy bike tours we did!

During my studies in Heidelberg I made many great friends that I sadly got to see less of in the last four years. But we still have a lifetime ahead of us that we can fill with sailing trips, see you soon!

The same goes for all friends from Lichtenfels, I am sad we cannot meet this year, but there are many more Formula E races to follow in the future!

I would like to thank my family for their continued support and love. Cornelius Daiber, its amazing to see you thrive in Chemistry, who

would have thought my little brother would be big so quickly? My parents, Thomas Daiber and Susanne Daiber, for looking out for me and supporting me all this time. Without you I would't be where I am now.

I would like to thank Jenny Lamphere for her support and love during all this time, I will never forget it.

# Curriculum Vitæ

## Personal Information


Benjamin Daiber
benjamin.daiber@gmail.com
linkedin.com/in/benjamindaiber


21.02.1992 Born in Stuttgart, Germany

## Education

2011 Abitur
Meranier Gymnasium Lichtenfels, Germany

2011-2014 Bachelor of Science
Physics
University of Heidelberg, Germany

2014-2016 Master of Science
Advanced Matter and Energy Physics
University of Amsterdam, The Netherlands

*Thesis* Indirect to Direct Bandgap Transition in methylammonium Lead Halide Perovskite
*Promotor* Dr. Bruno Ehrler

2016-2020 Ph.D. in Physics
from University of Groningen
Research at AMOLF, Amsterdam, The Netherlands

*Thesis* Transfer of Triplet Excitons in Singlet Fission-Silicon Solar Cells
*Promotor* Dr. Bruno Ehrler